Radiation Safety

Radiation Safety

1. Introduction

The major safety hazard associated with accelerators is obviously the radiological hazard. This course deals with this hazard. The subject however is very vast and cannot be covered in an exhaustive way in this short introductory course. We have therefore tried to present the basic, general ideas involved, presenting numerical data to show the relative importance of the different processes, give practical rules of thumb, and provide reference to literature where more details can be found.

Chapter 2 gives a short overview of the interaction processes of the different types of radiation with matter.

Chapter 3 defines the main quantities used in radiation physics and radiation protection, and explains the fundamental rules of radiation protection.

Chapter 4 describes the prompt radiation sources that exist around the different types of accelerators.

Chapter 5 gives a short introduction to the problem of induced radiation.

Chapter 6 deals with the shielding of accelerators.

Chapter 7 gives a short introduction to radiation monitoring.

2. Introduction to radiation physics

2.1 Introduction

Radiation is energy transmitted either in the form of waves, particularly as electromagnetic radiation, or in the form of charged or uncharged particles. It is appropriate to characterise radiation into two main groups: *ionising radiation* and *non-ionising radiation*. The decisive property of radiation for this grouping is the ability to ionise atoms and molecules, i.e. to remove or add an electron to an atom or molecule, resulting in the formation of ions. Non-ionising radiation such as ultraviolet radiation, microwaves or low-frequency electromagnetic radiation are not capable of ionisation and are not discussed here.

Table 1 gives the mean ionisation potential for a few elements, i.e. the energy required to ionise an atom.

Element	Ionisation potential [eV]
carbon	11.260
oxigen	13.618
potassium	4.341
iron	7.870
lead	7.416

Table 1 – Mean ionisation potential for a few elements.

One sees that the energy required to ionise an atom is of the order of 10 eV. For electromagnetic radiation this corresponds to a wavelength of the order of 100 nm (hard ultra-violet).

Ionising radiation can be *directly ionising* or *indirectly ionising*. Directly ionising radiation includes charged particles including for example electrons, positrons, protons and heavy ions. This radiation can ionise the medium promptly. Indirectly ionising radiation may only ionise by means of secondary charged particles such as electrons or recoil nuclei. Indirectly ionising radiation encompasses any uncharged particles, such as neutrons and photons.

All radiation transport problems can in principle be solved with the help radiation transport equations, if the basic microscopic processes and the properties of the material are known. It is however sufficient and easier in many practical cases to describe the interaction of radiation with material using characteristic macroscopic quantities. In this chapter, we will describe the microscopic processes and the corresponding macroscopic description for the interaction of the different types of ionising radiation, of importance in accelerator radiation physics.

2.2 Interactions of electrons / positrons with matter

2.2.1 The physical processes

The interaction of electrons and positrons with matter can be divided into elastic and inelastic collisions with orbital electrons and atomic nuclei.

Inelastic collisions with orbital electrons result in the excitation of the atom, or, if the energy of the incident electron (or positron) is sufficiently high, in the ionisation of the atomic nuclei. This process is called *ionisation slowing down*.

Inelastic collisions occur with an atomic nucleus when the electron or positron enters the vicinity of the atomic nucleus; it will be deflected from its original direction by the Coulomb field of the nucleus. The electron loses energy which is emitted as photon radiation, bremsstrahlung. This interaction is called *radiation slowing down*.

Elastic scattering by atomic nuclei, without emission of photons, occurs essentially at low electron/positron energies. Rutherford scattering is of no importance in radiation protection physics, but as a result of this process more than 95% of the energy transferred to matter will produce a heating up effect.

Positrons which have been slowed down to nearly zero kinetic energy will finally annihilate. The most important process is two-photon annihilation, which results in the emission of two 511 keV photons.

2.2.2 Macroscopic description

In radiation physics the interaction of charged particles such as electrons or positrons is described using " stopping powers". The stopping power is the average rate at which the charged particles lose energy at any point along their tracks. For electrons and positrons it is customary to separate the total linear stopping power into two components: (a) the collision stopping power, which is the average energy loss per unit path length due to ionisation slowing down and (b) the radiative stopping power, which is the average energy loss per unit path length due to radiation slowing down. The separation of the stopping power into these two components is useful because most of the energy lost via ionisation and excitation of atoms is absorbed in the medium close to the electron track, whereas most of the energy lost in the form of bremsstrahlung travels far from the track before being absorbed.

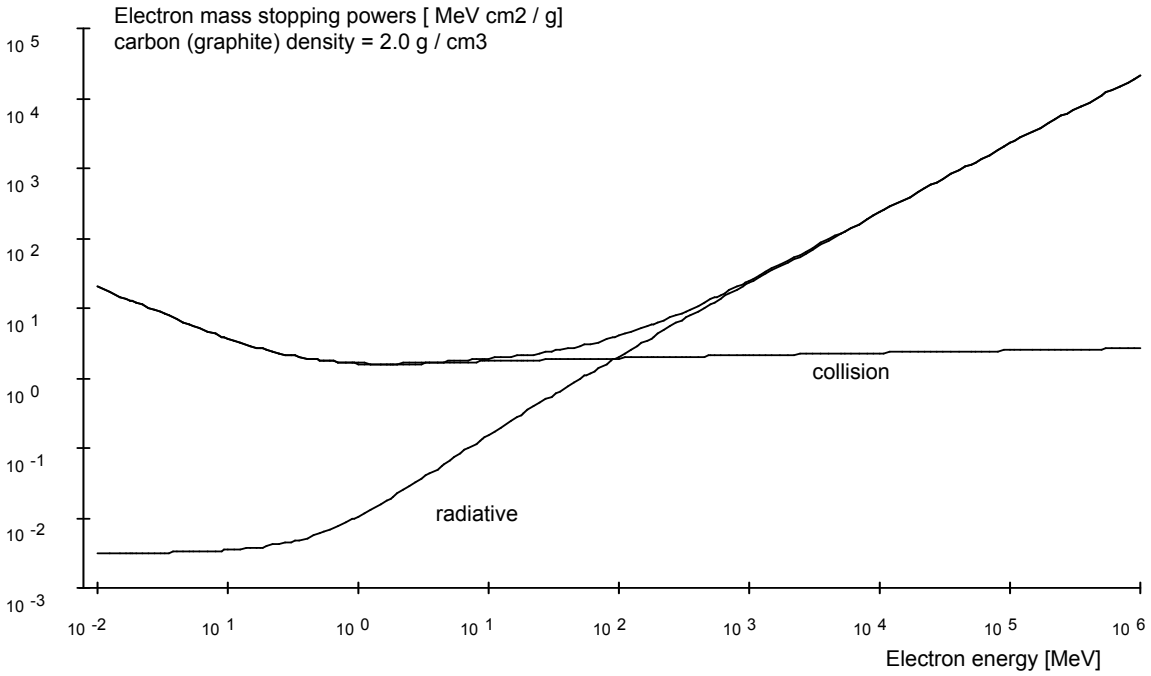

Figure 1.a – Electron stopping powers for graphite as a function of energy.

Figures 1.a and 1.b show the collision stopping power, radiative stopping power and total stopping power for graphite and lead respectively [1]. The graphite case is representative for light elements, the lead case for heavy elements.

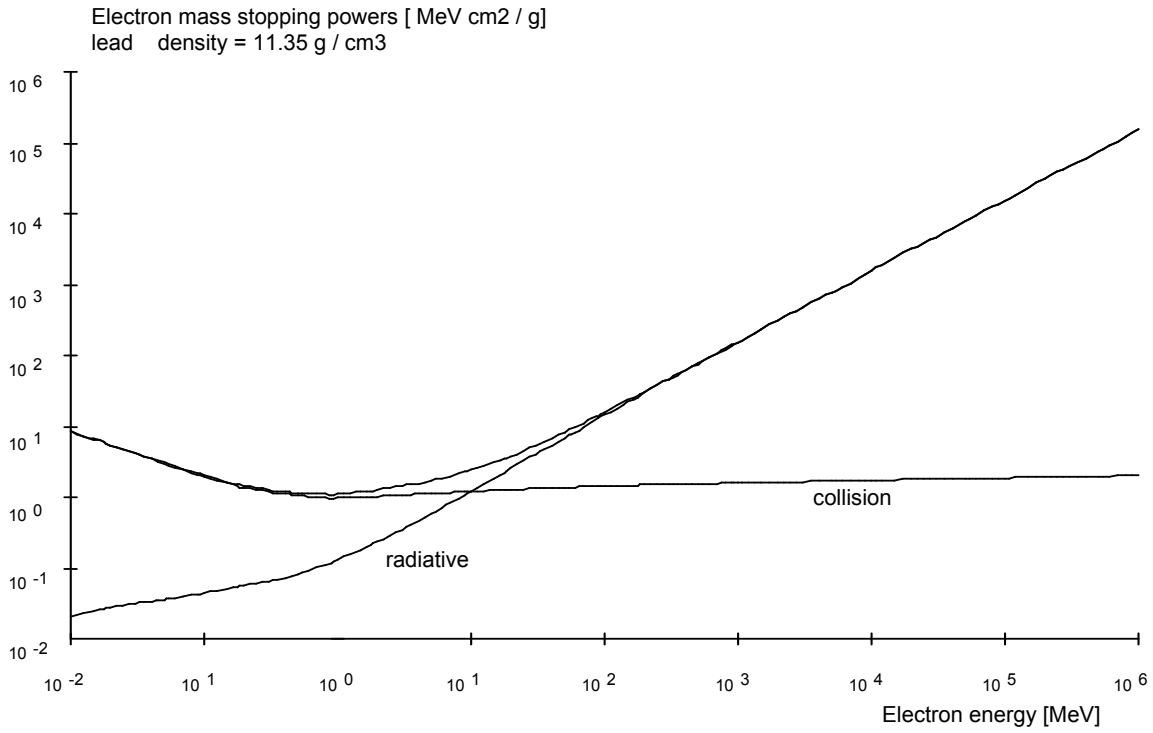

Figure 1b – Electron stopping powers for lead as a function of energy.

2.2.2.1 Collision stopping power

The collision stopping power is due to the energy transfer from the incident electrons to bound atomic electrons. If we denote by dσ/dW the differential cross-section per atomic electron for inelastic collisions resulting in an energy transfer of W, the mass collision stopping power can be expressed as

$$\frac{1}{\rho} S_{coll} = \frac{N_A}{A} Z \int W \frac{d\sigma}{dW} dW, \qquad (1)$$

where N_A is Avogadro's number (6.022045×10^{23} mol^{-1}), Z the atomic number of the medium, A the atomic weight of the medium and ρ its density ($g \cdot cm^{-3}$). The mass stopping power is expressed in units of $MeV \cdot cm^2 \cdot g^{-1}$.

The ionisation and excitation energy loss is described by the Bethe-Bloch formula [1]

$$S_{coll} = \frac{2\pi r_e^2 m_0 c^2}{\beta^2}\frac{Z}{A}\left\{\ln\left[\frac{\tau^2(\tau+2)}{2(I/m_e)^2}\right] + (1-\beta^2) + \frac{\tau^2/8 - (2\tau+1)\ln 2}{(\tau+1)^2} - \delta\right\}, \quad (2)$$

with r_e the classical electron radius (r_e = 2.817938 $\times$ 10^{-15} m), m_0c^2 the electron rest energy (0.511 MeV), I the mean excitation energy of the medium, β the electron velocity divided by the speed of light, and τ the ratio of the kinetic energy of the incident electron to its rest energy. δ is the density effect: when an electron passes through matter, polarization of the atoms in the medium occurs, decreasing the electrical field experienced by the electron, causing a decrease in the stopping power. In the high-energy limit, i.e. $\beta \sim 1$, the density effect is well approximated by the form [2]

$$\delta \approx 2\ln\left[\frac{28.816}{I}\sqrt{\frac{\rho Z}{A}}\right] + 2\ln(\tau+1) - 1. \quad (3)$$

Some selected values for the mean excitation energy are shown in table 2.

Element	Z	mean excitation energy I [eV]
beryllium	4	63.7
carbon (graphite)	6	78
aluminum	13	166
iron	26	286
copper	29	322
germanium	32	350
tungsten	74	727
lead	82	823
uranium	92	890

Table 2 – Mean excitation energy for different materials

2.2.2.2 Radiative stopping power

The radiative energy loss due to the deflection of the electron trajectory in the electric field of an elementary charge is known as the phenomena of bremsstrahlung. The scattering charge is generally a nucleus, but bremsstrahlung in the field of orbital electrons is not negligible, especially in materials of low atomic number. Three particles are involved in the collision: the electron, the emitted photon and the scattering nucleus or electron. The nucleus takes up negligible energy, due to its high mass, but its momentum may be comparable to that of the other two partners. For this reason, although one single photon is emitted per interaction, its energy and emission angle are not uniquely related.

Since the deflection is obviously stronger when the nucleus charge is large, radiation energy loss is especially important in high-Z materials. The cross-section is approximately proportional to the square of the atomic number.

Bremsstrahlung is emitted even at low electron energies, but the cross-sections are small and about constant up to a few MeV, where they begin to increase rapidly with increasing electron energy. Since collision losses decrease with increasing electron energy, the bremsstrahlung contribution to energy loss becomes important above energies of about 10 MeV for high-Z and about 100 MeV for low-Z materials (see figures 1.a and 1.b).

The energy spectrum of radiated photons ranges from zero to the kinetic energy of the incident electron and the number of photons in a given energy interval is approximately inversely proportional to the photon energy.

The angular distribution of the emitted photons becomes increasingly forward-peaked as the electron energy increases: at keV energies such as those found in common X-ray tubes, the photons are emitted at about 30^o to 90^o, but at energies E large compared to the electron rest mass the average angle of emission is of the order of m_0c^2/E (in radians).

As an example we show in figures 2.a and 2.b the differential bremsstrahlung cross-sections as a function of photon energy for 4 different electron energies, for copper and lead respectively (taken from reference [2]).

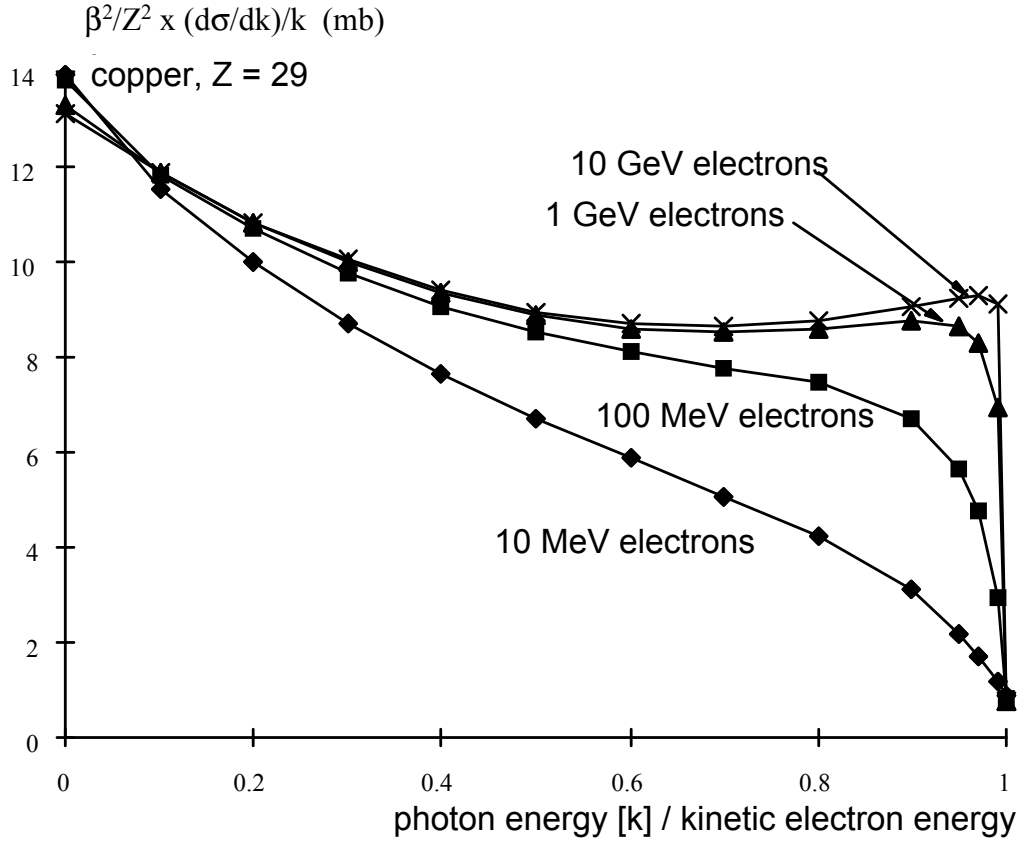

Figure 2.a – Differential bremsstrahlung cross-sections of copper for 4 different electron energies.

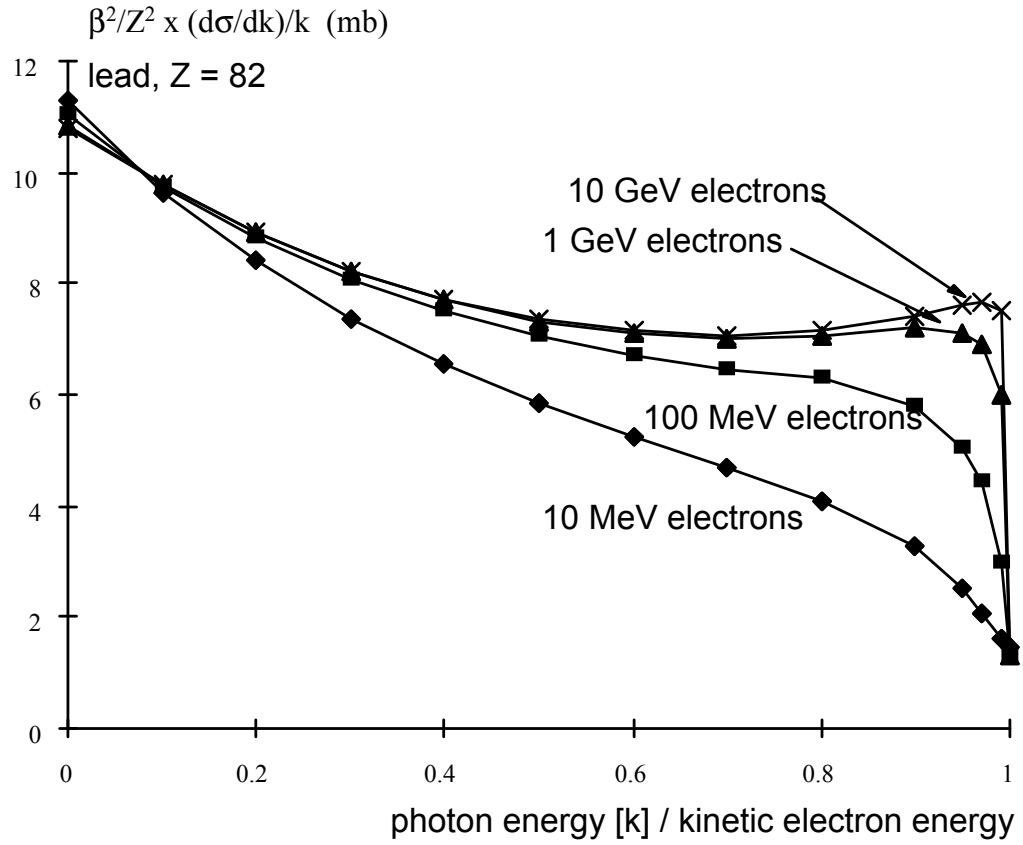

Figure 2.b – Differential bremsstrahlung cross-sections of lead for 4 different electron energies.

2.2.2.3 Continuous slowing-down range

If it is assumed that, when an electron of initial energy E_0 is slowed down in a uniform medium, the rate of energy loss along the track is always equal to the mean energy loss rate, a continuous slowing-down range r_0 can be defined as:

$$r_0 = \int_0^{E_0} \frac{1}{S_{tot}} dE \,, \tag{4}$$

where $S_{tot} = S_{col} + S_{rad}$ is the total stopping power. When S_{tot} is given in MeV·cm^2·g^{-1}, the continuous slowing down range r_0 has the unit g·cm^{-2}. This continuous slowing-down approximation (CSDA) range is the mean distance travelled by the electron, which is larger than the mean depth the electron will penetrate inside the medium. The CSDA ranges for graphite, copper and lead are shown in figure 3 [1,2].

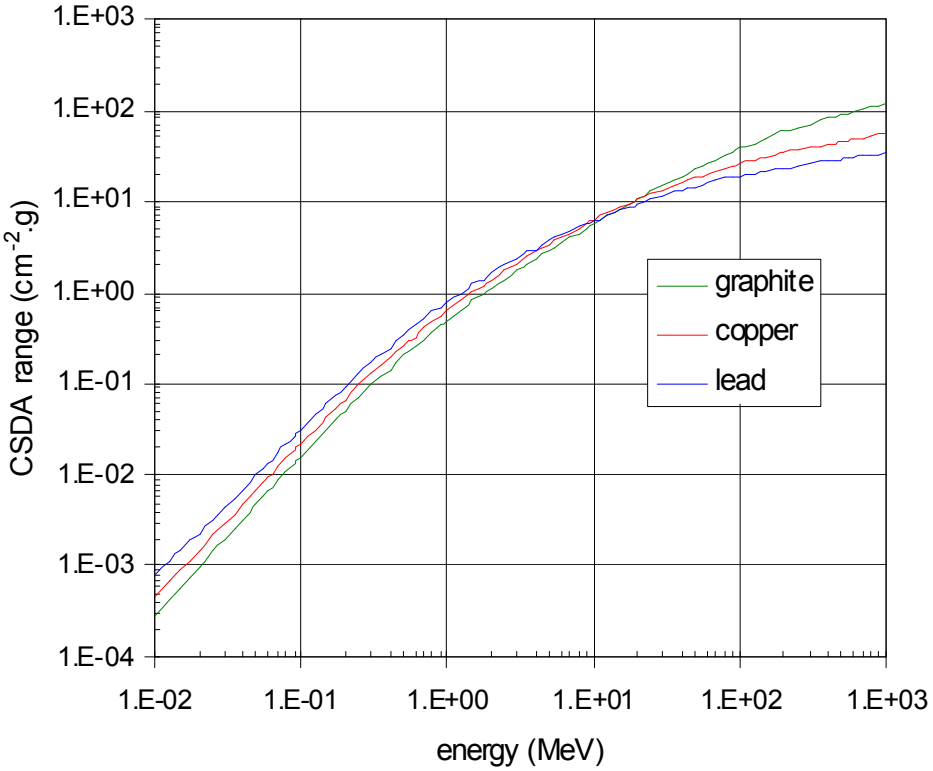

Figure 3 - CSDA ranges for graphite, copper and lead

2.2.2.4 Multiple scattering

An electron passing near a nucleus may undergo elastic scattering. The behaviour of a charged particle interacting with matter is determined by a superposition of successive single scattering processes resulting in multiple scattering.

An approximate formula for the mean scattering angle is given by

$$\left\langle \theta^2 \right\rangle = \left(\frac{E_s}{\beta p} \right)^2 \frac{X}{X_0}, \tag{5}$$

where X is the distance expressed in g/cm^2 , X_0 is the radiation length of the material in question., and E_s = 21.2 MeV.

In expression (5) the radiation length X_0 is used. In the case of pure radiative energy losses, the electron energy decreases exponentially on average with distance and a characteristic relaxation length X_0 called radiation length can be defined.

Since the square angle of the scattering increases linearly with the thickness of an absorber, a mass scattering power S_{sc} can be defined as

$$S_{sc} = \frac{1}{\rho}\frac{d\langle\theta^2\rangle}{dx}. \tag{6}$$

Values for mass scattering powers for carbon, copper and lead are shown in figure 4 [2].

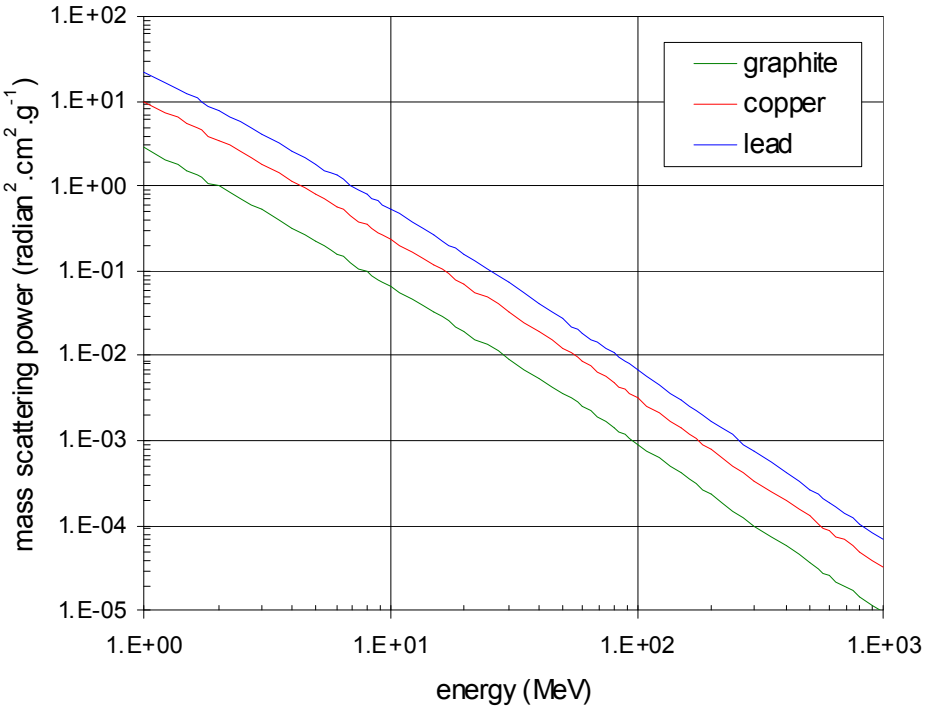

Figure 4 - Mass scattering powers for carbon, copper and lead.

2.3 Interactions of photons with matter

2.3.1 The physical processes

As an example, the photon cross-sections for Pb and C are shown in the figures 5.a and 5.b (taken from reference [3]). The total cross-section is the sum of 4 different contributions, the photoelectric absorption process, the Compton scattering process, the pair production and the coherent (Rayleigh) scattering. As can be seen, the photo-electric effect is the predominant

effect at low energies, pair production is the predominant process at high energies, and Compton scattering is the dominant process in the intermediate energy range.

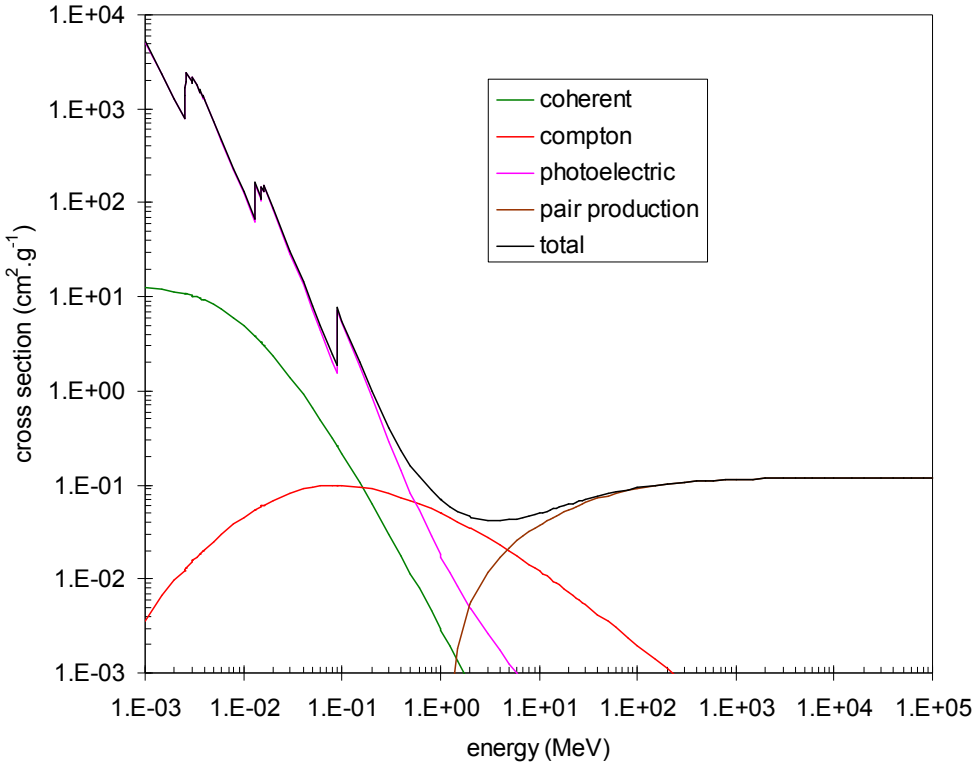

Figure 5.a – Photon cross-sections of lead as a function of photon energy.

At low energies Rayleigh scattering is dominated by the photo-electric effect, at intermediate energies by Compton scattering. Furthermore since Rayleigh scattering does not change the photon energy and essentially scatters at small angles it can be neglected generally in radiological problems and will only play its role in very specific X-ray shielding problems.

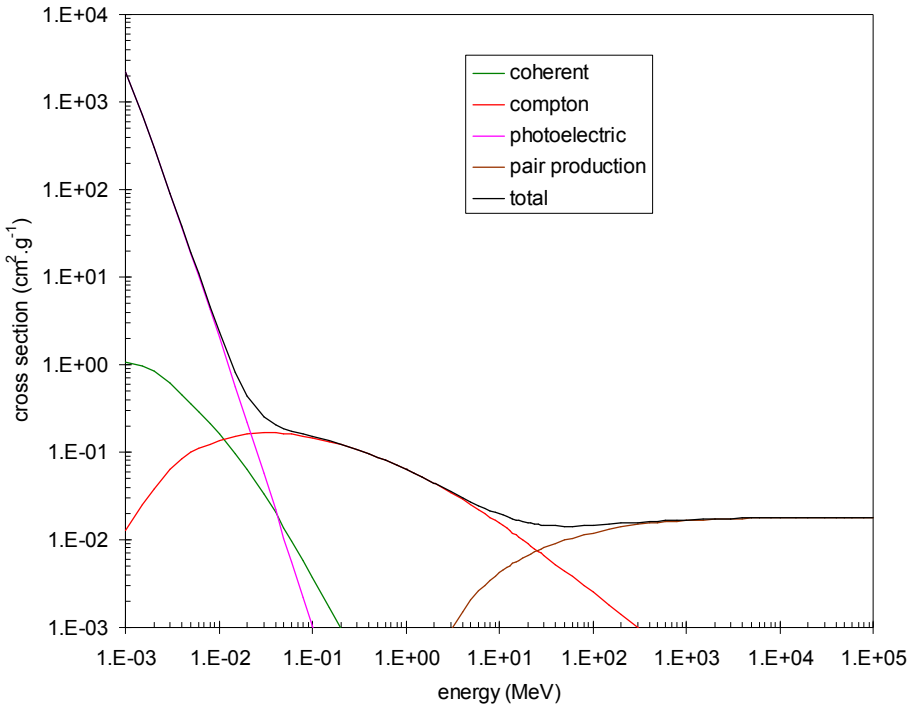

Figure 5.b – Photon cross-sections of graphite as a function of photon energy.

2.3.1.1 Photoelectric effect

In the photoelectric effect an electron is removed from one of the inner shells (K, L, M) of an atom by the absorption of a photon. Since a photon can only remove an electron from a given shell if its energy is higher than the corresponding electron binding energy, the photoelectric cross section exhibits sharp resonances, the absorption edges, corresponding to the binding energies of the different shells. The energy of the ejected photo-electron equals the energy of the photon minus the electron binding energy. In all practical X-ray shielding problems, the photo-electron can be discarded. The vacancy created in the atomic shell will be filled by an electron coming from a higher shell. The difference in binding energy between the two shells is either released as a characteristic fluorescent X-ray, or leads to the ejection of another bound electron (Auger electron), creating a new vacancy, etc.

Therefore, the photoelectric absorption will give rise to the emission of a number of fluorescent X-rays and Auger electrons. The fluorescence yield of a given (sub)shell is the probability that a vacancy in that (sub)shell is filled by a radiative transition. While we can again ignore the emission of the Auger electrons, the fluorescent X-rays have some importance in shielding calculations. Indeed the difference between the binding energies of the K-shell and the L-subshells of the heavier elements, such as Pb which is the main material used for the shielding of X-rays, is sufficiently high to result in fluorescent K X-rays with non-negligible energies. Figure 6 shows the situation for Pb, where the K-shell has a binding energy around 88 keV, compared to roughly 15 keV for the L-shell, and 3 keV for the M-shell.

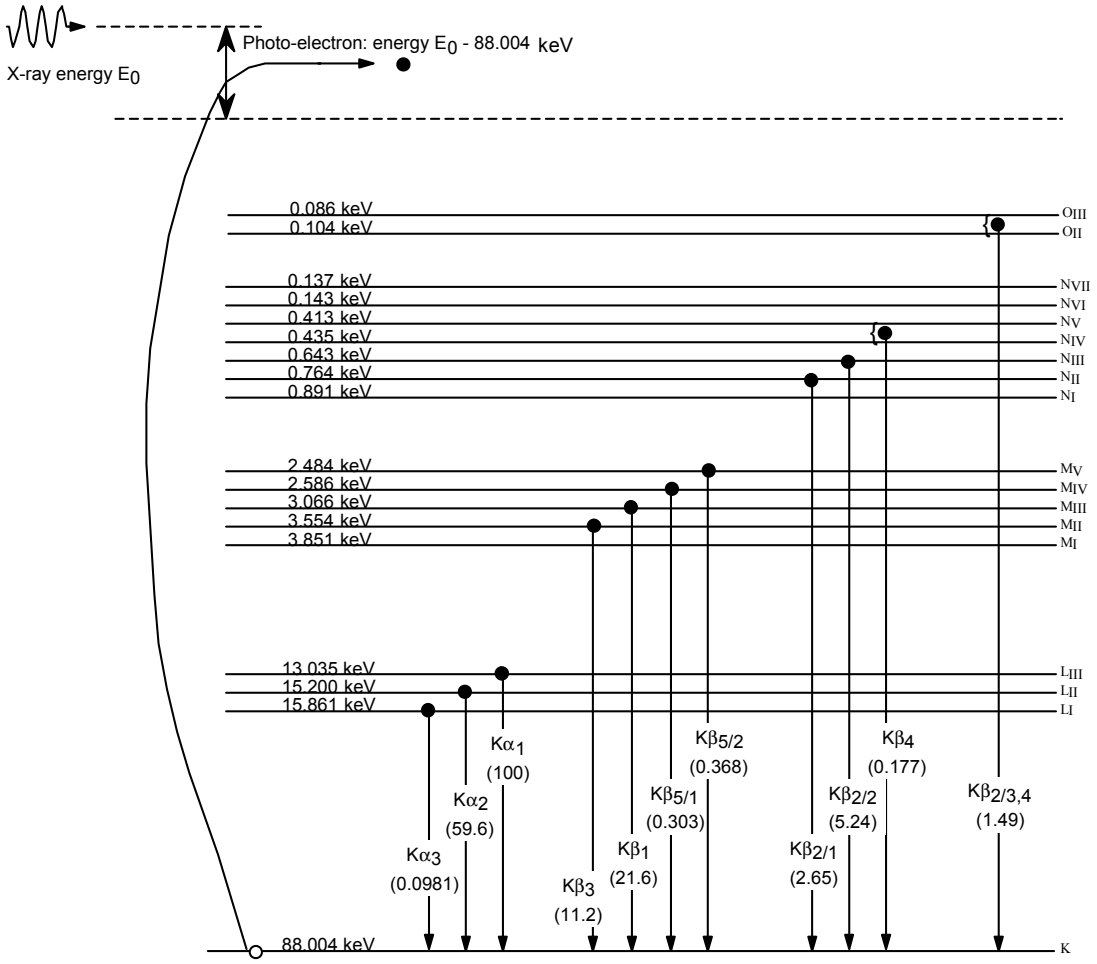

Figure 6 – The photoelectric effect in lead.

2.3.1.2 Compton scattering

If a photon scatters on a loosely bound electron, some of the photon energy is transmitted as kinetic energy to the electron, whereas the scattered photon keeps the remaining energy.

If a photon with energy E_0 is scattered at an angle θ, the energy E_c of the scattered photon will be given by

$$E_c = \frac{E_0}{1 + \frac{E_0}{m_0 c^2}(1 - \cos\theta)}, \tag{7}$$

with m_0c^2 the electron rest energy (511 keV).

The angular differential cross-section for Compton scattering is given by the Klein-Nishina formula [2]:

$$\frac{d\sigma}{d\Omega} = \frac{r_e^2}{2} \frac{1+\cos^2\theta}{\left[1+\left(E_0/m_0c^2\right)(1-\cos\theta)\right]^2} \left\{1+\frac{\left(E_0/m_0c^2\right)^2(1-\cos\theta)^2}{\left(1+\cos^2\theta\right)\left[1+\left(E_0/m_0c^2\right)(1-\cos\theta)\right]}\right\} \quad (8)$$

with r_e the classical electron radius (r_e = 2.817938 $\times$ 10^{-15} m). Figure 8 shows this angular distribution for different initial photon energies.

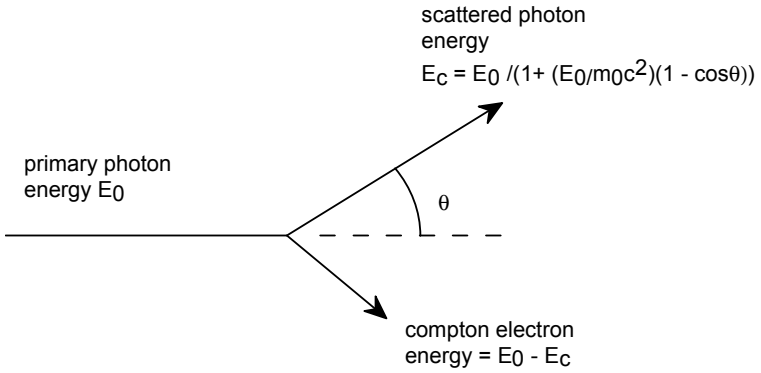

Figure 7 – Compton scattering.

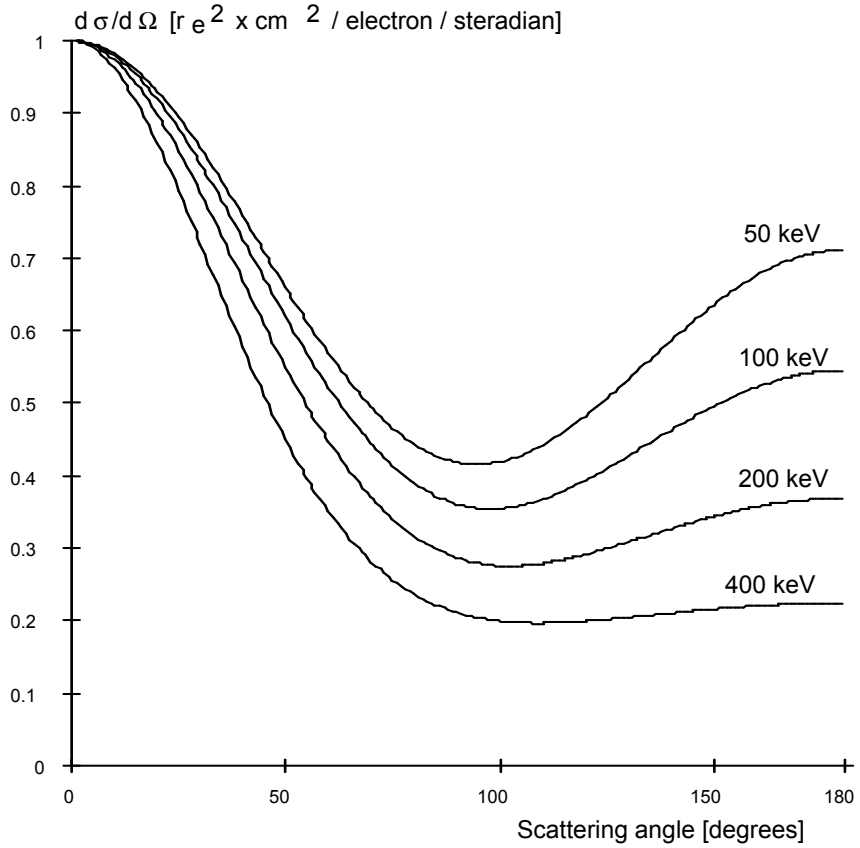

Figure 8 – Differential Compton cross-section for 4 different incident photon energies.

2.3.1.3 Pair production

In this effect, which is the most likely photon interaction at high energies, a photon disappears in the field of a charged particle, and an electron positron pair appears. The cross-section κ_n in the field of a nucleus varies as

$$\kappa_n \sim Z^2.$$

The cross-section κ_e in the field of all the atomic electrons varies as Z times the square of the unit charge, or

$$\kappa_e \sim Z,$$

and is of minor importance except for the lowest-Z-materials.

As an example, the differential energy distribution of the electron/positron pair is shown in figure 9 in case of 1 GeV photons, for a ^{82}Pb nucleus (using the differential Bethe-Heitler Born-approximation cross-section, in the high energy approximation and for partial screening, see reference [5]). The distribution shows perfect symmetry between the electrons and the positrons, and shows a predominance for events where one of the two particles takes up nearly 100 % of the available kinetic energy.

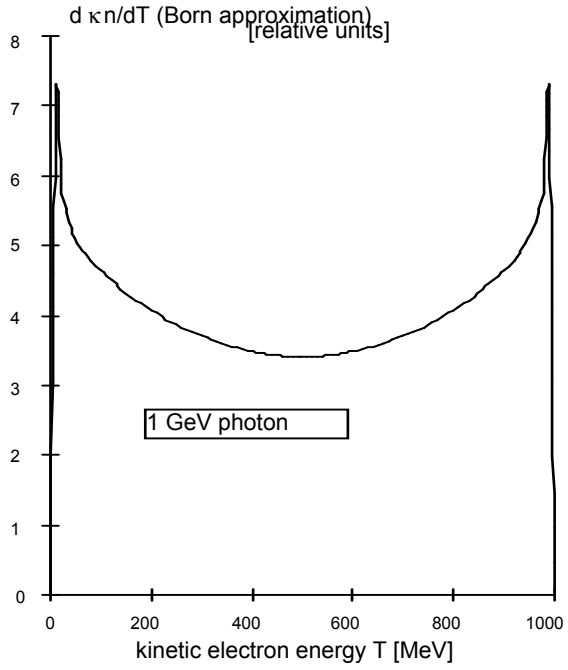

Figure 9 - Differential electron/positron energy distribution for 1 GeV photons, for a ^{82}Pb nucleus

2.3.2 Macroscopic description

2.3.2.1 Attenuation factors

Unlike directly ionising radiation (charged particles), when indirectly ionising radiation like photons passes through material, it interacts with atoms in a more discontinuous way and any

such interaction may result in a substantial loss of energy. It is no longer useful to consider one single particle in terms of its actual energy deposition or its range. Instead one has to observe a sufficiently high number of particles and define global attenuation coefficients.

The *mass attenuation coefficient*, μ/ρ of a given material and for photons of a given energy is given by

$$\frac{\mu}{\rho} = \frac{1}{\rho N}\frac{dN}{dl}, \tag{9}$$

where dN/N is the fraction of the photons that experience interactions in traversing a distance dl in a material of density ρ. Mass attenuation coefficients are expressed in units $cm^2 \cdot g^{-1}$. The *linear attenuation coefficient*, μ, is expressed in units cm^{-1}, and contrary to the mass attenuation coefficient, depends on the density of the medium.

There is a direct relationship between the cross-section σ of photons and their attenuation coefficient. In accordance with the definition of the cross-section, the number of interactions produced by mono-directional photons of fluence Φ per unit path length in a material containing N target centres per unit volume is $\sigma\Phi N$. The number of such interactions in an infinitesimal path length will be $\sigma\Phi N dl$. The product σN is actually the linear attenuation coefficient (in neutron physics this is sometimes called the *macroscopic cross section* Σ).

The number of target centres (atoms) N per unit volume of a material of density ρ and atomic mass A is given by

$$N = \frac{\rho}{A} N_A, \tag{10}$$

where N_A is Avogadro's number. Consequently the mass attenuation coefficient can be expressed as

$$\frac{\mu}{\rho} = \frac{N_A}{A}\sigma \tag{11}$$

Cross sections are often expressed in barns·atom^{-1}, i.e. 10^{-24} $cm^2 \cdot atom^{-1}$. The conversion factor to go from σ [barns·atom^{-1}] to μ/ρ [$cm^2 \cdot g^{-1}$] will then be

$$\frac{\mu}{\rho} = 10^{-24}\frac{N_A}{A}\sigma. \tag{12}$$

2.3.2.2 Build-up factor

Since in the case of the interaction of photons with matter, scattering processes are always significant, the contribution from the scattered photons has to be taken into account. In photon beam attenuation experiments for example, conditions may correspond to a narrow-beam geometry where pure exponential attenuation takes place, or to broad-beam geometry where a *build-up factor* B must be considered, defined as

$$B = \frac{\text{Primary} + \text{scattered} + \text{secondary radiation}}{\text{Primary radiation alone}}. \tag{13}$$

2.4 The electromagnetic cascade

The electromagnetic cascade is a multiplicative phenomena arising from the combined action of bremsstrahlung and pair production processes. The interactions of both electrons and

photons at high energies consist of a kind of chain reaction: photons created by electrons and/or positrons in the field of nuclei materialize again into electron/positron pairs. The latter radiate more photons in turn, and an avalanche process goes on until the energy of the cascade particles is reduced below an energy limit at which no further multiplication is possible.

Electromagnetic cascades are a very efficient way of energy dissipation. The energy of the initial high energy electrons or photons is rapidly distributed among an exponentially growing number of particles of the two kinds. Eventually, energy is deposited in matter via collision processes, but at a rate which is proportional to the number of particles present in the shower.

Several shower theories have been developed, but a detailed description of the problem goes beyond the scope of this introductory course.

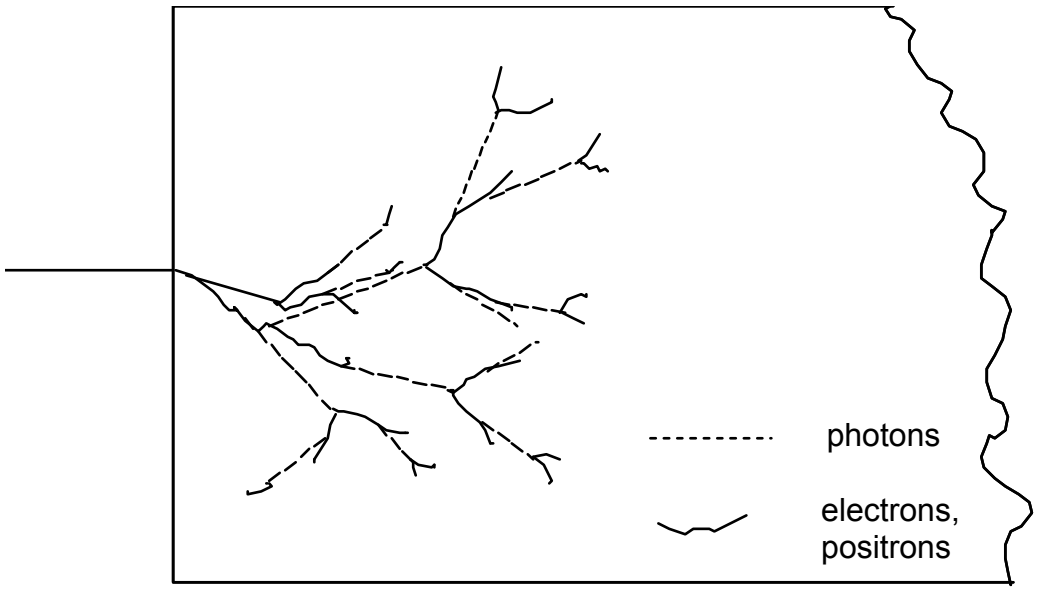

Figure 10 – The electromagnetic cascade

2.5 Interactions of neutrons with matter

2.5.1 Mechanisms of neutron interaction

Neutrons interact with matter by way of three different mechanisms, compound nucleus formation, potential or shape scattering and direct interaction.

2.5.1.1 Compound nucleus formation

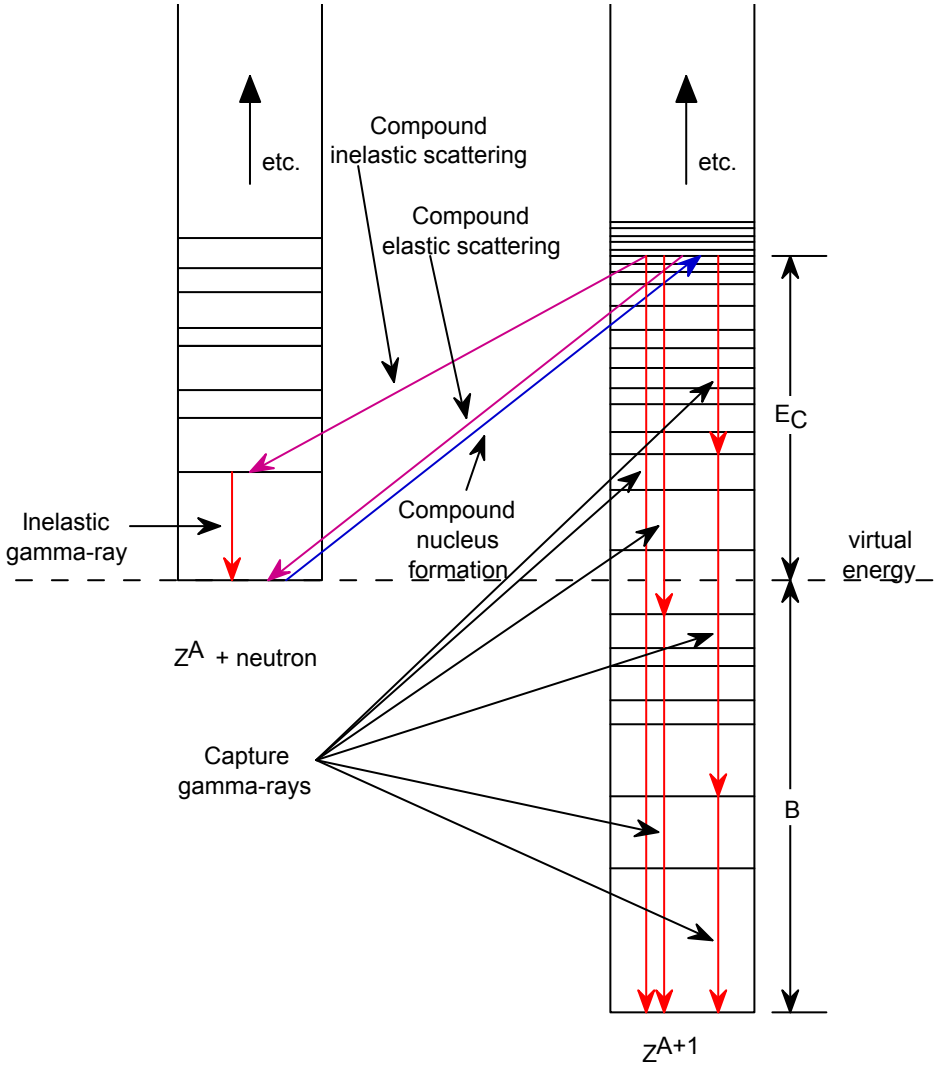

Figure 11 - Principle of compound nucleus formation (from reference [6]).

This process corresponds to the absorption of a neutron by a nucleus Z^A and the subsequent formation of a system known as the *compound nucleus* Z^{A+1}. The center-of-mass total kinetic energy E_C is transferred into internal energy of the compound nucleus. The excitation energy of the compound nucleus is given by the sum of the kinetic energy E_C and the neutron binding energy B.

The de-excitation of the compound nucleus can occur in different ways.

- In *compound elastic scattering* or *resonance elastic scattering* a neutron is emitted and the residual nucleus Z^A is returned to its ground state.
- In *compound inelastic scattering* or *resonance inelastic scattering* a neutron is emitted and the residual nucleus Z^A remains in an excited state.
- The compound nucleus can also decay by emitting one or more gamma rays (*radiative capture*) or by the emission of nucleons or groups of nucleons (*(n, p), (n, α), etc.*).

The probability to form a compound nucleus is high when there is an excited state in Z^{A+1} in the vicinity of the energy E_C + B, and is small if this is not the case. The cross-section will therefore show distinct peaks, called resonances.

2.5.1.2 Potential scattering

While compound elastic scattering is only important in the vicinity of a resonance, potential scattering describes a type of elastic scattering that occurs at any neutron energy. Potential scattering does not involve the formation of a compound nucleus, and can be compared to the scattering of one billiard ball by another. Potential scattering depends on the forces acting on the neutron as it passes through or neat a nucleus. These forces depend on the size and the shape of the nucleus (hence the alternative name *shape elastic scattering*).

2.5.1.3 Direct interaction

Neutrons of relatively high energy can interact with nuclei by direct interaction, where the nucleon interacts directly with one of the nucleons in the nucleus. An example is the (n, p) reaction, where a proton is ejected from the nucleus and the incident neutron is retained in the nucleus. The incident neutron can also raise one of the nucleons in an excited state and leave itself the nucleus with a reduced energy, in which case the reaction is called *direct-interaction inelastic scattering*.

2.5.2 Elastic scattering

The general behaviour of the elastic scattering cross section can be summarized as follows:

- *Light and some magic nuclei*: the cross section is constant from low energy up to about the MeV region, where a number of fairly wide resonances occur. Above the resonance region the cross section becomes smooth and rolling.
- *Heavy nuclei*: the cross section is constant at low energy. In the resonance region the cross section remains constant in between the resonances but varies rapidly in the vicinity of each resonance. Above the resonance region the cross section becomes smooth and rolling.
- *Intermediate nuclei*: the behaviour of the cross section is intermediate between the light and heavy nuclei.

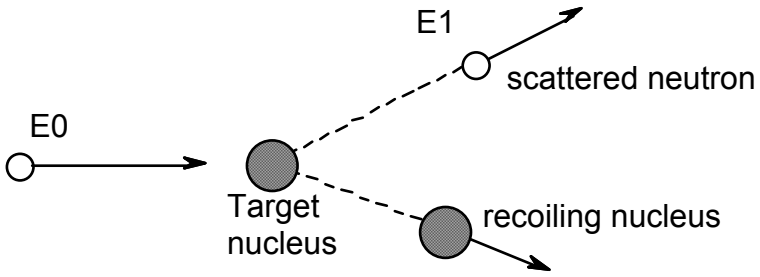

Figure 12 – Elastic neutron scattering

The only energy absorbed is in the form of kinetic energy and the energy transferred to the scattering nucleus depends on the angle of the scattering and the mass of the scattering nucleus. The total kinetic energy is conserved.

For radiation protection purposes, elastic scattering is most important for light nuclei, since they can absorb a large fraction of the neutron's energy. Indeed, if A denotes the atomic mass of the nucleus, it is easy to show from the laws of conservation of energy and momentum that the minimum energy of the scattered neutron, corresponding to neutron backscattering, will be given by [6]:

$$(E_1)_{\min} = \left(\frac{A-1}{A+1}\right)^2 E_0 = \alpha E_0 . \tag{14}$$

The average energy loss per collision (for isotropic scattering in the center-of-mass) will be given by

$$\overline{\Delta E} = \frac{1}{2}(1-\alpha)E_0 , \tag{15}$$

which is maximal for hydrogen (A=1), equal to $E_0/2$. This is the reason why elements rich in water (hydrogen) will be most suited for neutron shielding.

2.5.3 Inelastic scattering

For inelastic scattering to occur, the kinetic energy of the neutron E_l (in the laboratory system) must be greater than the inelastic threshold energy E_t given by:

$$\mathrm{E_t} = \frac{\mathrm{A}}{\mathrm{A}+1}\mathrm{E_1} , \tag{16}$$

where A is the mass of the target nucleus and E_1 its first excited level. Although there are many exceptions, the energy of the first excited state E_1 generally decreases with increasing mass number. For this reason heavier nuclei are important in radiation shielding for slowing down fast neutrons via inelastic scattering.

2.5.4 Absorption reactions

2.5.4.1 Radiative capture

Radiative capture is the process where a neutron is absorbed and the compound nucleus will decay to its ground state by emitting one or more gamma rays. Radiative capture can occur at all energies but is most probable at low energies and in particular at energies leading to long-lived states of the compound nucleus. For neutron energies well below a resonance, the radiative capture cross section behaves as 1/v, where v is the speed of the neutron. For most medium and high Z nuclei the first nuclear level lies well above the virtual energy, and the radiative capture cross section will show a long 1/v tail (see figure 13.a the neutron cross sections for iron). An atypical behaviour is shown in cadmium, where the first resonance in ^{113}Cd occurs at only 0.178 eV above the virtual energy, and the low-energy cross section is therefore quite large with a short 1/v tail (see figure 13.b).

2.5.4.2 Charged-particle reactions

Charged-particle reactions are reactions where the neutron enters the nucleus and knocks out a proton [(n,p) reaction] or a group of nucleons [e.g. (n,α) reaction]. These reactions are normally endothermic, which means that they do not occur below a threshold reaction. For a few light nuclei they are exothermic. Well known examples of exothermic charged-particle reactions are $^{10}B(n, \alpha)^{7}Li$ (see figure 13.c) and $^{3}He(n, p)^{3}H$. The first reaction explains why boron is largely used to absorb slow neutrons, and is also used in BF_3 neutron counters. The operation of ^{3}He proportional neutron counters is based on the second reaction (see § 7.3.1).

2.5.4.3 Fission

With a small number of very heavy elements the nucleus hit by a neutron can become unstable and break up in two or more fragments. This process is called fission.

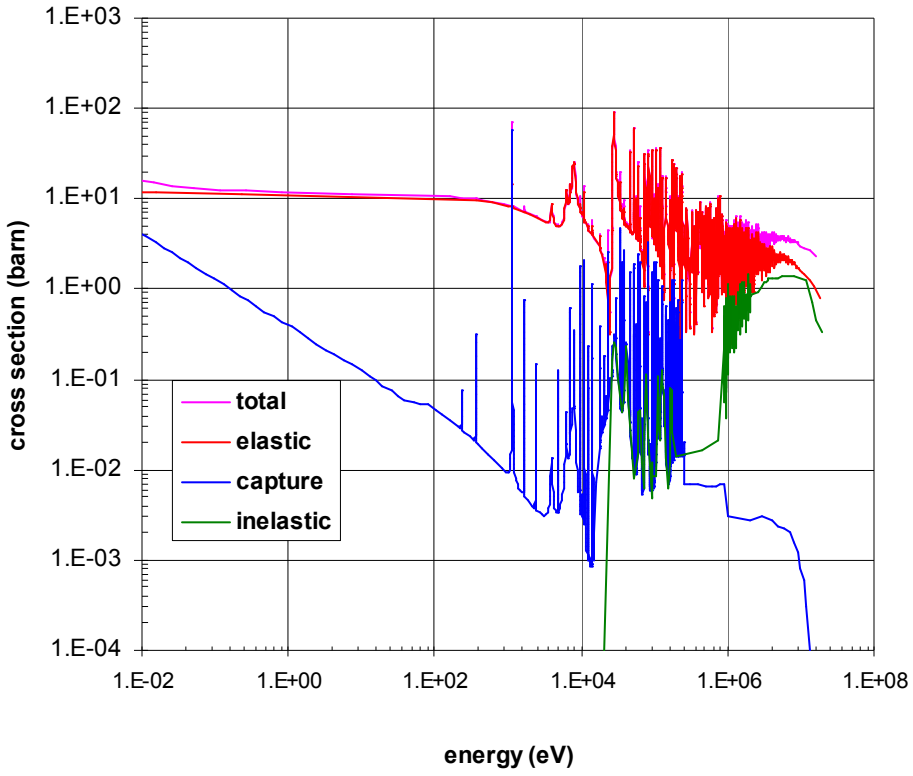

Figure 13.a - Neutron cross-sections of iron (reference [7]).

2.5.5 Examples of neutron cross-sections

In the figures 13.a to 13.c a few typical examples of neutron cross-sections are shown. These figures are copyright (c) 1997 by the Japan Atomic Energy Research Institute (JAERI) and are copied with kind permission of JAERI [7].

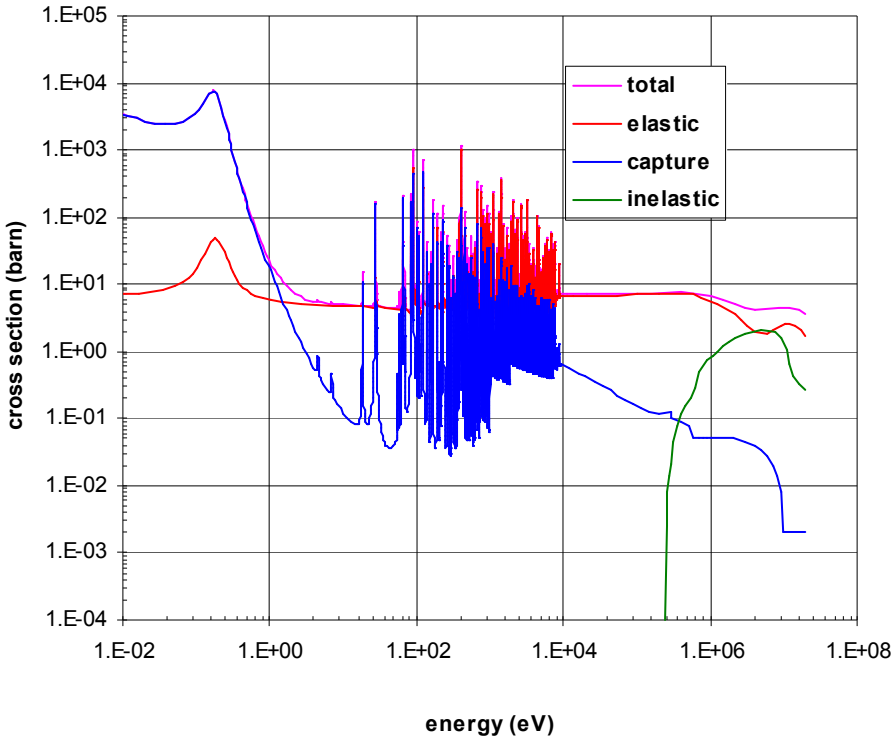

Figure 13.b - Neutron cross-sections of cadmium (reference [7]).

2.5.6 Macroscopic description

Neutron scattering interactions are thus important, particularly at high energies, and they lead to fast neutrons being slowed down to thermal energies facilitating their subsequent absorption by means of neutron-capture reactions. Neutron cross-sections for these reactions are very different from and more complicated than photon-cross sections. Neutron cross-sections may for example be very dependent on the energy of the incident neutron. They can also vary very erratically for different elements.

Although the attenuation of neutrons as a result of scattering and capture reactions is in broad terms similar to the attenuation of photons, the shielding problem is far more complex. If one considers a flux of fast neutrons passing through a shielding medium they are in the first instance slowed down by elastic and inelastic scattering. It is only, however, when the neutrons have been reduced to low energies that they will be captured or absorbed and may then be regarded as having been removed from the incident neutron flux. In this connection the presence of hydrogen in the shield is of great importance because when a neutron collides with a nucleus of a hydrogen atom it usually results in the neutron losing a large amount of energy.

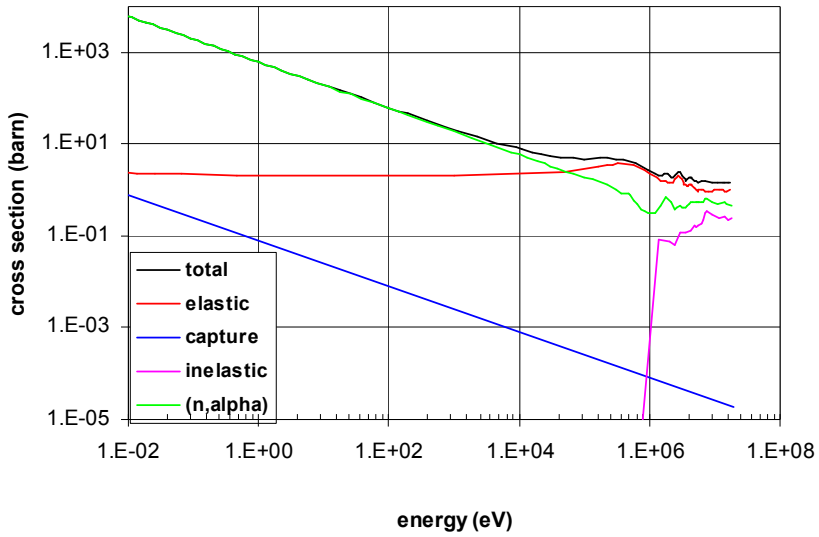

Figure 13.c - Neutron cross sections of boron (reference [7]).

Inelastic scattering from heavy nuclei can also be considered as an effective removal process of neutrons, on condition that a minimum amount of uniformly distributed hydrogen atoms is present in the shield, to further reduce the energy by elastic scattering, finally resulting in the capture of the neutron. The concept of an effective neutron-removal cross-section was introduced by Albert and Welton, with the idea to describe neutron attenuation by means of a simple exponential law. After a shield wall of thickness d, the neutron flux I will be given according to the initial flux I_0 by

$$I = I_0 e^{-\Sigma_R d}, \qquad (17)$$

where Σ_R is the effective macroscopic removal cross-section for the material, in units cm^{-1}. Chapman and Storrs have determined experimentally the removal cross-section per unit mass (Σ_R/ρ) for fission or fast neutrons of 8 MeV, and for atomic weights between 8 and 240 they found that Σ_R/ρ ($cm^2 \cdot g^{-1}$) was approximately equal to $0.21A^{-0.58}$ [8] (see also § 6.3).

2.6 Interactions of high energy protons with matter

The interaction of high energy charged protons is a complex process, including:

- Ionisation energy loss and multiple Coulomb scattering
- Elastic and inelastic proton – nucleus scattering
- Electromagnetic cascades initiated by photons from the decay of unstable particles

These different physical processes are described in the following paragraphs, with the emphasis of those aspects that are important for shielding.

2.6.1 Ionisation energy loss and multiple Coulomb scattering

Protons interact with bound electrons in the atoms and molecules of the target material by inelastic collisions resulting in the ionisation or excitation of the atoms and molecules. The energy loss associated with these inelastic collisions is called stopping power, expressed in units of $MeV.cm^{-1}$ or $MeV.g^{-1}.cm^2$.

For incident energies > 1 MeV, the proton stopping power can be written as [9]:

$$-\frac{1}{\rho}\frac{dE}{dx} = \frac{2\pi N_A z^2 e^4}{mc^2\beta^2}\frac{Z}{A}\left[\ln\frac{2mc^2\beta^2 W}{I^2(1-\beta^2)} - 2\beta^2 - 2\frac{C}{Z} - \Delta + \pi\alpha z\beta\right], \quad (18)$$

where W is given by:

$$W = \frac{2mc^2\beta^2}{1-\beta^2}\left[1 + \frac{2m}{M(1-\beta^2)^{0.5}} + \left(\frac{m}{M}\right)^2\right]^{-1}. \quad (19)$$

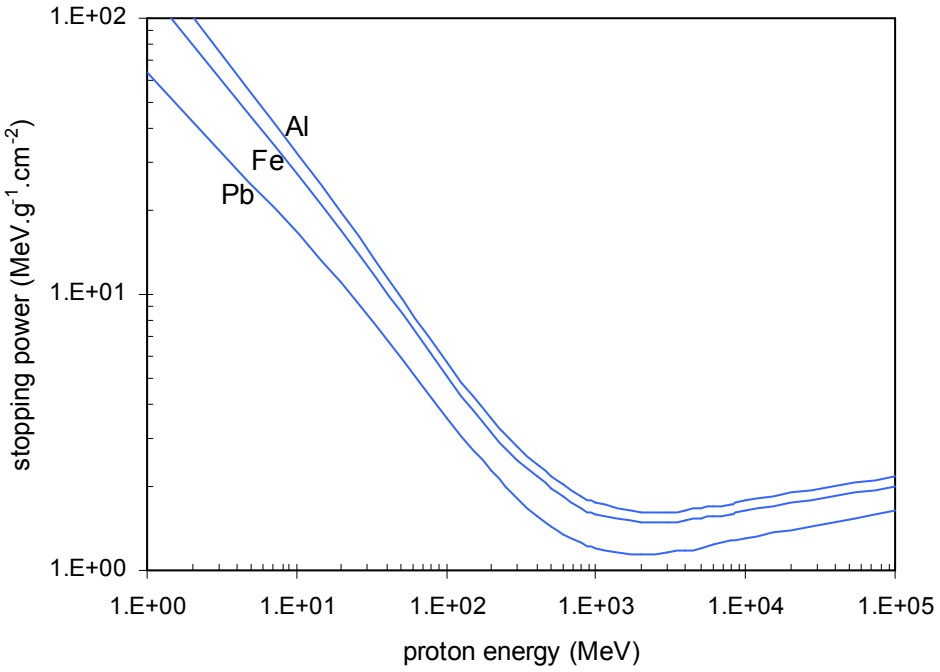

Figure 14 - The stopping power of protons in different materials as a function of energy.

In expressions (19) and (20) m and M are respectively the electron and the proton rest mass, β is the ratio of the proton laboratory speed to the speed of light, α is the fine structure constant, D is the polarisation effect correction, C is the shell correction effect, N_A is Avogadros number, I is the adjusted ionisation potential of the target material, ρ is the target material density and A and Z are respectively the atomic weight and the atomic number of the target material.

The stopping power as a function of energy is plotted for three different materials in figure 14 (from reference [9]). As shown in this figure, the stopping power initially decreases with increasing energy, passes through a broad minimum and then slowly increases again with increasing energy. Particles in the energy range where the minimum stopping power occurs (around about 2 GeV) are commonly referred to as *minimum ionising particles*.

2.6.2 Inelastic proton – nucleus scattering

When a high energy proton strikes a nucleus it has a high change of making an inelastic scattering where a range of secondary particles are emitted in a so-called spallation reaction. After the initial intra-nuclear cascade, where the incident proton interacts directly with nucleons, the residual nucleus is left in an excited state from which it decays via the emission of lower-energy particles in the so-called evaporation process. The inelastic proton-nucleus scattering is illustrated in figure 15. If the energy of the secondary particles emitted from the intra-nulcear cascade is high enough, they can induce further intra-nuclear cascades, leading to the development of a hadron cascade.

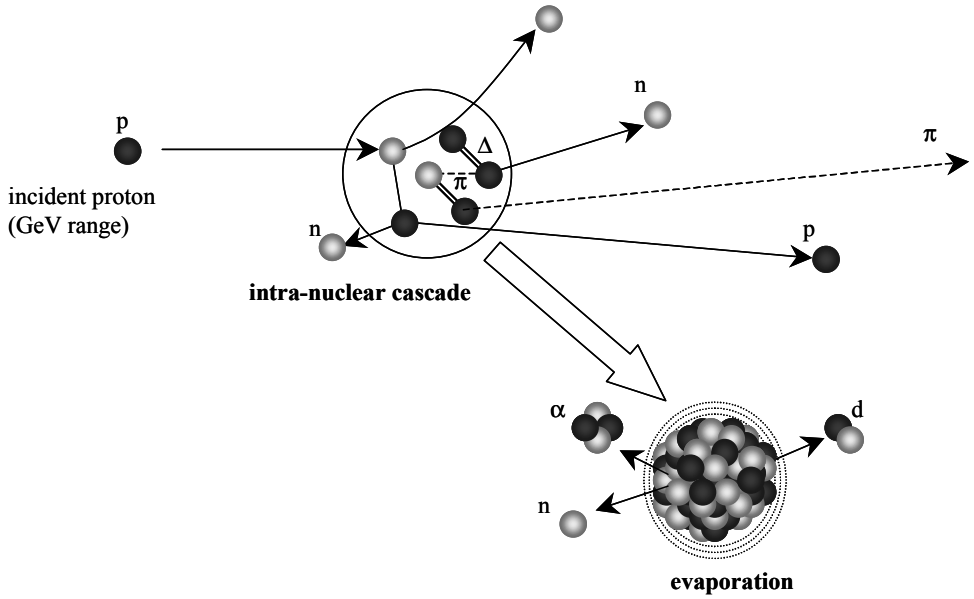

Figure 15 – Inelastic proton-nucleus scattering.

2.6.2.1 Inter-nuclear cascades

At high incident energies (higher than about 120 MeV), the incident proton reacts directly with individual nucleons inside the nucleus (intra-nuclear cascade). The secondary hadrons ejected from the nucleus can have enough energy to initiate further intra-nuclear cascades: the development of so-called inter-nuclear cascades becomes important. The multiplicity of the emitted secondary particles as well as their energy and angular distributions are complicated and depend on the individual interaction cross sections. The detailed description of these inter-nuclear cascades can therefore only be done using complex Monte-Carlo codes. Paragraph 4.2 describes a simple macroscopic model, providing a powerful tool for shielding calculations for high energy particle accelerators.

Figure 16 shows the proton non-elastic cross-section for a selection of materials, for energies up to 1000 GeV [10, 2]. One sees that the cross-sections vary little for proton energies above 1 GeV.

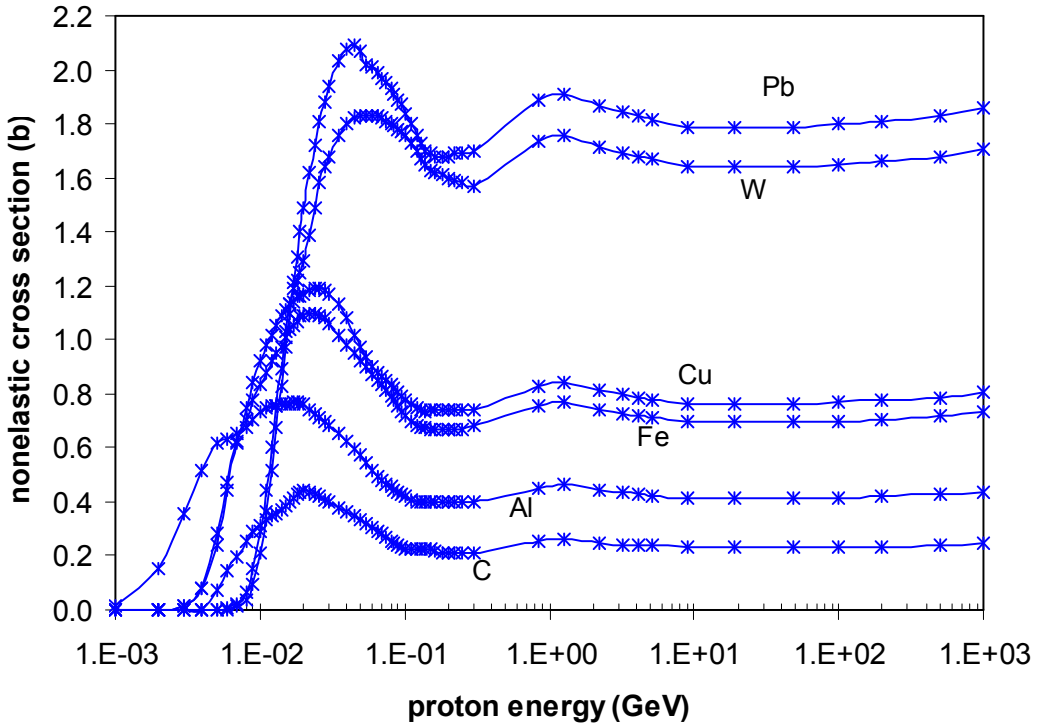

Figure 16 - Inelastic proton cross-sections for protons incident on different materials. Cross-sections below 300 MeV proton energies are taken from reference [10], cross-sections above 300 MeV are taken from reference [2] and various references given herein.

For high energies the dependence of the inelastic cross-section σ_{inel} on the atomic mass of the target nucleus A can be approximated by [11]

$$\sigma_{inel} = \sigma_0 \times A^{0.7} \tag{20}$$

where σ_0 is the corresponding proton-nucleon total cross-section. Table 3 gives the nuclear inelastic cross sections for a number of materials [12]. For proton energies above about 120 MeV the inelastic cross-section σ_{inel} can be approximated by [11]:

$$\sigma_{inel} = 42 \times A^{0.7} \times 10^{-27} \quad cm^2. \tag{21}$$

Material	A	Nuclear inelastic cross-section (barn}
Graphite	12.01	0.231
Aluminium	26.98	0.421
Iron	55.85	0.703
Copper	63.55	0.782
Tungsten	183.85	1.65
Lead	207.19	1.77

Table 3 – Nuclear inelastic cross sections for various materials [12].

2.6.2.2 Nuclear evaporation

At the end of the intra-nuclear cascade, where the residual nucleus is left in an excited state. It decays to its ground state via the emission of lower-energy particles. The emission of these particles is best described by an evaporation process. The energy distribution of the evaporation neutrons is described by the equation [13]:

$$n(E)dE \propto E\, e^{-E/T}, \tag{22}$$

where T is the so-called nuclear temperature.

Similar equations can be used for the energy distribution of emitted protons, deuterons and heavier particles. The emission is isotropic. The energy of evaporation neutrons extends to typically 8 MeV.

At lower incident proton energies, where the intra-nuclear interaction mechanism ceases, the interaction of a proton with a nucleus goes via the compound nucleus formation. For increasing energy of the incident particle a large number of (overlapping) excited states in the compound nucleus become available and the decay of the compound nucleus is again best described by an evaporation process

2.6.3 Comparison between ionisation energy loss and inelastic nuclear scattering

Figure 17 shows the proton range as a function of initial proton energy for various materials. These ranges were calculated using the ionisation and excitation stopping powers [9]. Inelastic nuclear interactions are not taken into account in the definition of range. The probability that a proton will undergo an inelastic nuclear interaction before it reaches the end of its range is also shown in figure 17. One sees that for energies above 1 GeV this probability is 100 %. This means that above this energy all protons hitting a (sufficiently thick) target will undergo a spallation reaction.

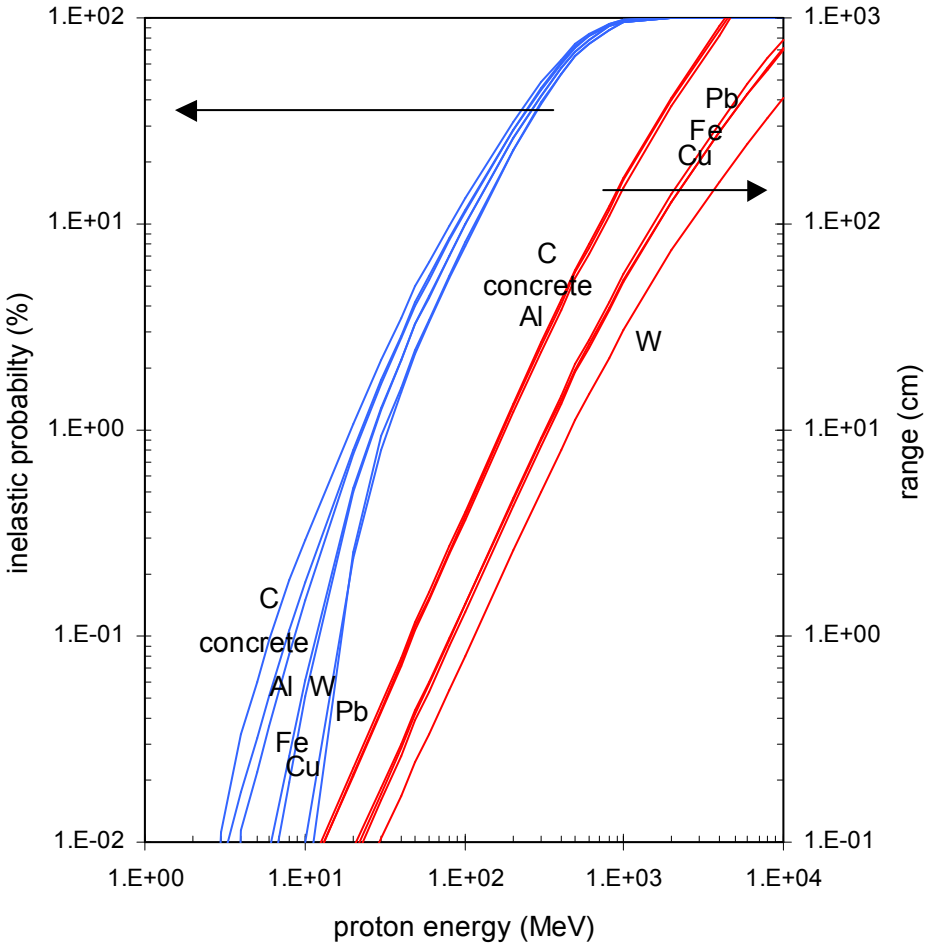

Figure 17 – Range of protons (right hand scale) and probability of inelastic nuclear scattering within this range (left hand scale) (from reference [9]).

2.6.4 Elastic proton – nucleus scattering

Elastic nuclear collisions contribute very little to the energy loss above 1 MeV. Compared to the energy loss due to ionisation and excitation their contribution is less than 0.1 % at 1 MeV, and even smaller at higher energies.

2.6.5 Bremsstrahlung

Proton bremsstrahlung is completely negligible at all energies considered here. For 10 GeV protons bremsstrahlung only contributes for a fraction of a percent to the energy loss, and this contribution drops rapidly at lower energies.

3. Introduction to radiation protection

3.1 Definitions

3.1.1 Activity

Activity is the main quantity that is used for the assessment of radioactive sources. Radioactivity describes the instability of the atomic nuclei of certain atoms whereby the nucleus experiences a spontaneous nuclear transition or transformation with the resulting emission of radiation. The decay process of a radioactive source can be described by the well-known equation

$$\frac{dN}{dt} = -\lambda N(t) \tag{23}$$

which shows that the number of decays per time unit is proportional to the number of available radioactive nuclei at that time. The proportionality factor λ is called the *decay constant* and has the unit s^{-1}.

Integration of the expression (23) leads to the following expression for the number of nuclei

$$N(t) = N(0)e^{-\lambda t}. \tag{24}$$

The *half-life* $T_{1/2}$ of a radioactive isotope is the time it takes for the number of radioactive nuclei to fall to half its initial number. Its relationship with the decay constant λ is given by

$$T_{1/2} = \frac{\ln 2}{\lambda}. \tag{25}$$

The unit of activity is the becquerel (Bq), where 1 Bq = 1 s^{-1}. The old unit for activity is the curie (Ci), with 1 Ci = 3.7×10^{10} Bq.

Some common types of radioactivity are listed in table 4.

Type	Symbol	Particles emitted	Example
Alpha	α	Helium nucleus	$^{226}Ra \rightarrow {}^{222}Ra + \alpha$
Beta minus	β^-	Electron and antineutrino	$^{24}Na \rightarrow {}^{24}Mg + e^- + \bar{\nu}$
Beta plus	β^+	Positron and neutrino	$^{22}Na \rightarrow {}^{22}Ne + e^+ + \nu$
Electron capture	EC	Neutrino	$^{7}Be + e^+ \rightarrow {}^{7}Li + \nu$
Isomeric transition	IT	Gamma rays and/or conversion electrons	$^{137m}Ba \rightarrow {}^{137}Ba + \gamma$ or conversion electrons

Table 4 – Types of radioactive decay.

These notions of radioactivity will be used when discussing induced activity (see chapter 5).

3.1.2 Radiation fields

In order to study or evaluate radiation effects, it is important to specify the parameters of the radiation field at the point of interest. The relevant quantities, used for the description of radiation in free space or in matter, deal either with the particle number or the energy of the considered radiation. As to the particles, we may be interested in their number as well as in their distribution with respect to energy or direction.

The *particle fluence* ϕ is the quotient of dN by da

$$\Phi = \frac{dN}{da} \tag{26}$$

where dN is the number of particles incident on a sphere of a cross-sectional area da. The common unit of particle fluence is particles·cm^{-2}.

The *fluence rate* φ is the quotient of $d\Phi$ by dt, where $d\Phi$ is the increment of the particle fluence in the time interval dt

$$\varphi = \frac{d\Phi}{dt} = \frac{d^2 N}{dadt}. \tag{27}$$

The unit of the fluence rate is particles·cm^{-2}·s^{-1}.

3.1.3 Kerma and Absorbed dose

The *kerma* is the quotient of dE by dm, where dE is the sum of the initial kinetic energies of all the charged ionising particles liberated by uncharged ionising particles in a volume element of mass dm, thus:

$$\mathrm{K} = \frac{\mathrm{dE}}{\mathrm{dm}}. \tag{28}$$

The unit for kerma is J·kg^{-1}, for which the special name gray (Gy) has been adopted.

The *absorbed dose* D is the *mean energy imparted* by ionising radiation per unit mass at a point.

$$D = \frac{d\bar{\varepsilon}}{dm} \tag{29}$$

The unit for absorbed dose is gray. The old unit for absorbed dose was rad, where 1 Gy = 100 rad.

The *absorbed dose rate* $\dot{\mathrm{D}}$ is defined as

$$\dot{\mathrm{D}} = \frac{dD}{dt}, \tag{30}$$

and its units are Gy·s^{-1}.

In the definition of absorbed dose, the energy imparted by the ionising radiation to matter in a volume is given by

$$\varepsilon = R_{in} - R_{out} + \Sigma Q, \tag{31}$$

where R_{in} is the radiant energy incident on the volume, i.e. the sum of all the energies (excluding rest energies) of all those charged and uncharged ionising particles that enter the volume, R_{out} is the radiant energy emerging from the volume and ΣQ is the sum of all changes of the rest mass energy of nuclei and elementary particles in any interactions that occur in the volume. The *mean energy imparted* is the expectation value of ε.

3.1.4 Biological effects: Effective dose E and Ambient Dose Equivalent H*(d)

Biological tissues undergo alterations when exposed to ionising radiation. Some of these effects occur more or less immediately following the exposure, while others occur only a long time after the exposure. The first effects are called deterministic, the second ones are called stochastic effects.

The biological effect not only depends on the dose but also on the type of radiation. The biological effect also depends on the relative exposure of different tissues and organs.

3.1.4.1 ICRP: Protection quantities

In 1991 the International Commission on Radiological Protection (ICRP) has published new recommendations (ICRP Publication 60 [14]). In this publication the protection quantities used in radiological protection for external radiation are defined, namely the *effective dose E* and the *tissue or organ equivalent doses* H_T.

The **organ dose D_T** is the mean absorbed dose in a specified tissue or organ of the human body, T, given by:

$$D_T = \frac{1}{m_T}\int_{m_T} D dm\,, \tag{32}$$

where m_T is the mass of tissue or organ and D is the absorbed dose in the mass element dm. The unit of organ dose is the gray.

The **tissue or organ equivalent dose $H_{T,R}$** is the absorbed dose in an organ or tissue multiplied by the relevant radiation weighting factor:

$$H_{T,R} = w_R \cdot D_{T,R}\,, \tag{33}$$

where $D_{T,R}$ is the absorbed dose averaged over the tissue or organ T due to radiation R and w_R is the radiation weighting factor for radiation R. Values for the radiation weighting factors are given in table 5.

When the radiation is composed of radiations with different values of w_R, the absorbed dose is subdivised into blocks, each multiplied by its own value of w_R and summed to determine the total equivalent dose, i.e.

$$H_T = \sum_R w_R \cdot D_{T,R}\,. \tag{34}$$

The unit of equivalent dose is $J.kg^{-1}$ and its special name is **sievert (Sv)**.

The **effective dose E** is the sum of the equivalent doses in tissues or organs, each multiplied by the appropriate tissue weighting factor:

$$E = \sum_T w_T \cdot H_T \ , \tag{35}$$

where H_T is the equivalent dose in tissue or organ T and w_T is the tissue weighting factor for tissue T (see table 6).

Type and energy range of radiation	Radiation weighting factor w_R
Photons, all energies	1
Electrons and muons, all energies	1
Neutrons	
< 10 keV	10
10 - 100 keV	5
> 100 keV to 2 MeV	10
>2 - 20 MeV	20
> 20 MeV	10
	5
Protons, energy > 2 MeV	5
Alpha particles, fission fragments, heavy nuclei	20

Table 5 – Values for radiation weighting factors (ICRP publication 60 [14]).

The effective dose will depend on the irradiation geometry. The ICRP has defined a number of typical irradiation geometries of an anthropomorphic phantom for which calculations are carried out assuming whole-body irradiation by broad unidirectional or plane-parallel beams. We mention the following two geometries, the most applicable for accelerator environments:

Antero-posterior geometry (AP) – The irradiation geometry in which the ionising radiation is incident on the front of the body in a direction orthogonal to the long axis of the body.

Rotational geometry (ROT) – The geometry in which the body is irradiated by a parallel beam of ionising radiation, from a direction orthogonal to the long axis of the body, which rotates at a uniform rate around the long axis. Alternatively, this geometry may be defined by rotating the body at a uniform rate about its long axis, while irradiating the body by a broad beam of ionising radiation from a stationary source located on an axis at right angles to the long axis of the body.

3.1.4.2 ICRU: Operational quantities

The protection quantities defined by the ICRP are amenable to calculation if the conditions of irradiation are known, however these quantities are not directly measurable. The International Commission on Radiation Units and Measurements (ICRU) has defined a set of operational quantities for area and individual monitoring, designed to provide an estimate of the protection quantities of the ICRP. For this purpose they have defined the *dose equivalent H* and the *ambient dose equivalent H*(d) (see ICRU Report 51 [15])*.

Tissue or organ	Tissue weighting factor w_T
Gonads	0.20
Bone marrow (red)	0.12
Colon	0.12
Lung	0.12
Stomach	0.12
Bladder	0.05
Breast	0.05
Liver	0.05
Oesophagus	0.05
Thyroid	0.05
Skin	0.01
Bone surface	0.01
Remainder	0.05

Table 6 – Values for tissue weighting factors (ICRP publication 60 [14]).

The **dose equivalent H** is the product of Q and D in a point in tissue, where D is the absorbed dose and Q is the quality factor at that point, thus

$$H = Q \cdot D \,. \tag{36}$$

The unit of dose equivalent is sievert.

The quality factor Q is a function of the *unrestricted linear energy transfer L in water*.

Table 7 gives the relationship between the quality factor Q and linear energy transfer L in water.

Unrestricted linear energy transfer L ($keV \cdot \mu m^{-1}$)	Quality factor Q
$L < 10$	1
$10 \leq L \leq 100$	0.32 L - 2.2
$L > 100$	$300 / L^{1/2}$

Table 7 – Definition of quality factor Q.

The **ambient dose equivalent H*(d)** at a point in a radiation field is the dose equivalent that would be produced by the corresponding expanded and aligned field in the ICRU sphere (30 cm diameter tissue-equivalent sphere: density 1 $g.cm^{-3}$, composition by mass: 76.2 % O, 11.1 % C, 10.1 % H and 2.6 % N) at a depth d mm on the radius opposing the direction of the aligned field (see figure 18). The recommended value for d is 10 mm for penetrating radiation and 0.07

mm for low-penetrating radiation. The unit of ambient dose equivalent is sievert. Ambient dose equivalent rates are expressed in $Sv \cdot s^{-1}$.

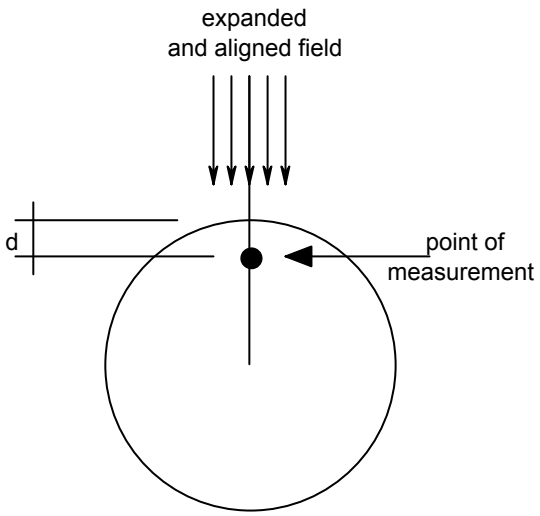

Figure 18 – Definition of H(d).*

An expanded and aligned radiation field is a hypothetical unidirectional field with the same energy distribution throughout the volume of interest as the actual field.

3.1.4.3 Comparison between protection and operational quantities

This section compares the protection quantity, effective dose E, with the operational quantity, ambient dose equivalent H*(10), and describes the performance of the latter as predictor of the protection quantity. The data presented in this section are taken from ICRU Report 57 [16].

Both the protection quantities and operational quantities can be related to the basic physical quantities fluence Φ and air kerma free-in-air K_a. Figures 19.a and 19.b compare both quantities for photons. We have chosen the AP and ROT geometries for the effective dose E because these are probably the most useful geometries to describe radiation exposures around accelerator tunnels. As can be seen H*(10) always overestimates E for photons with energies up to 10 MeV. For photon energies between 60 keV and 10 MeV the value of the ratio E/H*(10) ranges from 0.75 to 0.92 for the AP geometry and from the 0.48 to 0.85 for the ROT geometry. Hence, the ambient dose equivalent provides an overestimate of the effective dose exceeding 15 % over a wide range of photon energies. At low photon energies the extent of overestimation becomes significant, but at these energies the dose is essentially due to exposure of the skin and the eye lens and both quantities, E and H*(10), are of limited practical application.

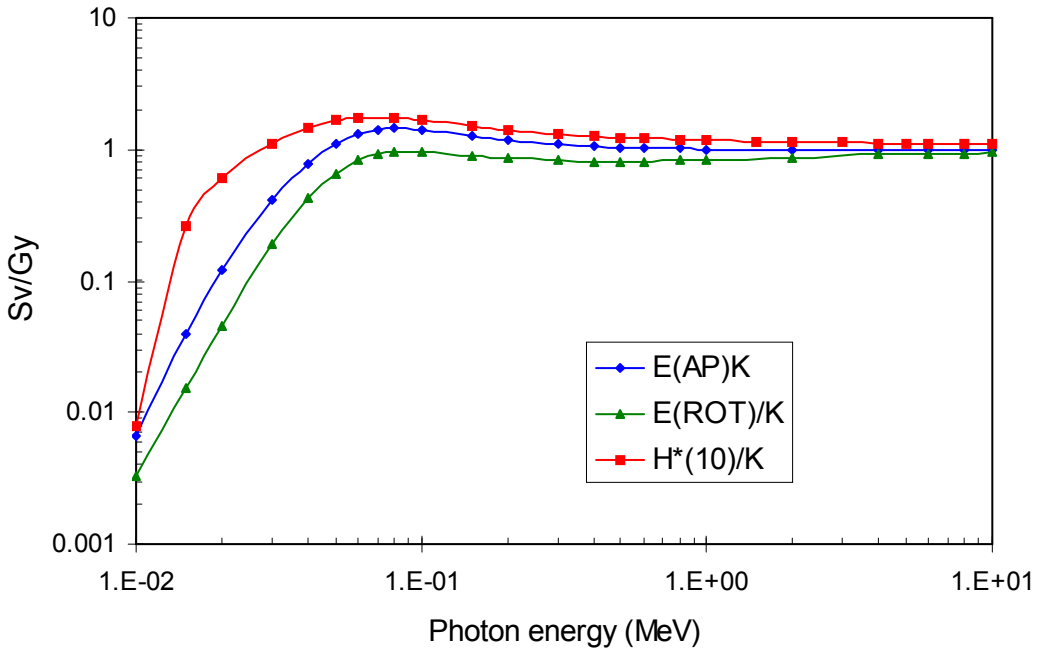

Figure 19.a – Ratio of effective dose E to air kerma free-in-air for two irradiation geometries (AP and ROT) and ratio of ambient dose equivalent H(10) to air kerma free-to-air as a function of photon energy.*

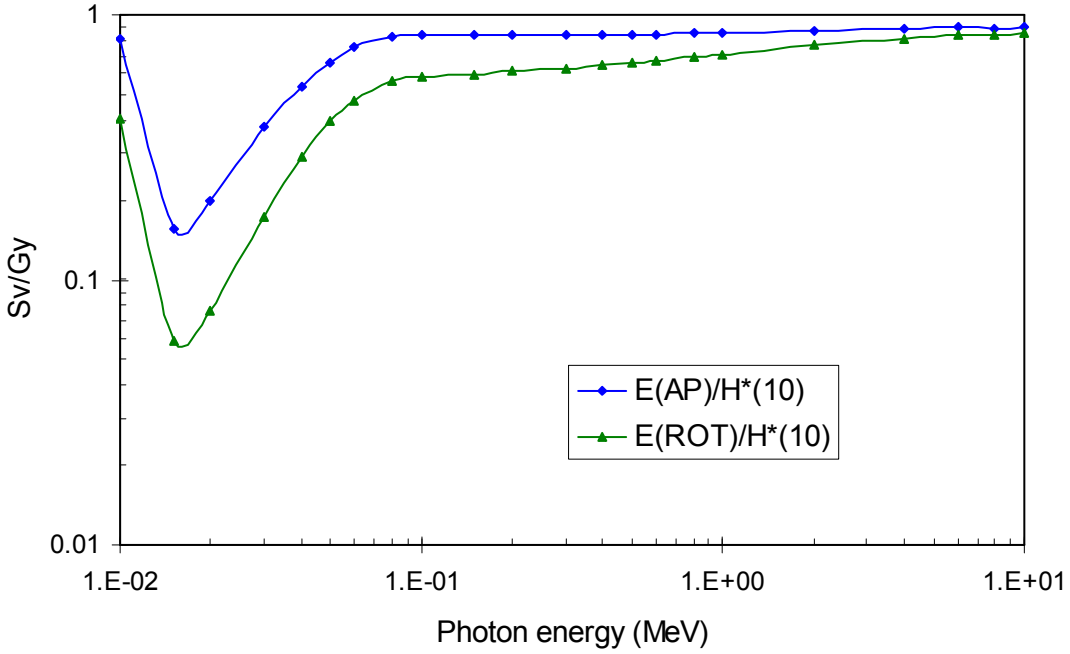

Figure 19.b – Ratio of effective dose E for two irradiation geometries (AP and ROT) to ambient dose equivalent H(10) as a function of photon energy.*

Figures 20.a and 20.b compare the effective dose E to the ambient dose equivalent H*(10) for neutrons. In the AP geometry the ambient dose equivalent underestimates the effective dose E in energy regions from about 1 eV to 40 keV, from about 3 MeV to 13 MeV and above 40 MeV. In practice, irradiation by monoenergetic neutrons rarely occurs. In the case of neutron irradiation over a wide range of energies, the ambient dose equivalent is usually a conservative (safe) estimate for the effective dose. However, for radiation fields around high-energy accelerators H*(10) may not be a prudent measure for E.

In the ROT geometry the ambient dose equivalent H*(10) is a better estimation for the effective dose E, it only slightly underestimates the effective dose for energies between 0.5 keV and 50 keV, and it again underestimates the effective dose for energies above 50 MeV.

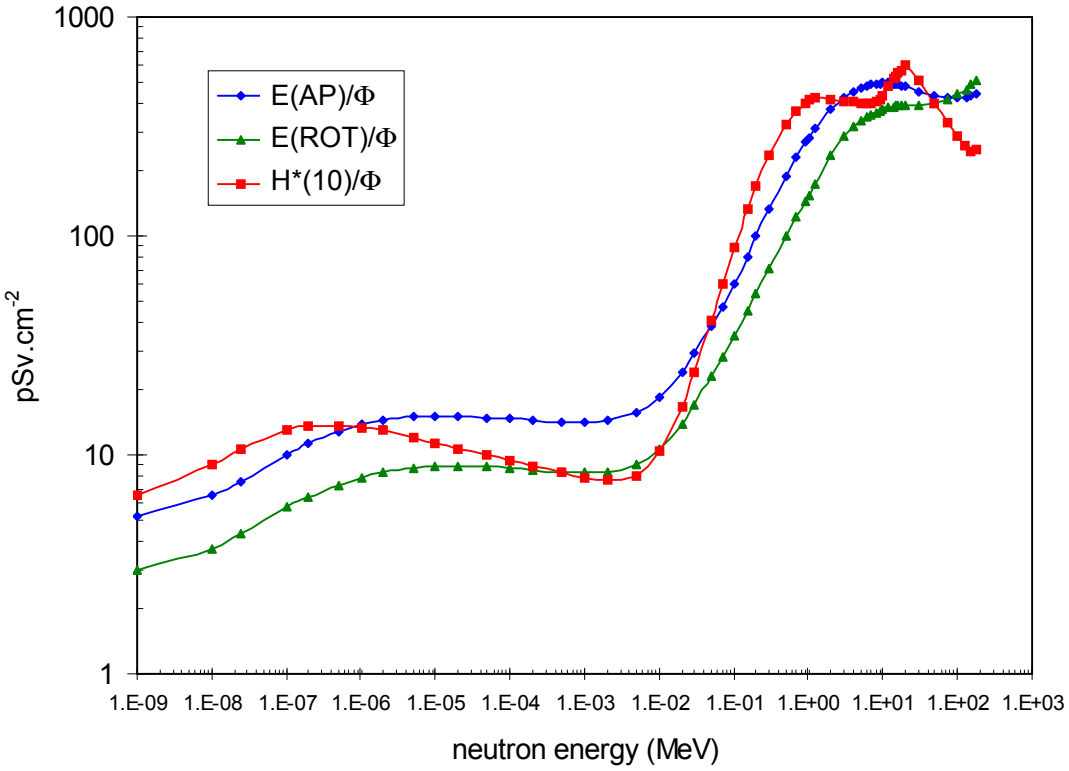

Figure 20.a – Effective dose E per unit neutron fluence for two irradiation geometries (AP and ROT) and ambient dose equivalent H(10) per unit neutron fluence as a function of neutron energy.*

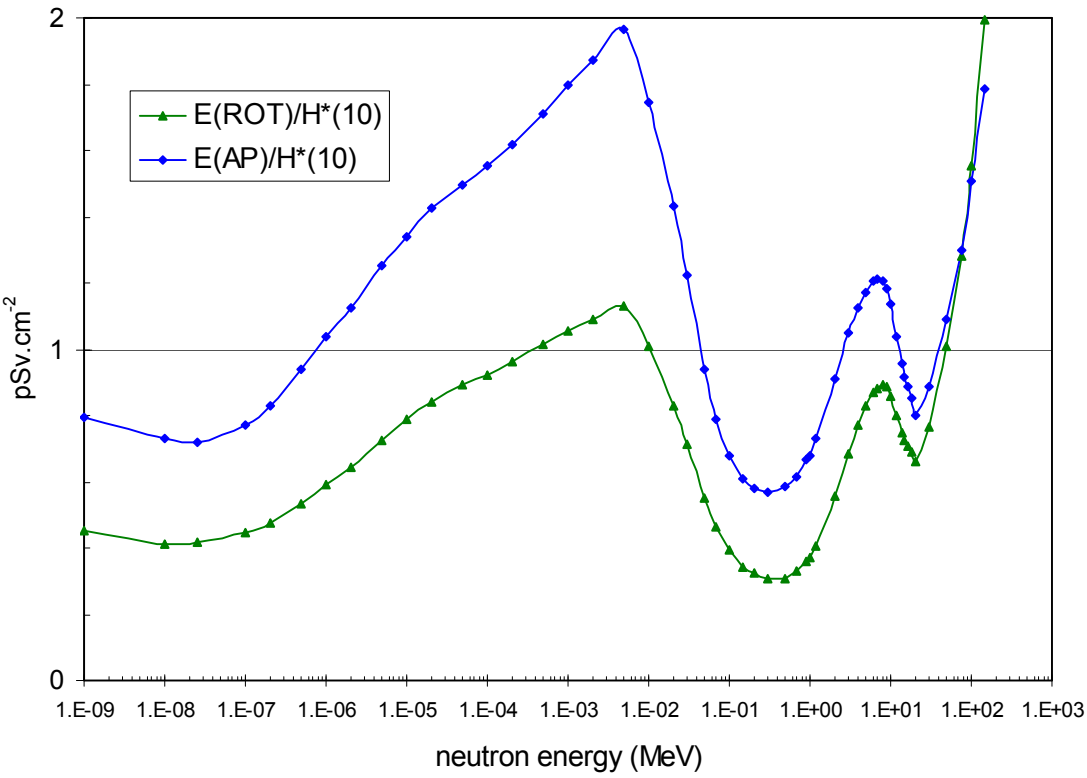

Figure 20.b – Ratio of effective dose E for two irradiation geometries (AP and ROT) to ambient dose equivalent H(10) as a function of neutron energy.*

3.2 Biological effect of ionising radiation

Two types of biological effects of ionising radiation exist. The first type, deterministic effects, involve the malfunctioning or loss of function of tissues in organs due mainly to cell loss. These effects result from high dose exposures and for them there is a threshold. The second type, stochastic effects, express themselves long after the exposure and include increased risk of cancer and of hereditary disorders. These stochastic effects appear to have no threshold and may occur after low radiation doses even though their frequency is then low. For a more detailed description of biological effects of ionising radiation we refer to references [14] and [17].

3.3 Radiation protection rules

The basic role of radiation protection consists in avoiding undue exposure of man and the environment to ionising radiation. The fact that the probability of both deterministic and stochastic damage is dose-dependent is the underlying reason for the two general criteria:

1. Radiation protection measures must guarantee that deterministic radiation damage is avoided. Since deterministic damage appears above a threshold dose, this dose must not be exceeded.
2. The probability of stochastic radiation damage, which has no threshold dose according to the dose-effect relationships currently taken as a basis, must not exceed a justifiable size.

The actual basic principles of radiation protection are defined in ICRP Publ. 60 [14]:

- The necessity of justifying each radiation application by its benefits.

- The demand for optimising radiation protection measures, i.e. the ALARA principle, which says that any exposure to personnel should be kept as low as reasonably achievable.
- The establishment of individual limits for radiation exposure of people on the basis of a justifiable risk.

Table 8 gives the recommended dose limits from ICRP publication 60:

Application	Dose limit	
	Occupational	Public
Effective dose	20 mSv per year, averaged over defined periods of 5 years, not exceeding 50 mSv in any single year	1 mSv in a year
Annual equivalent dose in		
The lens of the eye	150 mSv	15 mSv
The skin	500 mSv	50 mSv
The hands and feet	500 mSv	-

Table 8 – Recommended dose limits from ICRP Publication 60 [14].

Since a working year is normally counted as 2000 working hours, the occupational limits in mSv have to be divided by 2 to obtain limits in $\mu Sv.h^{-1}$, e.g. the occupational limit is 10 $\mu Sv.h^{-1}$ whereas a limit for non-exposed workers of 0.5 $\mu Sv.h^{-1}$ can be derived from the public dose limit.

The natural background is about 1 mSv per year. For human beings, doses above 1 Sv will lead to serious or lethal injuries, whereas a value of the order of 3 to 4 Sv is taken as the 50% lethal dose value $LD_{50/30}$, i.e. the dose which will lead to the death of 50% in an irradiated population within a period of 30 days after the acute exposure.

3.4 Different official radiation protection bodies

In this paragraph we give a non-exhaustive list of international and national organisations in the field of radiation physics and radiation protection

3.4.1 International Organisations

3.4.1.1 International Commission on Radiological Protection (ICRP)

Founded in 1928, the International Commission on Radiological Protection has, since 1950, been providing coherent and complete recommendations on the basic radiation protection rules and their practical implications. The ICRP has published an important list of publications, prepared by four different committees of experts.

The ICRP is a non-governmental organisation, and therefore its recommendations have no legal value. However the ICRP is internationally recognised for its high technical competence and its recommendations have always highly determined national and international laws and rules.

3.4.1.2 International Atomic Energy Agency (IAEA)

The International Atomic Energy Agency is a autonomous, inter-governmental organisation, founded in 1957, under the authority of the United Nations. The IAEA is based in Vienna, Austria. The general role of the IAEA is to promote the exchange of knowledge in the field of the pacific use of nuclear energy. One of its specific roles is to increase the safety level of nuclear installations.

The importance of the IAEA can be illustrated by the fact that the national laws concerning transport of radioactive material are based in the IAEA directives in 90% of all countries.

3.4.1.3 International Commission on Radiation Units and Measurements (ICRU)

This commission was created in 1925. Its principal role is to publish reports, providing recommendations for the scientific community with respect to:

- definitions and units concerning radioactivity and ionising radiation;
- measurement protocols, and their use in radiology and radiobiology;
- physical data required for the previous measurement protocols;
- the practical applications in the field of radiation protection of these recommendations.

3.4.2 European Organisations

3.4.2.1 European Agency for Nuclear Energy (EAN)

The European Agency for Nuclear Energy was founded in 1958. Its main role is to promote collaborations between the different countries of the European Community in the framework of nuclear energy, regarding safety, environmental and economic aspects.

3.4.2.2 The European Atomic Energy Community (EURATOM)

EURATOM was created in 1957. Its role is to provide the necessary rules for the development of the nuclear industry within the countries of the European Community.

European directives based on the recommendations of the ICRP and ICRU are published. These directives must be translated by the member states into national laws.

The European Community have adopted the recommendations of ICRP Publication 60, by publishing on 13/05/96 the European Directive 96/29/Euratom.

4. Prompt radiation sources

One has to distinguish between two types of radiation, namely prompt radiation and induced radiation. Prompt radiation includes all radiation fields that disappear immediately when the accelerator is switched off, i.e. when the accelerator beam is dumped. Protective measures against prompt radiation are straightforward. The accelerator must be installed inside a room with sufficiently thick walls to reduce the radiation levels outside the room to acceptable levels. A "personnel safety system" must guarantee that nobody can penetrate inside the room while the accelerator is switched on. Induced radiation, contrary to prompt radiation, does not disappear immediately when the accelerator is switched off, but will decay with a more or less long decay constant. Protective measures against induced radiation are less straightforward, since one cannot prevent people's access to the activated areas. Protective measures therefore must rely partly on safety procedures, as well as on people's respect of these procedures.

4.1 Radiation sources around electron accelerators

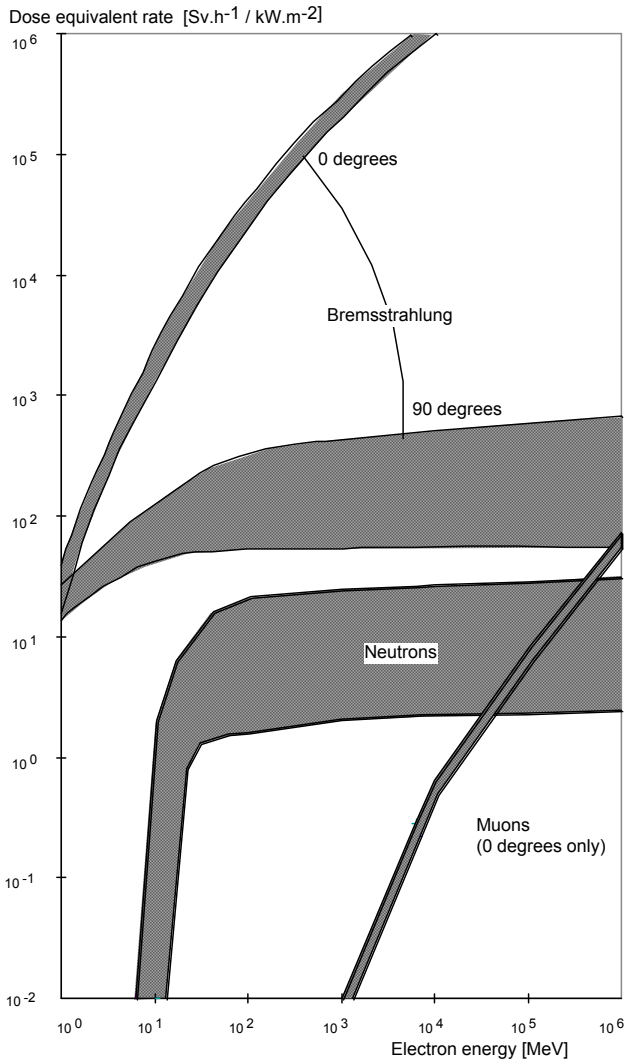

Figure 21 – Prompt radiation sources as a function of the electron energy.

Radiation hazards due to the presence of the primary electron beams are generally not to be taken into account because no access into the accelerator room can be allowed while the machine is in operation. Exceptions are medical accelerators used for radiation therapy. For all electron beam energies, the dominant prompt secondary radiation produced near electron accelerators consists of photons produced by bremsstrahlung in the materials which absorb the electron beam (targets, beam dumps,..). Neutron radiation will be the next important source of secondary radiation, if the electron energy exceeds the threshold for neutron production. Thresholds lie in the range between 6 to 13 MeV for most materials. Above these energies, giant-resonance neutron production must be considered. At high energies, neutrons are produced in photonuclear reactions via the quasi-deuteron effect or in processes involving p-meson production. Although fewer in number than other types of secondary particles, these neutrons are quite penetrating and in such installations may dominate shielding requirements.

Whenever neutrons are produced, they will not only contribute to the prompt radiation, but will also lead to induced activity (see paragraph 5).

The intensity of these types of radiation as a function of electron energy is qualitatively sketched in the figure 21 (taken from reference [18]). The width of the bands suggests the degree of variation due to differences in geometry, targets, etc. In accelerator shielding calculations, dose-equivalent rates are often expressed in $Sv \cdot h^{-1}$ $(kW \cdot m^{-2})^{-1}$, corresponding to the dose equivalent rate measured at 1 m from the target onto which a 1-kW beam is directed. The unit m^2 is included to describe an inverse-square dependence on distance from the target, which is strictly speaking only true for unshielded point radiation, but represents a sufficiently accurate assumption for most radiological safety problems.

4.1.1 Electron Beams

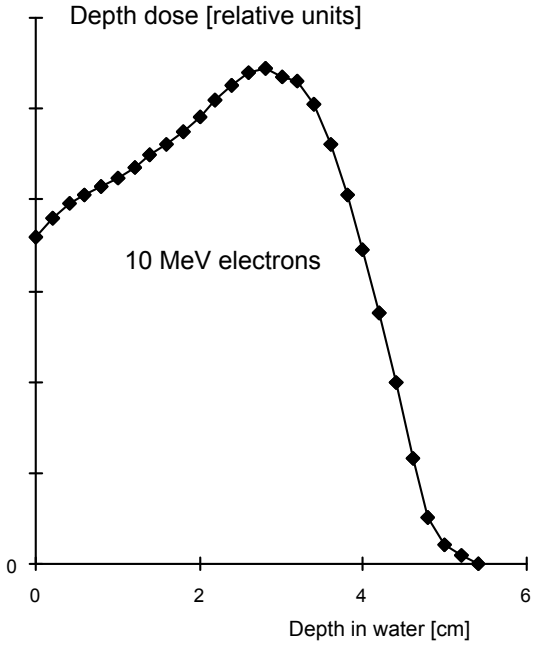

Figure 22 – Depth dose curve in water for 10 MeV electrons.

Except for radiation therapy, there is no installation in which access of personnel to a direct electron beam from an accelerator can be safely allowed. Inadvertent or deliberate access to a controlled area is prevented by the Personnel Safety System. Even when beams are

adjusted to negligible levels and limited by electronic devices, sufficient assurance cannot be provided that the mode of operation may not suddenly change, permitting dangerous beam levels in the primary beam line.

The fluence of electrons, together with the stopping power of the medium (tissue) determines the absorbed dose. The absorbed dose D in Gy of a monochromatic beam is approximately given by

$$D\ (Gy) = 1.602 \times 10^{-10}\ \Phi\ (S/\rho)_{coll,\infty} \qquad (37)$$

where Φ is the fluence (electrons·cm^{-2}) and $(S/\rho)_{coll,\infty}$ is the unrestricted collision stopping power in MeV·cm^2·g^{-1}. The actual absorbed dose is difficult to calculate precisely from stopping power curves, because buildup, scattering and spectral changes all modify dose distributions. An example of a depth dose curve is shown in figure 22, corresponding to a 10 MeV beam on a water phantom.

4.1.2 Photons

The secondary radiation with the greatest potential hazard at all energies are the photons produced by bremsstrahlung. Photons are radiated from any object struck by the primary electrons, such as a beam-stop or target in a linear accelerator or vacuum vessels or magnet yokes in circular machines.

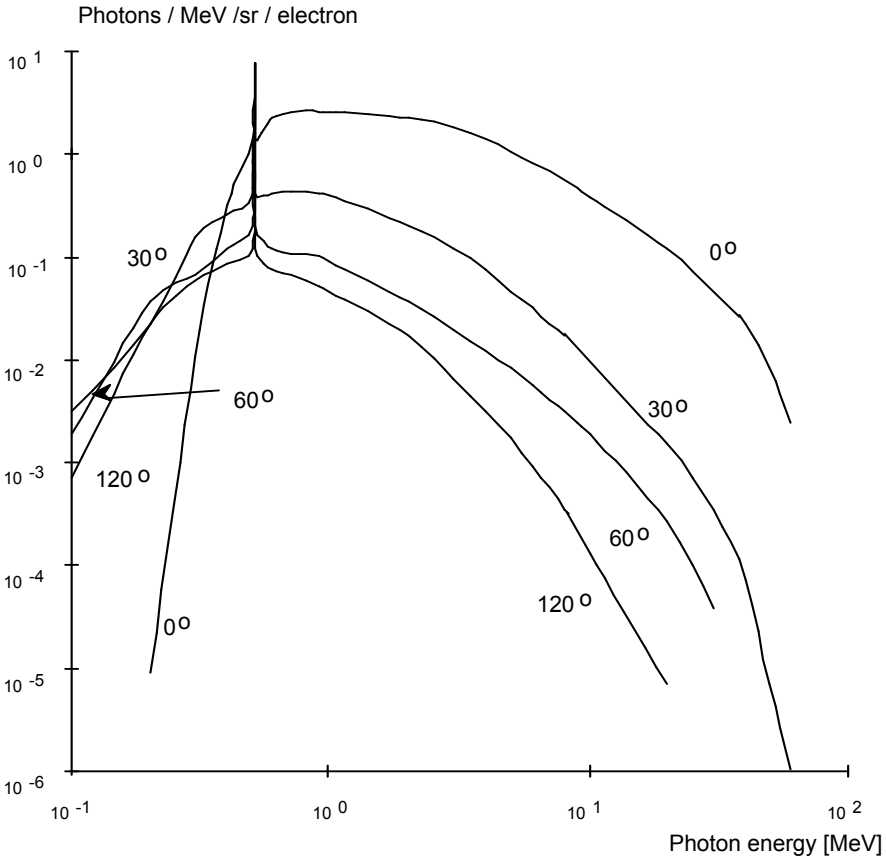

Figure 23 - Bremsstrahlung spectra produced by 60 MeV electrons hitting a thick tungsten target.

As explained in chapter 2, at low energies, the electrons incident on a target lose their energy primarily by ionising while at higher energies the bremsstrahlung production dominates. The bremsstrahlung yielded from a target as a function of the target thickness will first show an increase, until reabsorption in the target modifies this growth to produce a broad maximum, followed by a decline that becomes approximately exponential at very great thickness. A target of thickness corresponding to the maximum radiation is called a 'optimum' target and the photons emanating from such a target are described as 'thick target' bremsstrahlung. High-Z targets will produce more bremsstrahlung than low-Z targets.

An example of typical bremsstrahlung spectra produced by 60 MeV electrons hitting a thick tungsten target is shown in figure 23. The graph shows the photon fluences for different angles with respect to the electron beam (taken from reference [18]).

In accelerator shielding problems, the exact nature of the targets will not always be predictable, and one should therefore use thick target bremsstrahlung from high-Z targets as source terms. Figure 24 shows the absorbed dose rates from thick-target bremsstrahlung for high-Z targets.

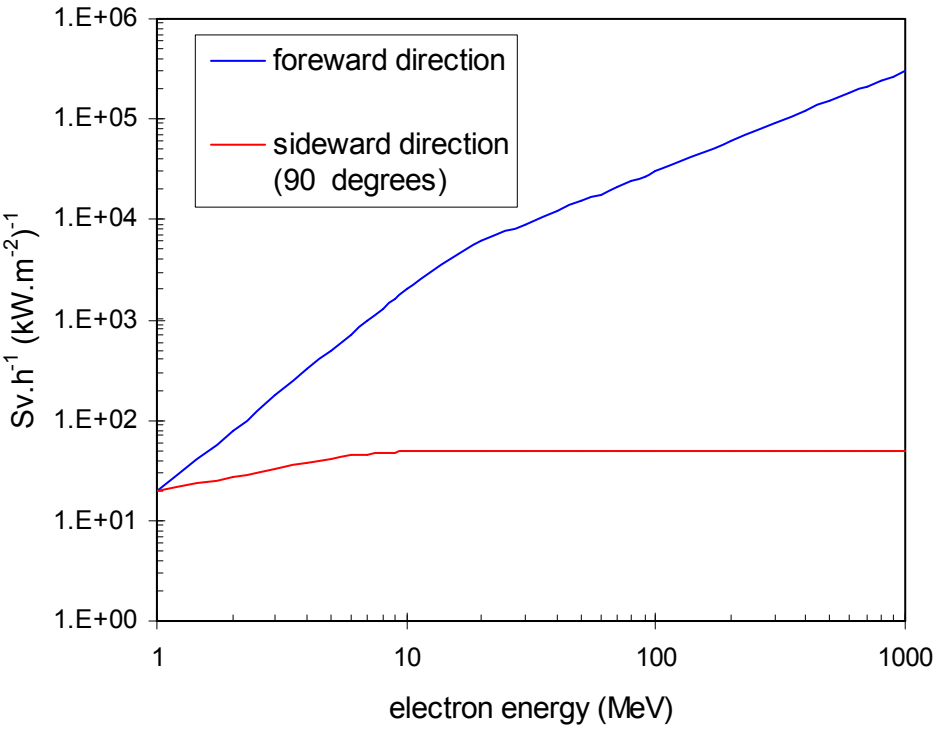

Figure 24 – Bremsstrahlung dose equivalent source terms for 0 and 90 degrees as a function of electron energy

As a rule of thumb, the following values can be used (E_0 in MeV):

$$\dot{D}\ [Sv \cdot h^{-1}\ (kW \cdot m^{-2})^{-1}] \approx 20\ E_0^{\,2} \qquad 0^o,\ E_0 < 20\ MeV$$

$$\dot{D}\ [Sv \cdot h^{-1}\ (kW \cdot m^{-2})^{-1}] \approx 300\ E_0 \qquad 0^o,\ E_0 > 20\ MeV \qquad (38)$$

$$\dot{D}\ [Sv \cdot h^{-1}\ (kW \cdot m^{-2})^{-1}] \approx 50 \qquad 90^o,\ E_0 > 100\ MeV$$

These values represent the more penetrating radiation component to be considered in shielding design. Dose rates from an unshielded target may be significantly higher because of the contribution of softer radiation components.

4.1.3 Neutrons

4.1.3.1 Giant Resonance Neutrons

Above a threshold energy that varies from 10 to 19 MeV for light nuclei (but which is 2.23 MeV in deuterium and 1.67 MeV in beryllium) and from 4 to 6 MeV for heavy nuclei, neutron production will take place in any material struck by the electron or bremsstrahlung beam. It should be realized that it is the photons interacting with components that release the neutrons, rather than direct interaction of the electrons. The produced neutrons represent a prompt radiation hazard and are also related to induced activity (see chapter 5).

Between threshold and approximately 30 MeV, neutron production results primarily from a process known as the 'giant photonuclear resonance'. The physical mechanism can be described as one in which the electric field of the photon transfers its energy to the nucleus by inducing an oscillation in which the protons as a group move opposite to the neutrons as a group.

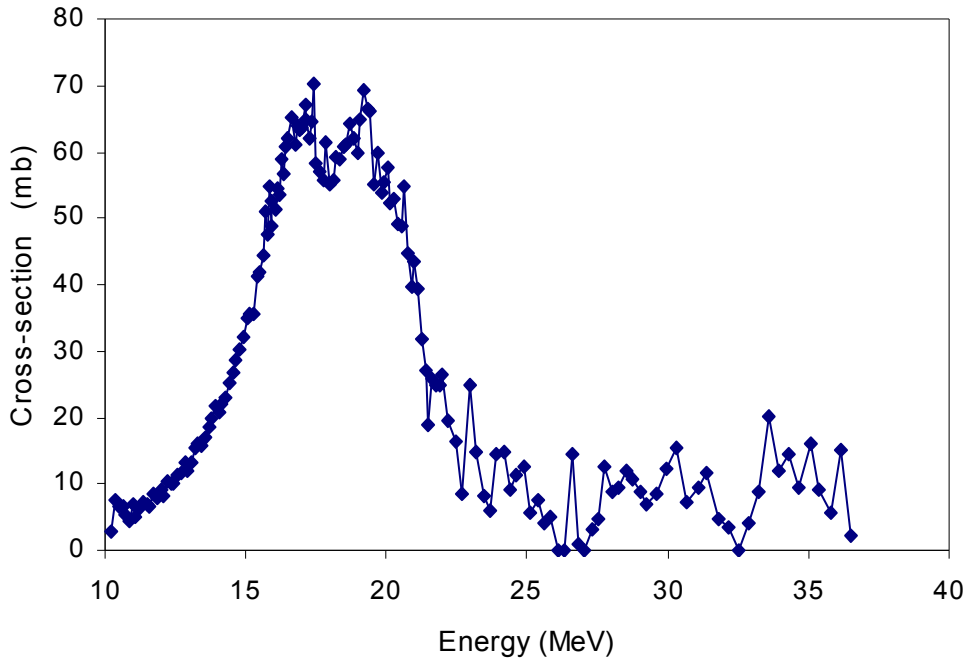

Figure 25 – Cross-section for the reaction $^{55}Mn(\gamma, n)^{54}Mn$.

The cross-section for this process has a large maximum at photon energies of approximately 20 - 30 MeV for light nuclei (atomic mass number A = 40), and 13 - 18 MeV for medium and heavy nuclei. The width of this peaking varies between about 3 MeV (heavy nuclei) and 10 MeV (light nuclei). This phenomenon occurs in all nuclei (except of course ^{1}H) and its general features are rather smooth functions of nuclear size. As an example the cross-section for the reaction $^{55}Mn(\gamma, n)^{54}Mn$ is shown in figure 25 [19]. One sees clearly the giant resonance peaking around 18 MeV.

The resulting neutron source is obtained from a folding of the neutron production cross-sections, with the bremsstrahlung photon spectrum, which as explained in the previous paragraph decreases strongly with the photon energy. The trend of such a spectrum strongly enhances the importance of the giant-resonance mechanism, relative to mechanisms that dominate at higher energy.

4.1.3.2 Quasi-deuteron neutrons

At photon energies above the giant resonance, the dominant neutron production is the 'quasi-deuteron' mechanism, where the photon interacts initially with a neutron-proton pair within the nucleus, rather than with the nucleus as a whole. The cross-section for this mechanism is about an order of magnitude below the giant resonance peak, and the neutron spectrum shows a rapid fall-off in neutron energy. The combination of both effects makes the neutrons released by the quasi-deuteron effect relatively less of a hazard than giant-resonance neutrons, even though they are more penetrating. If adequate protection is provided against giant-resonance neutrons and, if needed, against high-energy neutrons (discussed below), the quasi-deuteron neutrons are not generally a special hazard.

The cross-section Σ_{QD} [1/cm] for a given material (A,Z) is given by the expression [20]

$$\Sigma_{QD}\left[cm^{-1}\right] = \frac{(A-Z)\times Z}{A} \times \frac{N_{Av}}{A} \times \rho\left[g.cm^{-3}\right] \times 1.10^{-24}\,\sigma_d\,[mbarn] \qquad (39)$$

with σ_d the cross-section for the reaction $\gamma(d,p)n$, multiplied by $\exp(-60/E_\gamma)$, as described by Levinger [20]. Figure 26 shows these cross-sections.

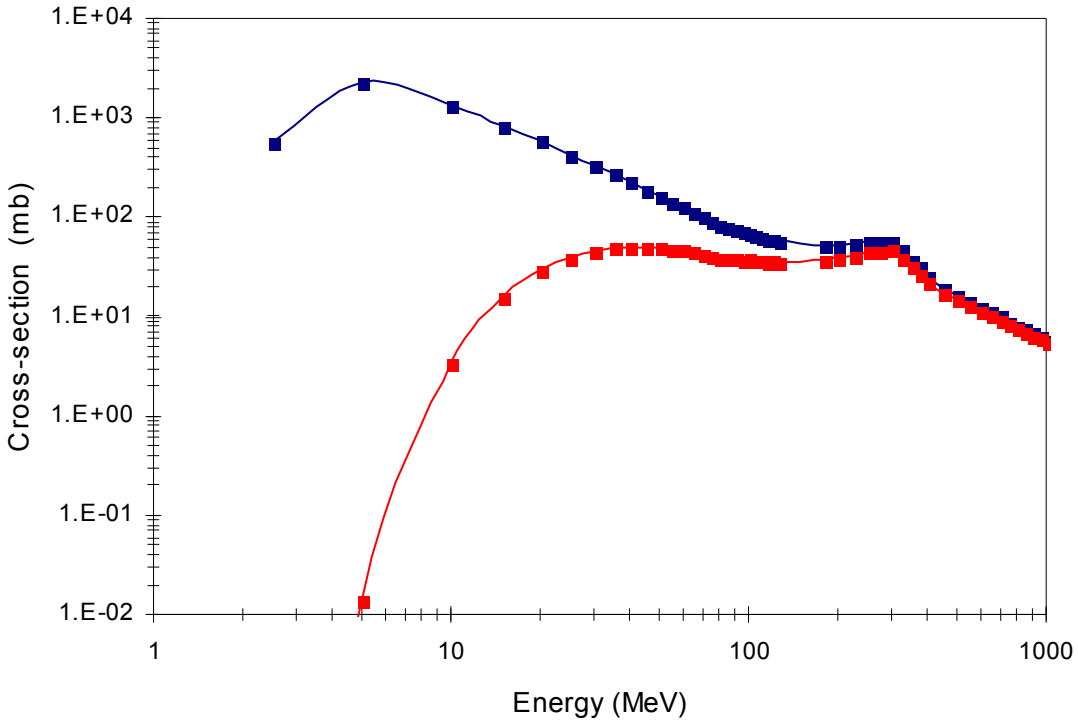

Figure 26 – γ(d,p)n cross-section (bue) [2] and cross-section multiplied by factor exp(-60/E_γ) (red).

4.1.3.3 High energy neutrons

Above 140 MeV, the cross section for photons on nuclei rises again, due to the opening of channels for photopion production. The cross-section goes through a number of resonance peaks, which are caused by nucleon isobar formation. The largest resonance, the first one, peaks at about 300 MeV.

Figure 27 shows the different neutron production cross-sections of copper, as a function of photon energy. Figures 28.a and 28.b show the neutron spectra produced in a 5 cm thick copper target bombarded with 600 MeV electrons.

4.1.3.4 Neutron yields from electron beams

To assess the radiological significance of neutrons released at electron accelerators, it is necessary to combine the cross-sections for photoneutron production with a realistic energy spectrum of the photons released within materials struck by the electrons. For radiation shielding problems, conservative assumptions are again made, namely the electrons are dumped in thick high-Z targets, and self- shielding is disregarded.

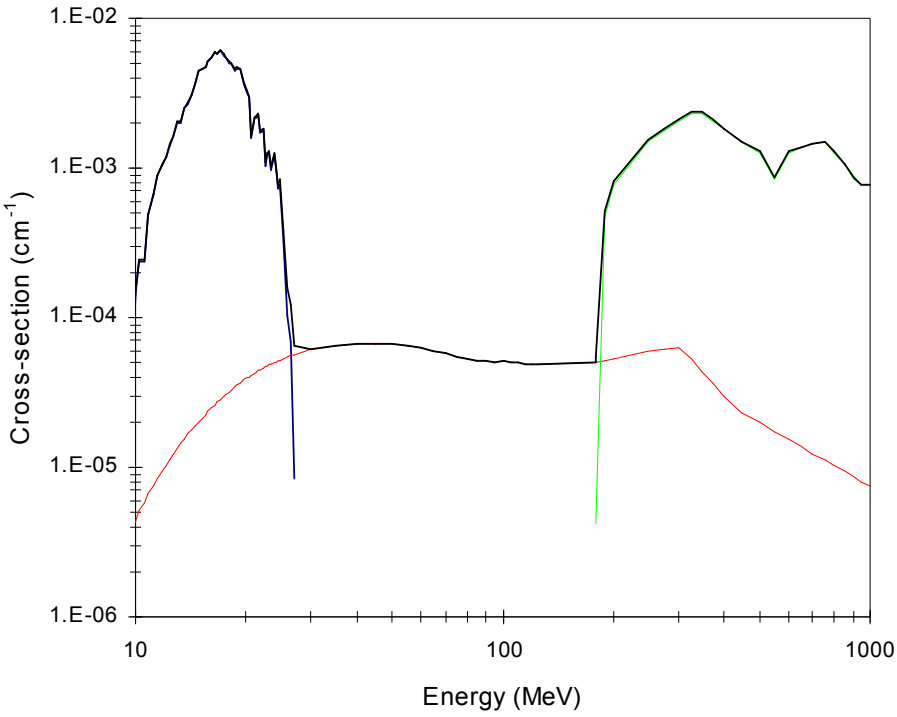

Figure 27 – Cross-section for neutron production of Cu – giant resonance: blue; quasi-deuteron: red; photo-pion: green ; total : black.

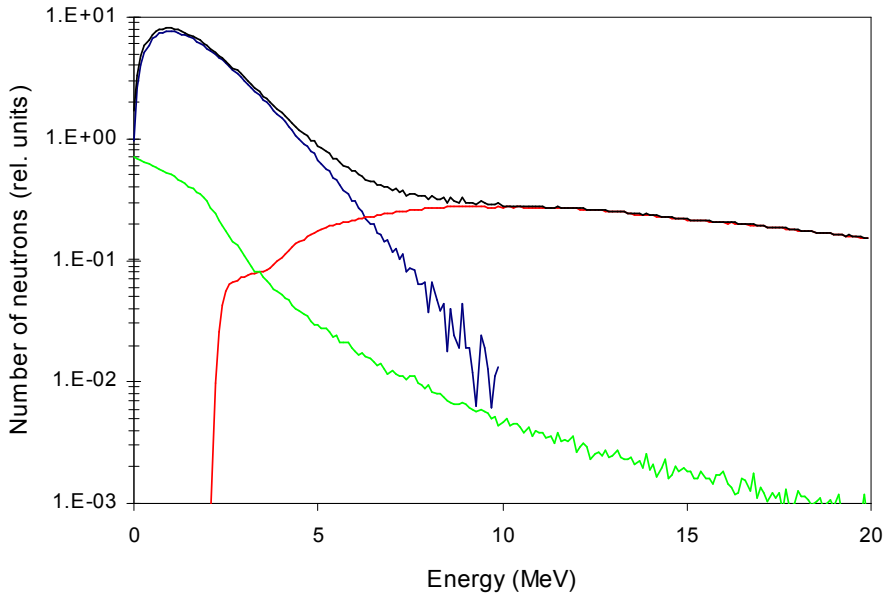

Figure 28.a – Number of neutrons with energy below 20 MeV produced in a 5 cm thick Cu target bombarded with 600 MeV electrons - giant *resonance (bleu), quasi-deuteron (red), photo-pion (green), total (black).*

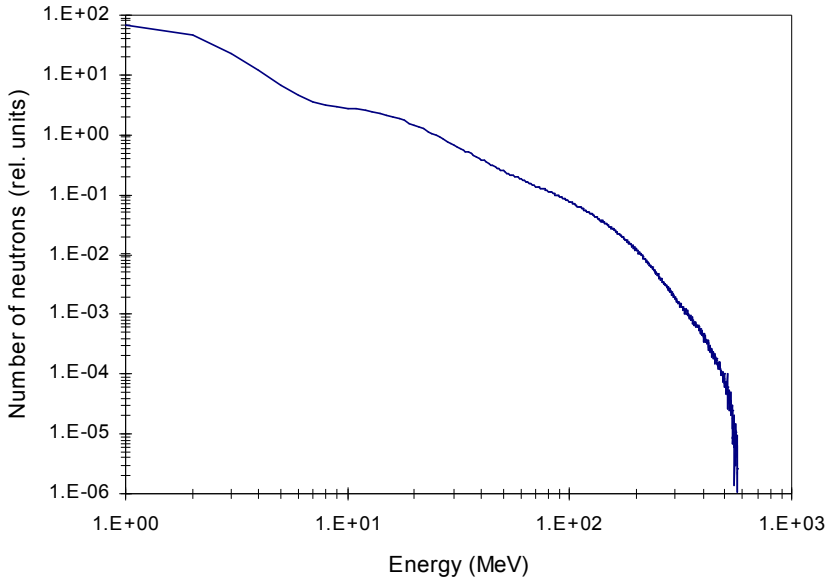

Figure 28.b – Total number of neutrons produced in a 5 cm thick Cu target bombarded with 600 MeV electrons

Some useful rule-of-thumb equations are:

Let:

Y = neutron yield, in units of $n \cdot s^{-1} \cdot kW^{-1}$,

φ = neutron fluence rate, in units of $n \cdot cm^{-2} \cdot s^{-1}$,

then we can write:

$$\varphi = Y \cdot P/(4p\ 10^4\ d^2), \tag{40}$$

with P being the electron beam power in kW and d the distance in m from the source to the location in question.

A. Giant resonance neutrons

Unless the neutron spectrum at the location in question has been measured and is found to be different, we can assume that the neutron spectrum peaks somewhere near 1 MeV, and that the energy is effectively 1 - 2 MeV. The conversion of neutron flux density to dose equivalent rates is then (see figure 20.a):

$$\dot{H}\ [Sv \cdot h^{-1}] \approx 1.4 \times 10^{-6}\ \varphi \tag{41}$$

or

$$\dot{H}\ [Sv \cdot h^{-1}] \approx 1.4 \times 10^{-6}\ Y \cdot P/(4p\ 10^4\ d^2) \tag{42}$$

One can take 2×10^{12} neutrons·s^{-1}·kW^{-1} as indicative of the maximum neutron yield for high-Z materials (excluding photo-fissionable materials Z > 82) [18]. This gives finally the following rule of thumb for the unshielded dose-equivalent rate:

$$\dot{H}\ [\mathrm{Sv \cdot h^{-1}}] \approx 23 \times P/d^2. \qquad (43)$$

B. High energy neutrons

For electron energies above 140 MeV, high energy neutrons are produced. As a rule of thumb, the following conversion factor for the unshielded dose equivalent rate can be used:

$$\dot{H}\ [\mathrm{Sv \cdot h^{-1}}] \approx 2.7 \times P/d^2. \qquad (44)$$

4.1.4 Muons

Above an energy of about 211 MeV, muon pair production (π^+, π^-) by photons in the Coulomb field of target nuclei becomes possible. This is a process analogous to ordinary electron-positron pair production, except that the cross-sections are several orders of magnitude smaller. Muon production will not present a radiation problem at an installation which is otherwise adequately shielded, unless the beam energy exceeds about 1 GeV. The muon fluence is very highly peaked in the forward direction. In cases where additional muon shielding is needed, it usually takes the form of iron blocks, one to several meters in length, positioned only in the forward direction. The only significant stopping process for muons is energy loss by ionisation. For more details we refer to reference [2].

4.1.5 Summary

Table 9 summarizes the unshielded dose equivalent source terms F_H to be used for electron accelerators.

Radiation Component	Radiation Dose Equivalent Factor F_H [Sv·h^{-1} (kW·m^{-2})$^{-1}$]
Bremsstrahlung	50
Giant Resonance Neutrons	23
High Energy Neutrons	2.7

Table 9 – Unshielded dose equivalent source terms for lateral shielding of electron accelerators.

4.2 Radiation sources around proton accelerators

The prompt radiation field around proton accelerators comes from the hadronic cascade, resulting from the interaction of the accelerated protons with matter (accelerator structure, shielding, …). Deep in the shield the cascade is propagated essentially by neutrons with energies above 150 MeV: ionisation energy losses for protons with energy below about 500 MeV become significant and high energy neutrons are therefore the most penetrating particles.

Outside the shield the radiation field will essentially consist of these high energy neutrons, who were created close to the primary proton interaction point, accompanied by many lower energy particles, mainly neutrons, created near the outer surface of the shield. The presence of these low energy neutrons created close to the outer surface of the shield explain why the equivalent dose outside a high energy proton accelerator is essentially due to neutrons with energies between 0.1 and 10 MeV, the dose contribution from thermal and very high energy neutrons being very small [21]. As an example, table 10 shows the radiation spectrum observed outside the 7 GeV proton synchrotron NIMROD [22].

Type of radiation	Energy range	Estimated % of neutron flux density	Estimated % of total dose equivalent
Neutrons	< 1 eV	< 7	<1
Neutrons	1 eV – 0.7 MeV	70	20
Neutrons	0.7 – 3 MeV	15	35
Neutrons	3 – 7 MeV	7	25
Neutrons	7 – 20 MeV	1.5	5
Neutrons + protons	20 – 100 MeV	1	5
Neutrons + charged particles	> 100 MeV	0.5	4
Other particles + gammas	-	-	< 2

Table 10 – Radiation spectrum above NIMROD extracted proton beam shielding [22].

4.2.1 Proton energies > 1 GeV

A simple, macroscopic description of the production of secondary hadrons from high energy proton interactions (> 1 GeV), useful for shielding calculations for high energy proton accelerators is given in reference [11]. In this paragraph we will explain the general ideas of this description.

Analysis of results from experiments and Monte-Carlo simulations show that the fluence of secondary hadrons, at 1 m and per proton interaction, produced by protons in the energy range 1 to 1000 GeV bombarding thin iron or copper targets can be described by the expression:

$$\varphi(\theta) = \frac{0.5}{\left(\theta + 35/\sqrt{E}\right)^2} \quad \text{hadrons.cm}^{-2}, \tag{45}$$

where θ is the emission angle in degrees and E the incident proton energy in GeV. Figure 29 shows the secondary hadrons angular distribution calculated from expression (45), for different emission angles, as a function of the energy of the interacting protons.

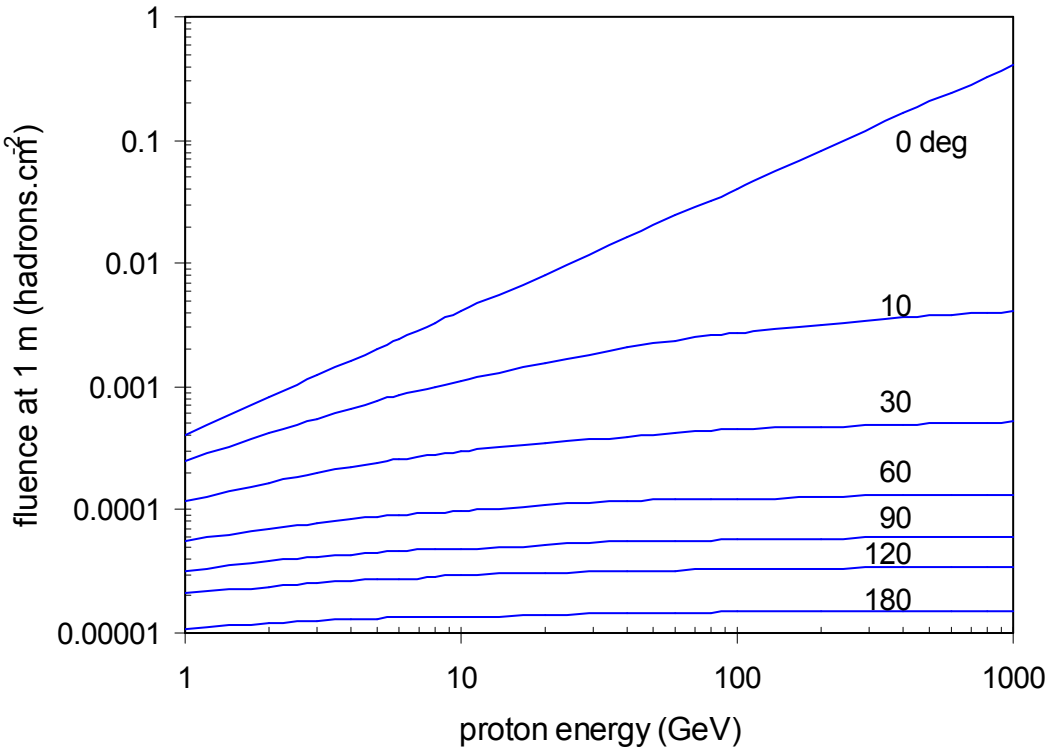

Figure 29 – Secondary hadron fluence per proton interaction at different angles as a function of incident proton energy

The particle multiplicity Q, i.e. the total number of secondary hadrons per interaction, is obtained by integrating equation (45) over all angles:

$$Q = 2\pi \int_{0^o}^{180^o} \frac{5000}{\left(\theta + 35/\sqrt{E}\right)^2} \sin\theta \, d\theta \, . \qquad (46)$$

Figure 30 shows the multiplicity Q obtained from expression (46) as a function of interacting proton energy. The curve thus obtained can be fitted with the following expression:

$$Q = 16E^{0.15} - 10 \quad \text{secondaries per interaction.} \qquad (47)$$

A large fraction of the kinetic energy of the interacting proton has been transferred to the kinetic energy of the secondary hadrons. Part of the initial energy however will have gone into the production of unstable secondary particles, into the production of particles with energy below that necessary to cause further spallation reactions, into elastic interactions and into ionisation. One can assume that some 80 % of the energy of the interacting hadron goes into the energy of the kinetic energy of secondary hadrons with energy above 120 MeV. With this assumption and using expression (47), the average energy of the secondary hadrons from an interaction by a proton of E GeV will be given by:

$$E_{sec} = 0.8\frac{E}{Q} = 0.8\frac{E}{1.6E^{0.15} - 10} \text{ GeV.} \quad (48)$$

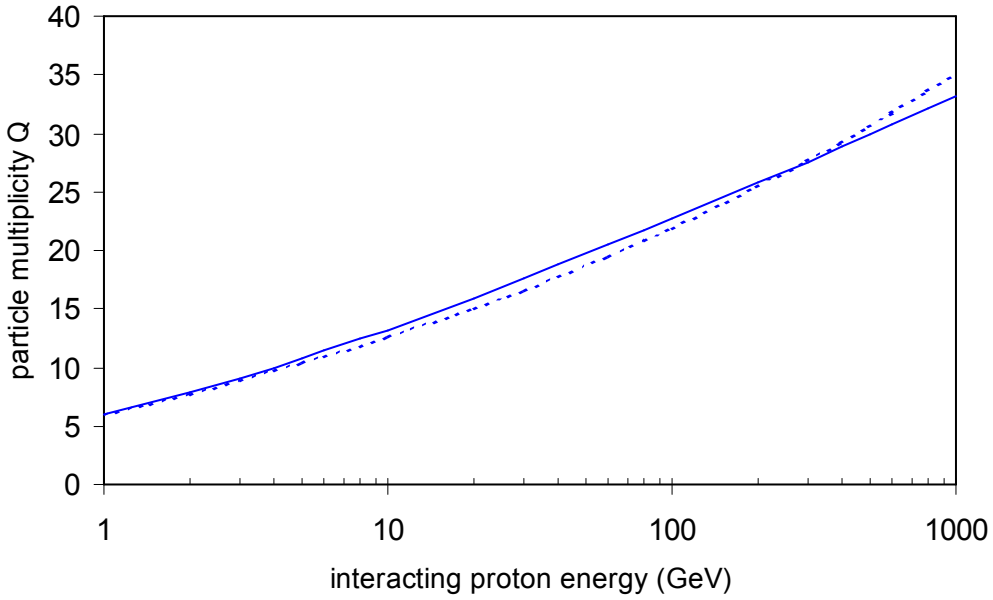

Figure 30 – Total number of secondary hadrons emitted per interaction as a function of the incident proton energy (solid line). The dashed line corresponds to the multiplicity given by equation (47).

Figure 31 shows the secondary particle average energy obtained with expression (48), as a function of the primary proton energy. The curve can be reasonably well fitted using the following relation:

$$E_{sec} = 0.12\,E^{0.76} = (0.06\,E)^{0.76} \quad \text{GeV.} \quad (49)$$

The dose equivalent H at a distance R meters from a high energy proton interaction and behind a thickness t of a shield with a mean free path for hadron attenuation λ, is given by:

$$H = \frac{H_0 e^{-t/\lambda}}{R^2}. \quad (50)$$

H_0 is the so-called source term (units: Sv.m^2), which is the effective equilibrium dose equivalent per interacting proton, normalized to 1 m from an interaction and to zero shield thickness.

In A. H. Sullivan's description, an expression for the source term H_0 is obtained in the following way. The equilibrium dose D_{eq} from a hadron fluence Φ is given by:

$$D_{eq} = -E_{sec}\frac{d\Phi}{dx} = E_{sec}\frac{\Phi}{\lambda}. \quad (51)$$

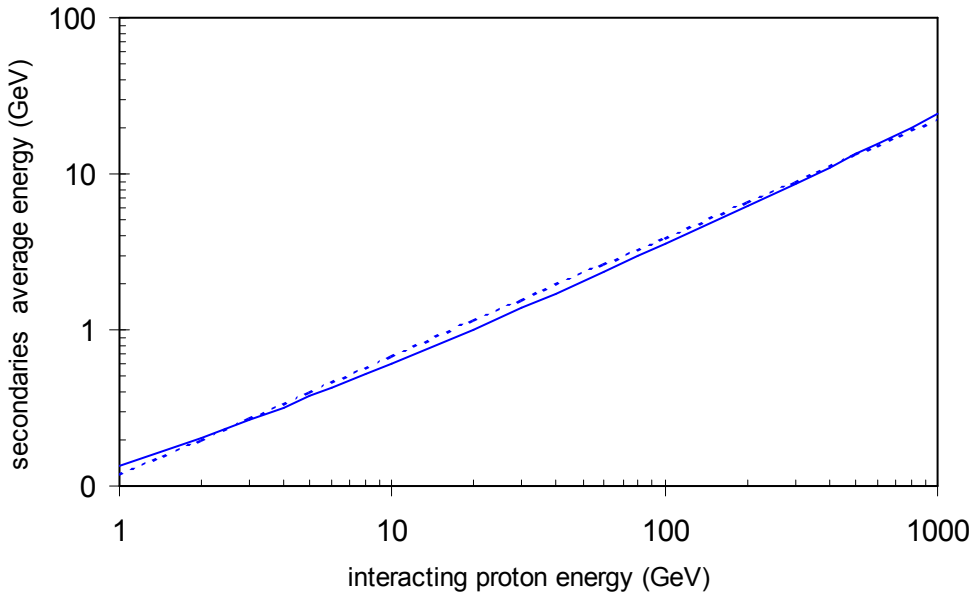

Figure 31 – The average energy of the secondary hadrons as a function of the incident proton energy. The solid line corresponds to the equation (48), the dashed line corresponds to the average energy given by equation (49).

The dose at the outer surface of the shield is estimated to about 50 % of the equilibrium dose inside the shield at the same thickness, due to lack of the dose contribution from backscattering. It is furthermore assumed that the absorbed dose to a person is about 90 % of that at the surface of a uniformly irradiated shield, due to the differences in the absorption coefficients for hadrons in human tissue and in the shield. Assuming a quality factor of 4, the source term H_0 is thus obtained from:

$$H_0 = 0.5\times0.9\times4\times D_{eq} = 0.5\times0.9\times4\times E_{sec}\frac{\Phi_1}{\lambda}, \quad (52)$$

where Φ_1 is the first generation hadron fluence, given by the equation (45). Using expression (49) for the secondary hadron average energy E_{sec}, and using a value of 100 g.cm^{-2} for λ (see § 2.6.2.1) we finally obtain the following expression for the source term $H_0(\theta)$ for primary protons of energy E_0 GeV:

$$H_0(\theta) = \frac{1.8\times10^{-10}\ E_0^{0.76}}{\left(\theta + 35/\sqrt{E_0}\right)^2} \text{ Sv.m}^2 \text{ per proton.} \quad (53)$$

Figure 32 shows the $H_0(\theta)$ obtained with equation (53) for various angles as a function of the incident proton energy.

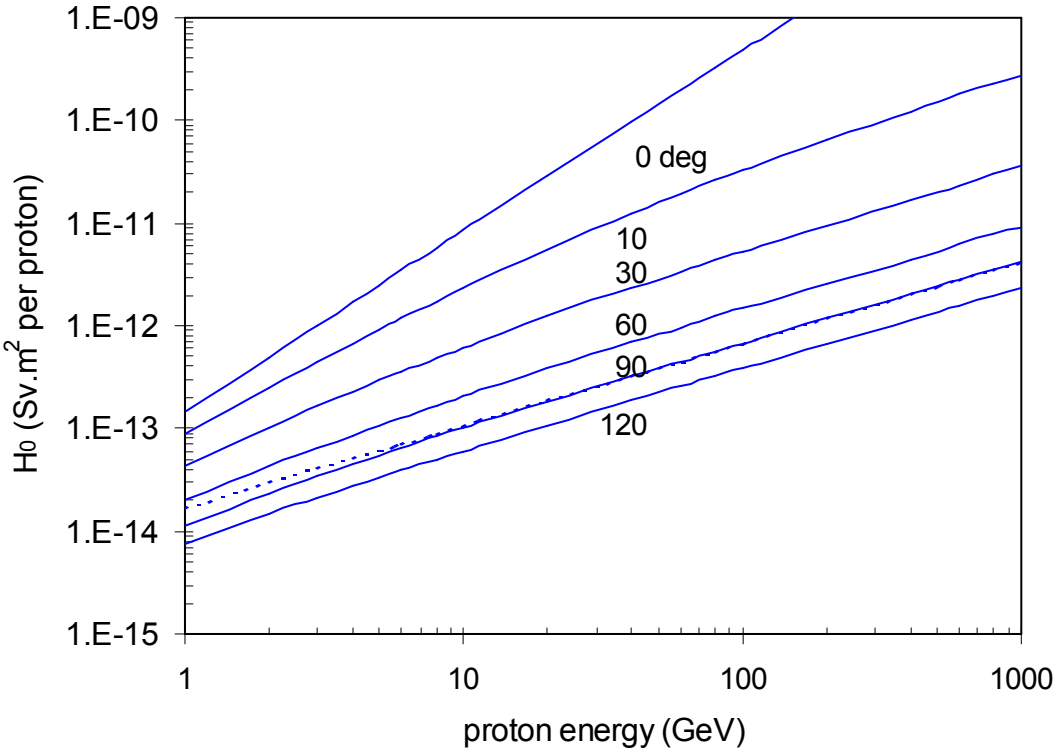

Figure 32 –Dose equivalent source term H_0 obtained with equation (53) for various angles θ as a function of the incident proton energy. The dashed line corresponds to the 90 degrees source term given by equation (54).

In shielding calculations the source term for radiation emitted at 90 degrees is normally used to define lateral shielding requirements. As shown in figure 32 the 90 degrees source term can be approximated by:

$$H_0(90^o) = 1.7 \times 10^{-14}\ E_0^{0.8} \quad \text{Sv.m}^2 \text{ per proton.} \tag{54}$$

4.2.2 Secondary radiation for proton energies < 1 GeV

Protons with energies below about 1 GeV will start to lose significant fractions of their energy by ionisation before they interact with a target nucleus. The interaction with the nucleus will give rise to the emission of cascade-neutrons, which will be the important secondary radiation source for shielding calculations of proton machines below 1 GeV. Indeed, charged particles emitted in the interaction by protons with energies below 1 GeV are very likely to lose all their energy via ionisation, before they can further interact. Evaporation neutrons (with energies < 8 MeV), emitted by the excited nucleus left after the proton interaction must also be taken into account, especially at lower proton energies.

It has been found that expression (45), describing the angular distribution of the neutrons emitted in interactions by protons of energies > 1 Gev, gives a reasonable approximation for proton energies below 1 GeV, when suitably modified to take into account of the energy loss of

the incoming proton by ionisation before undergoing the spallation reaction. One can assume that protons of energy less than 1 GeV incident on a thick target lose on average 20 % of their energy by ionisation before interacting [11].

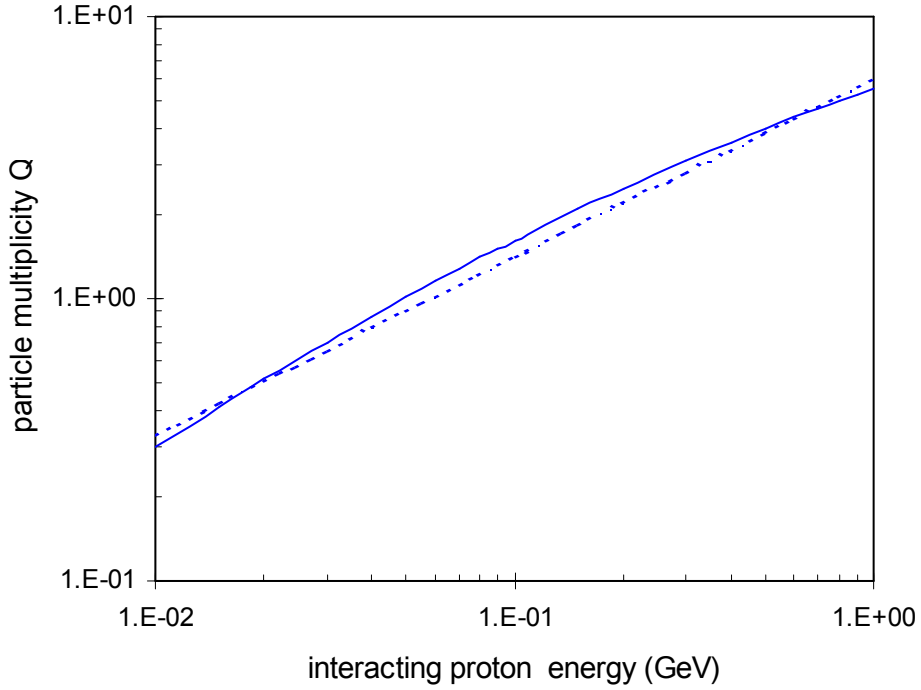

Figure 33 – Total number of secondary hadrons emitted per interaction as a function of the incident proton energy (solid line). The dashed line corresponds to the multiplicity given by equation (56).

Using expression (45) we thus obtain the following expression for the differential secondary hadron fluence

$$\varphi(\theta) = \frac{0.5}{\left(\theta + 35/\sqrt{0.8\times E}\right)^2} = \frac{0.5}{\left(\theta + 40/\sqrt{E}\right)^2} \quad \text{hadrons.cm}^{-2}, \tag{55}$$

Integrating expression (55) over all angles we obtain the multiplicity Q shown in figure 33. This multiplicity can be fitted to the relation

$$Q = 6\,E^{0.63} \quad \text{neutrons per proton} \tag{56}$$

At low incident proton energies not all protons will interact before coming to rest (see figure 17). The fraction that interacts will be approximated by

$$f = 1 - e^{-R/\lambda} \tag{57}$$

where R is the proton range in the target material and λ is the nuclear interaction mean free path. Figure 34 shows the ratio R/λ, using the values for R from reference [9] and using expression (22) for λ. A reasonable fit of this ratio for energies up to 1 GeV is given by

$$\frac{R}{\lambda} = 3.6\ E^{1.6} \quad \text{with E in GeV.} \tag{58}$$

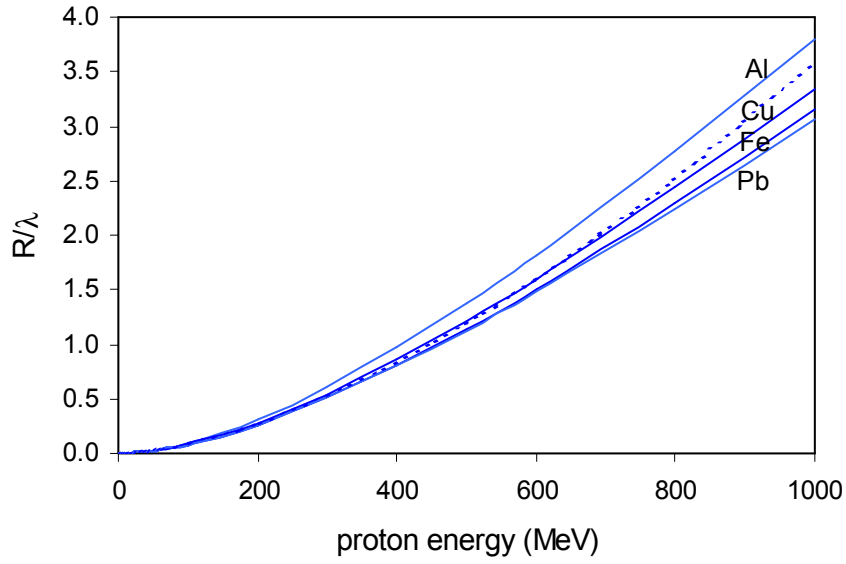

Figure 34 – Ratio R/λ as a function of the incident proton energy for 4 different materials (solid lines). The dashed line corresponds to the equation (58).

The total number of neutrons emitted per proton incident on a thick (copper or iron) target will therefore be equal to fQ. This total neutron emission is plotted in figure 35. This expression is in reasonable agreement with experimental data [23].

The resulting neutron fluence is given by

$$\varphi(\theta) = \frac{0.5\left(1 - e^{-3.6E^{1.6}}\right)}{\left(\theta + 40/\sqrt{E}\right)^2} \quad \text{neutrons·cm}^{-2} \tag{59}$$

Applying a fluence to dose equivalent conversion factor for neutrons in the energy range of 0.5 – 100 MeV of 40×10^{-11} Sv per neutron·cm^{-2} (see figure 20.a), we get the following source term

$$\dot{H} = \frac{7.2\times10^{-7}\left(1 - e^{-3.6E^{1.6}}\right)}{\left(\theta + 40/\sqrt{E_0}\right)^2} \quad \text{Sv·h}^{-1}\text{.m}^2 \text{ per proton·s}^{-1}, \tag{60}$$

which reduces at 90 degrees to:

$$\dot{H}(90^{o}) = \frac{8.9\times10^{-11}\left(1-e^{-3.6E^{1.6}}\right)}{\left(1+0.44/\sqrt{E_0}\right)^2} \quad \text{Sv·h}^{-1}\text{.m}^2 \text{ per proton·s}^{-1}. \tag{61}$$

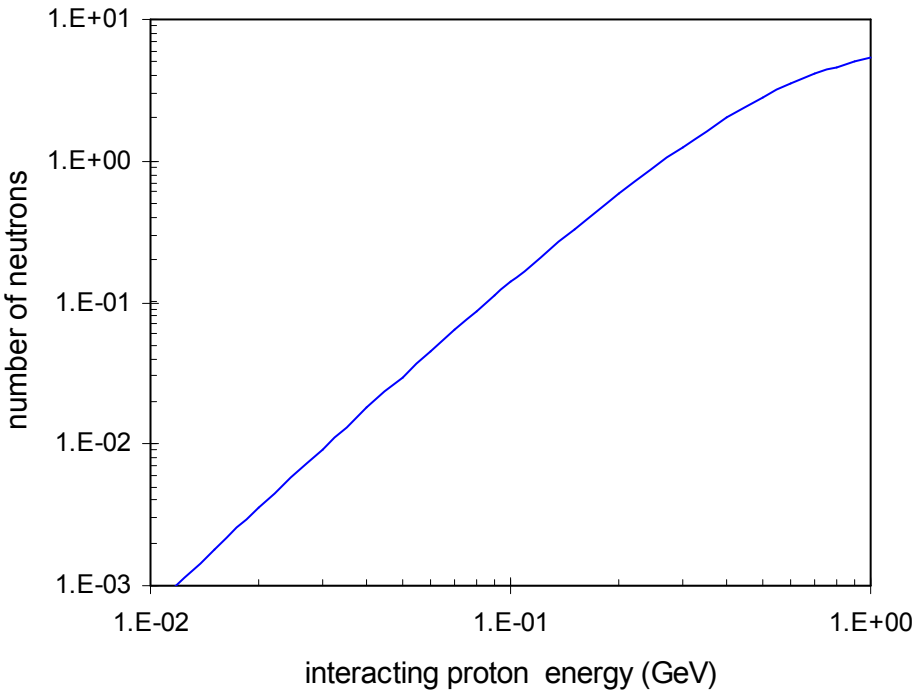

Figure 35 – Total number of neutrons emitted per proton incident on a thick copper or iron target.

Expression (45) that was used to derive the dose equivalent source terms for proton energies above and below 1 GeV was obtained for iron and copper target. Table 11 gives the relative secondary particle yield for different target materials.

Target material	Relative yield
Cu	1.0
Fe	1.0
Be	0.4
Al	0.6
Pb	1.5
U	1.7

Table 11 – Relative high energy secondary particle yield in different target materials.

5. Induced radiation

5.1 Introduction

The activation of matter, i.e. the process of making them radioactive by irradiating them with particles or photons, can take place via a large number of different processes. We will

briefly mention the most important ones. For a detailed description of the process we refer to the work of M. Barbier (reference [24]).

The overall quantity of radioactivity induced in an accelerator will depend on the primary beam loss (power), whereas the probability of producing a particular isotope will depend essentially on the composition of the material struck and the production cross section of this isotope.

The activation is a two-step process. The first step is the nuclear reaction that leaves the target nucleus in an excited state, the second step is the nuclear decay.

5.2 The activation formula

We will derive a formula to calculate the activity of a target bombarded by a given particle flux.

We define the following quantities:

Φ: the incident fluence rate, defined as the number of particles incident on the target per cm^2 and per s.

$\sigma_{target,i}$: the cross section for the production in the target material of the i^{th} isotope (cm^2).

λ_i: the decay constant of the i^{th} isotope

n_{target}: the number of target atoms per gram of target material

n_i: the number of nuclei of the i^{th} isotope per gram of target material

a_i: the activity of the i^{th} isotope, in Bq per gram of target material

The number of target atoms per gram of target material is given by:

$$n_{target} = \frac{N_A}{A_{target}}, \tag{62}$$

where N_A is Avogadro's number and A_{target} is the atomic weight of the target material.

Using the definition of cross section, the number of radioactive nuclei of the i^{th} isotope per gram of target material produced per unit time is thus given by:

$$n_i = \Phi \frac{N_A}{A_{target}} \sigma_{target,i}. \tag{63}$$

The number of nuclei of the ith isotope at any time is the result of two competing mechanisms, the production of these nuclei, given by expression (63) and their decay, due to their unstable nature. Their decay law is given by:

$$n_i(t) = n_i(0)\, e^{-t/\lambda_i}. \tag{64}$$

Using expressions (63) and (64), the number of nuclei of the i^{th} isotope at a given time t during the irradiation time will therefore be given by:

$$\begin{aligned} n_i(t) &= \Phi \frac{N_A}{A_{target}} \sigma_{target,i} \int_0^t e^{-\frac{t-\tau}{\lambda_i}} d\tau \\ &= \Phi \frac{N_A}{A_{target}} \sigma_{target,i} \lambda_i \left(1 - e^{-t/\lambda_i}\right). \end{aligned} \tag{65}$$

At the end of an irradiation period of duration T_{irr}, after a cooling time T_{cool} (see figure 36) the number of nuclei of the i^{th} isotope will therefore be given by

$$n_i(T_{irr}, T_{cool}) = \Phi \frac{N_A}{A_{target}} \sigma_{target,i} \lambda_i \left(1 - e^{-T_{irr}/\lambda_i}\right) e^{-T_{cool}/\lambda_i}. \tag{66}$$

The activity a_i of the i^{th} isotope, per gram of target material, is given by:

$$\begin{aligned} a_i(T_{irr}, T_{cool}) &= -\frac{dn_i}{dt}(T_{irr}, T_{cool}) \\ &= \frac{n_i(T_{irr}, T_{cool})}{\lambda_i}. \end{aligned}$$

Using expression (65) we finally obtain:

$$a_i(T_{irr}, T_{cool}) = \Phi \frac{N_A}{A_{target}} \sigma_{target,i} \left(1 - e^{-T_{irr}/\lambda_i}\right) e^{-T_{cool}/\lambda_i}. \tag{67}$$

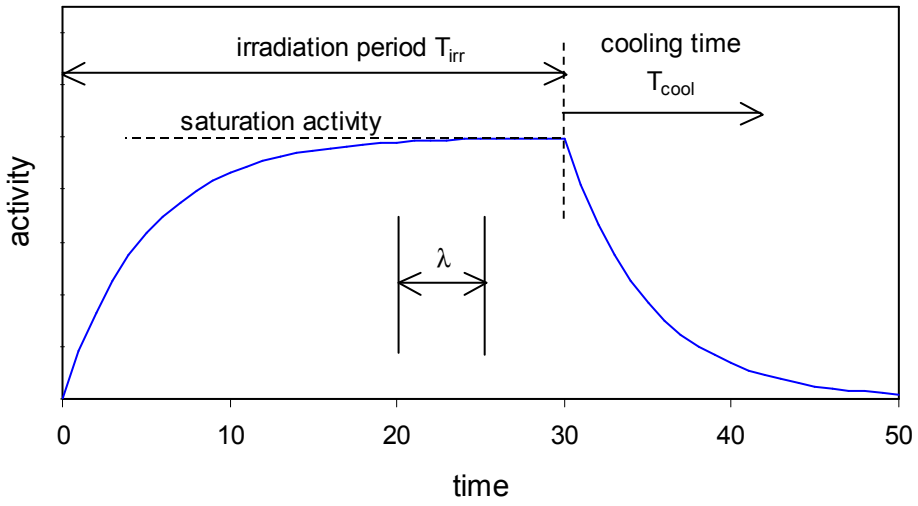

Figure 36 – The evolution of the activity as described in equation (67).

Expression (67) is the so-called "activation formula", describing the activity per gram of target material for a given isotope, following an irradiation of length T_{irr}, and after a subsequent cooling period T_{cool}.

5.3 Saturation activity

From formula (67) one sees that if the irradiation time t_i is large compared to the decay constant λ_i of a given isotope, the activity at zero cooling time for this isotope will reach a limit. This limit is called the saturation activity and is given by:

$$\left(-\frac{dn_i}{dt_c}\right)_{saturation} = \Phi \frac{N_A}{A_{target}} \sigma_{target,i} \,. \tag{68}$$

This is explained by the fact that part of the unstable nuclei that have been created during the irradiation have decayed before the end of the irradiation. The saturation value is therefore the maximum activity that can be obtained with a given particle flux. Although the irradiation time required for obtaining the saturation activity of a given isotope depends on the decay constant of this isotope, formula (68) shows that the value of the saturation activity itself is independent of the decay constant.

5.4 Physical processes involved in activation

5.4.1 Thermal and slow neutron reactions

Neutrons, due to their zero electric charge, can come within reach of the nuclear forces practically up to zero velocity, unlike charged particles such as protons, which need a certain energy to overcome the Coulomb barrier of the nucleus. As an example protons need a minimum of 5 MeV to undergo a nuclear reaction with an iron nucleus of the type (p,γ), whereas a neutron will undergo a (n,γ) reaction down to zero relative velocity.

The product of a (n,γ) reaction is an atom of the same kind but heavier by one neutron:

$$^{56}\mathrm{Fe}(n,\gamma)^{57}\mathrm{Fe}.$$

This reaction is called radiative capture.

5.4.2 Medium energy reactions

The Coulomb barrier prevents charged particles to induce nuclear reactions at low kinetic energies. In the energy range from a few MeV to about 50 MeV, protons can induce different types of reactions, such as (p,n), (p,pn), (p,2n), (p,p2n), (p,α), etc. Each of these reactions begins at a threshold energy that is higher than that of the preceding one. We have a similar situation for the neutron-induced reactions (n.p), (n.pn), (n,2p), (n,n2p), (n,α), etc .

5.4.3 Nuclear reactions at high energies

When a high energy proton or neutron interacts with a nucleus, neutrons, protons and other nuclear fragments are emitted. The target nucleus is converted to a different isotope, which has a high chance of being radioactive. As described in chapter 2, the intra-nuclear cascade may lead to an inter-nuclear cascade, producing further spallation reactions.

5.4.4 Photonuclear reactions

These are the nuclear reactions induced by high energy gamma rays. One can distinguish between giant resonance reactions, and photospallations, where nucleons or fragments are knocked out directly by the incoming photon.

5.5 Activation from electron accelerators

Many practical results about activation produced with electron accelerators are found in reference [18]. We reproduce a representative number of them hereafter.

5.5.1 Activation produced from accelerators below 35 MeV electron energy

Saturation activities for various targets for different electron energies are shown in table 12.

Target material	Radio-nuclide	$T_{1/2}$	Threshold (MeV)	Saturation Activity (GBq / kW) Accelerator energy [MeV]					
				10	15	20	25	30	35
Al	Na-24	14.96 h	23.71	–	–	–	0.02	0.37	1.1
	Al-26m	6.37 s	13.03	–	0.74	37.	140.	244.	425.
Fe	Mn-54	303 d	20.42	–	–	–	5.9	17.	22
	Mn-56	2.576 h	10.57	–	0.22	0.52	0.89	1.1	1.2
	Fe-53	8.51 min	13.62	–	0.37	9.6	19.	25.	27.
Ni	Ni-56	6.10 d	22.5	–	–	–	0.11	1.26	2.4
	Co-56	77.3 d	–	–	–	–	0.11	1.26	2.4
	Ni-57	36.0 h	12.19	–	3.7	44.	96.	133.	155.
	Co-57	270 d	–	–	3.7	44.	96.	133.	155.
Cu	Cu-61	3.32 h	19.73	–	–	0.004	8.5	24.	32.
	Cu-62	9.76 min	10.84	–	28.	177.	318.	407.	407.
	Cu-64	12.80 h	9.91	0.0004	22.	103.	155.	177.	185.

Table 12 – Saturation activities of the most important isotopes produced around electron accelerators with energy below 35 MeV.

5.5.2 Activation produced at high energy accelerators

As explained before, the number of radioisotopes that can be formed at higher energies is much larger. Tables 13.a to 13.e give an overview of the most important ones.

Material: Concrete					
Radio-nuclide	$T_{1/2}$	Threshold (MeV)	Parent isotope	Type	Saturation Activity (GBq / kW)
C-11	20.34 min	18.72	C-12	(γ,n)	0.13
O-15	123 s	15.67	O-16	(γ,n)	96.
Na-22	2.62 a	12.44	Na-23	(γ,n)	3.7
Mg-23	12.1 s	16.55	Mg-24	(γ,n)	0.27
Al-26m	6.37 s	13.03	Al-27	(γ,n)	0.034
Si-27	4.14 s	17.18	Si-28	(γ,n)	74.
K-38	7.71 min	13.08	K-39	(γ,n)	3.7
Fe-53	8.51 min	13.62	Fe-54	(γ,n)	3.7×10^{-3}

Table 13.a – Saturation activities produced in concrete at high energy electron accelerators.

Material: Aluminium

Radio-nuclide	$T_{1/2}$	Threshold (MeV)	Parent isotope	Type	Saturation Activity (GBq / kW)
Be-7	53.6 d	32.95	Al-27	(γ,sp)	4.8
C-11	20.34 min	33.53	Al-27	(γ,sp)	1.9
N-13	9.96 min	25.56	Al-27	(γ,sp)	0.5
O-15	123 s	44.43	Al-27	(γ,sp)	2.5
F-18	109.7 min	34.39	Al-27	(γ,sp)	5.2
Ne-24	3.38 min	33.11	Al-27	(γ,3p)	0.11
Na-22	2.62 a	22.51	Al-27	(γ,3n2p)	9.3
Na-24	14.96 h	23.71	Al-27	(γ,1n2p)	10.
Al-25	7.24 s	24.41	Al-27	(γ,2n)	1.4
Al-26	7.4×10^5 a	13.03	Al-27	(γ,n)	330.
Al-26m	6.37 s	13.03	Al-27	(γ,n)	330.
Mg-27	9.46 min	140	Al-27	(γ,π^+)	0.59

Table 13.b – Saturation activities produced in aluminium at high energy electron accelerators.

Material: Iron					
Radio-nuclide	$T_{1/2}$	Threshold (MeV)	Parent isotope	Type	Saturation Activity (GBq / kW)
Sc-46	83.9 d	37.41	Fe-54	(γ,sp)	7.4
V-48	16.0 d	25.86	Fe-54	(γ,sp)	15.
Cr-51	27.8 d	19.74	Fe-54	(γ,sp)	15.
Mn-52	5.60 d	20.89	Fe-54	(γ,np)	1.3
Mn-52m	21.1 min	20.89	Fe-54	(γ,np)	1.3
Mn-54	303 d	20.42	Fe-56	(γ,np)	22.
Mn-56	2.567 h	10.57	Fe-57	(γ,p)	1.2
Fe-52	8.2 h	24.06	Fe-54	(γ,2n)	2.1
Fe-53	8.51 min	13.62	Fe-54	(γ,n)	27.
Fe-55	2.60 a	11.21	Fe-56	(γ,n)	490.
Fe-59	45.6 d	–	Fe-58	(n,γ)	–

Table 13.c – Saturation activities produced in iron at high energy electron accelerators.

Material: Nickel					
Radio-nuclide	$T_{1/2}$	Threshold (MeV)	Parent isotope	Type	Saturation Activity (GBq / kW)
Ni-56	6.10 d	22.45	Ni-58	(γ,2n)	3.7
C0-56	77.3 d				3.7
Ni-57	36.0 h	12.19	Ni-58	(γ,n)	218.
C0-57	270 d				218.
C0-60	5.263 a	9.86	Ni-61	(γ,p)	3.7

Table 13.d – Saturation activities produced in nickel at high energy electron accelerators.

Material: Copper					
Radio-	$T_{1/2}$	Threshold	Parent	Type	Saturation

nuclide		(MeV)	isotope		Activity (GBq / kW)
Co-58	71.3 d	41.75	Cu-63	(γ,sp)	24.
Co-58m	9.2 h	41.75	Cu-63	(γ,sp)	24.
Co-60	5.263 a	18.86	Cu-63	(γ,n2p)	24.
Ni-63	92 a	17.11	Cu-65	(γ,np)	17.
Cu-61	3.32 h	19.73	Cu-63	(γ,2n)	32.
Cu-62	9.76 min	10.84	Cu-63	(γ,n)	407.
Cu-64	12.80 h	9.91	Cu-65	(γ,n)	185.
Cu-66	5.10 min	–	Cu-65	(n,γ)	–

Table 13.e – Saturation activities produced in copper at high energy electron accelerators.

Finally, as an example, table 14 lists the radionuclides detected in steel shielding around a 200 kW 20 GeV electron accelerator at zero cooling time [18]. Figure 37 shows the evolution of the activity of the various isotopes as a function of the cooling time.

Nuclide	$T_{1/2}$	Specific activity (t=0), [kBq/g]
Mn-56	2.576 h	4800.
Cr-51	27.8 d	590.
Mn-52	5.60 d	280.
Mn-54	303 d	190.
V-48	16 d	115.
Fe-59	45.6 d	59.
Sc-44m	2.44 d	37.
Sc-46	83.9 d	13.
K-43	22.4 h	7.8
Cr-48	23 h	7.0
Sc-48	1.83 d	6.3
Co-58	71.3 d	4.1
Co-60	5.263 a	2.2
Co-57	270 d	1.9

Table 14 – Example of activation of steel shielding in the vicinity of a 20 GeV linear accelerator [18].

An example of an activation spectrum measured on the ESRF Storage Ring injection septum stainless steel vessel is shown in figure 38.

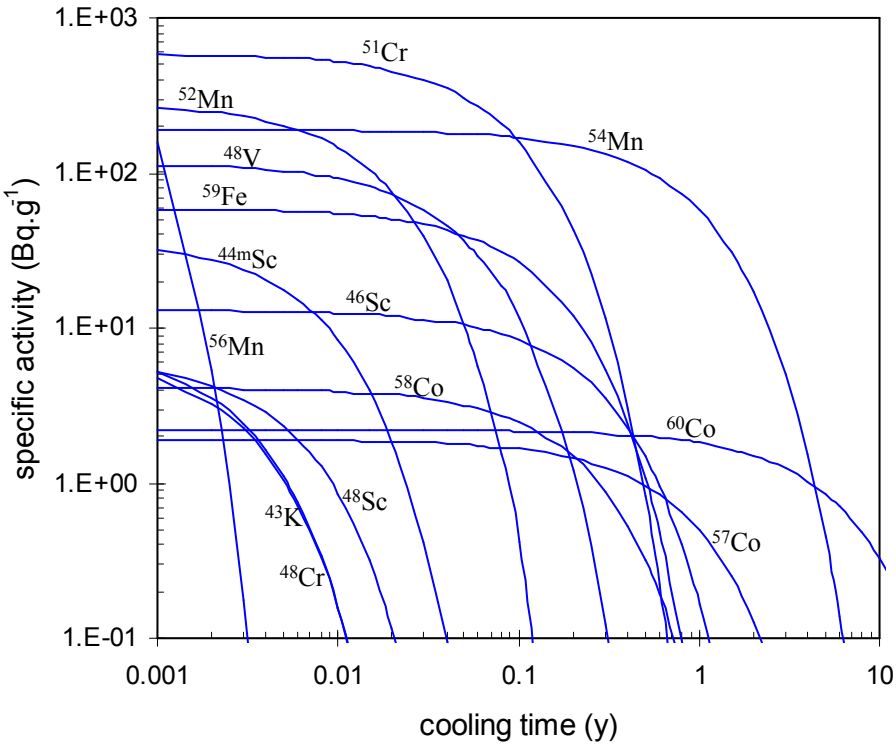

Figure 37 – Evolution of activity as a function of cooling time, corresponding to the initial activation given in table 14.

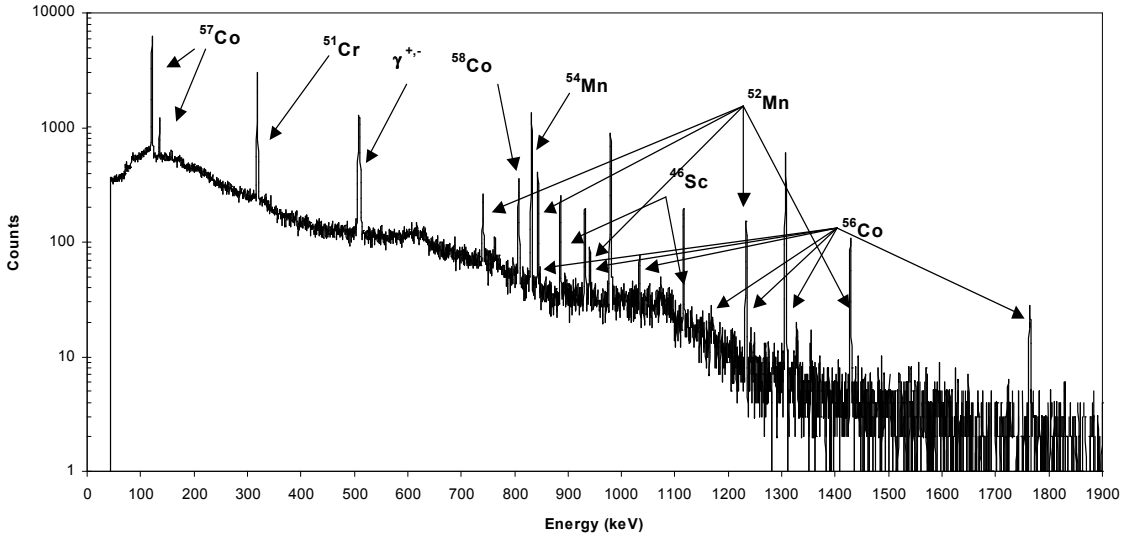

Figure 38 – Example of activation spectrum measured on a stainless steel vessel at the ESRF.

5.6 Activation from proton accelerators

As explained above, part of the activation will come from spallation reactions and part of it will come from thermal neutron activation. Table 15 lists the principal radioactive isotopes produced in accelerator structures by spallation reactions, as well as the corresponding gamma dose rates (dose rate at 1 m per Bq) [11].

Isotope	Half-life	Decay mode	$FSv.h^{-1}.Bq^{-1}$ at 1 m
^{7}Be	53 d	EC	7.8
^{11}C	20 min	β^+	140
^{18}F	1.8 h	β^+	132
^{22}Na	2.6 y	β^+	298
^{24}Na	15 h	β^+	560
^{46}Sc	84 d	β^+	283
^{48}Sc	1.8 d	β^+	455
^{48}V	16 d	β^+	397
^{51}Cr	28 d	EC	4.3
^{52}Mn	5.7 d	β^+	326
^{54}Mn	303 d	EC	114
^{56}Co	77 d	β^+	350
^{60}Co	5.3 y	β^+	340
^{65}Zn	245 d	EC	76

Table 15 – Principal radioactive isotopes produced in accelerator structures by spallation reactions.

Table 16 gives the properties of the most important isotopes near high energy particle accelerators formed by thermal neutron capture [11].

Parent isotope	Natural (%)	σ (barn)	Active isotope	Half-life	fSv.h-1 at 1m	
					per Bq	per g

^{23}Na	100	0.53	^{24}Na	15 h	560	7.7
^{40}Ar	99.6	0.61	^{41}Ar	1.8 h	150	1.4
^{44}Ca	2.0	0.70	^{45}Ca	165 h	-	-
^{50}Cr	4.3	17	^{51}Cr	28 d	4	0.04
^{55}Mn	100	13	^{56}Mn	2.6 h	2520	35
^{59}Co	100	37	^{60}Co	5.3 y	340	128
^{63}Cu	69	4.5	^{64}Cu	13 h	28	0.84
^{64}Zn	49	0.46	^{65}Zn	245 d	76	0.16
^{121}Sb	57	6.1	^{122}Sb	2.8 d	60	1.0
^{123}Sb	43	3.3	^{124}Sb	60 d	200	1.4
^{133}Cs	100	31	^{134}Cs	2.1 y	116	17
^{151}Eu	48	8700	^{152}Eu	12 y	45	750
^{153}Eu	52	320	^{154}Eu	8 y	286	190
^{186}W	28	40	^{187}W	1d	73	2.6

Table 16 – Properties of the most important isotopes near high energy particle accelerators formed by thermal neutron capture.

6. Radiation shielding

6.1 Introduction

Simple analytical models for shielding calculations, used to define the required thickness of the accelerator rooms, are based on the following expression:

$$\dot{H} = \sum_i \frac{F_{H_i} W e^{-X/\lambda_i}}{d^2} \tag{69}$$

with:

- $\dot{H}$ Dose equivalent rate, in $Sv \cdot h^{-1}$,
- W The primary beam loss rate, in kW,
- F_{H_i} Unshielded dose equivalent source term, in $Sv \cdot h^{-1}$ $(kW \cdot m^{-2})^{-1}$,
- X Shield wall thickness, in $g \cdot cm^{-2}$,
- λ_i Attenuation length for the ith radiation component, in $g \cdot cm^{-2}$,
- d Distance from the source to the dose point, in m.

Values for the unshielded dose equivalent source term F_{H_i} were obtained in chapter 4. In the present chapter we will essentially present values for the attenuation lengths λ_i and compare various shielding materials.

In chapter 4 the unshielded dose equivalent source terms were given in units $Sv \cdot m^2$ per proton or $Sv \cdot h^{-1}$ $(proton.s^{-1} \cdot m^{-2})^{-1}$. To obtain the source terms in the correct unit for expression (69) the following conversions must be used for protons of energy E GeV:

$$\begin{aligned} F_H\left(Sv.h^{-1}.m^2.kW^{-1}\right) &= \frac{1}{10^6 \cdot eE} \times F_H\left(Sv.h^{-1}.m^2 \ / \ proton \ per \ s\right) \\ F_H\left(Sv.h^{-1}.m^2.kW^{-1}\right) &= \frac{3600}{10^6 \cdot eE} \times F_H\left(Sv.m^2 \ per \ proton \ \right) \end{aligned} \tag{70}$$

with e = 1.6 10^{-19} C.

Before discussing in more detail the shielding against the two main radiation sources around accelerators, bremsstrahlung photons and neutrons, a few general remarks must be made concerning shielding materials.

Strictly speaking, whether a given material is suitable for shielding purposes or not depends only on its atomic weight A and/or its atomic number Z. Therefore for each type of radiation a large number of materials could be selected. However, in practice the range of useful materials is rather limited, because other criteria will determine the final choice, such as structural properties, cost, availability of space, etc. Finally the most economic, and most commonly used shielding material will be concrete. Another commonly used material is lead, for bremsstrahlung photon and especially X-ray shielding. Where neutron shielding is predominant special light materials such as dense polyethylene are used. Finally, earth is often used, because accelerator tunnels are often built underground. When shielding calculations take earth

layers into account, one has to warrant the thickness of this earth layer during the lifetime of the accelerator.

6.2 Shielding for electron accelerators

For shielding calculations around electron accelerators, one has to use the formula (69), with the unshielded dose equivalent conversion factors summarized in section 4.1.4. Table 17 gives values for the attenuation lengths for the most commonly used shielding materials [25].

Radiation Component	Shielding Material	Attenuation Length λ ($g \cdot cm^{-2}$)
Bremsstrahlung	Lead (11.34 $g \cdot cm^{-3}$)	25
	Concrete (2.3 $g \cdot cm^{-3}$)	49
	Iron (7.8 $g \cdot cm^{-3}$)	37
	Earth (1.6 $g \cdot cm^{-3}$)	70
	Dense Polyethylene (1.01 $g \cdot cm^{-3}$)	70
Giant Resonance Neutrons	Lead (backed by H)	161
	Concrete (2.3 $g \cdot cm^{-3}$)	40
	Iron (backed by H)	200
	Earth	33
	Dense Polyethylene	6.3
High Energy Neutrons	Lead	191
	Concrete (2.3 $g \cdot cm^{-3}$)	115
	Iron	138
	Earth	90
	Dense Polyethylene	62

Table 17 – Attenuation lengths for electron accelerator shielding.

6.3 Shielding for proton accelerators

6.3.1 Proton energies above 1 GeV

Analytical shielding models used for high energy proton accelerators (E > 1 GeV) are based on two fundamental ideas:

(1) At proton energies above 1 GeV the dose outside the shield wall will be caused by high energy neutrons (E ≥ 150 MeV) and low energy neutrons in radiation equilibrium with them. Because of the energy dependence of the inelastic cross sections for neutrons the attenuation in the shield can be described using a single dose attenuation length independent of neutron energy.

(2) The dose equivalent source term ($Sv.m^2$ per proton) is approximately proportional to the primary proton energy.

6.3.1.1 A. H. Sullivan's model

In chapter 4 we have derived the expressions (53) and (54) for the effective dose source term.

The attenuation mean free path λ, to be used in the shielding equation (69),in Sullivan's model is given in table 18 for various materials.

Material	Attenuation mean free path	
	$g.cm^{-2}$	cm
Water	85	85
Concrete	100	43
Earth	100	56
Baryte	112	35
Iron	132	17.8
Lead	194	17.0
Uranium	199	10.5

Table 18 – High energy particle attenuation mean free paths for various shielding materials [11].

6.3.1.2 The Moyer model

For a detailed description of the Moyer model, we refer to reference [21], pp. 282 – 307. We simply reiterate below the basic ideas of this model.

Figure 39 gives the general geometry used for shielding calculations in the case of a proton beam hitting a target.

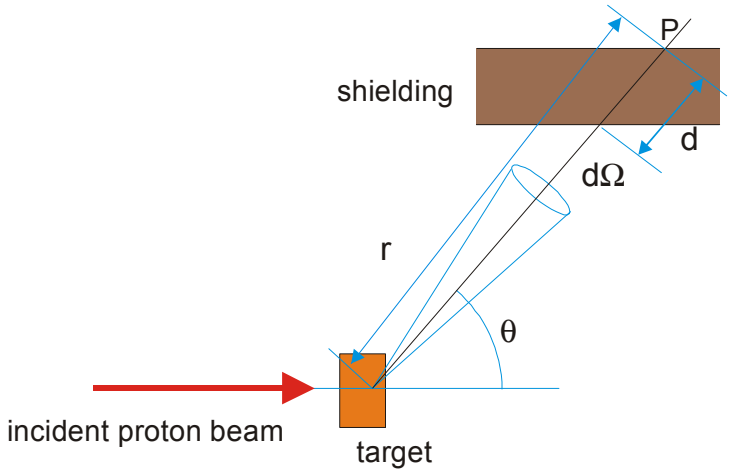

Figure 39 - Geometry used for shielding calculations

For shielding calculations we can assume that neutrons are the only secondary particles. Considering the target as an effective point source, we obtain the following expression for the dose equivalent rate $\dot{H}$ at a point P behind the shield wall:

$$\dot{H} = \frac{1}{r^2}\int F(E)B(E,\theta)\, e^{-d(\theta)/\lambda(E)}\, \frac{d^2n(E,\theta)}{dEd\Omega}\, dE\,, \tag{71}$$

where:

F(E): fluence to dose equivalent conversion factor,

B(E,θ): build-up factor,

λ(E): effective attenuation mean free path,

$\frac{d^2n(E,\theta)}{dEd\Omega}$: differential neutron yield.

The use of energy groups in neutron shielding is widely used, e.g. in nuclear reactor theory, and equation (71) can be written as:

$$\dot{H} = \frac{1}{r^2}\sum_i F_i B_i\, e^{-d(\theta)/\lambda_i}\left(\frac{dn}{d\Omega}\right)_i \tag{72}$$

In the Moyer model, the above expression is approximated by a single neutron energy group, based on the characteristic variation of neutron attenuation lengths as a function of energy, as shown in Figure 40 (high energy pions and protons in the hadronic cascade have very similar cross-sections). As shown in this figure, the actual variation in attenuation length with energy may be approximated by a step function:

λ (E > 150 MeV) = λ,

λ (E ≤ 150 MeV) = 0.

The essence of the Moyer model, therefore, is that the dose equivalent at any point outside the accelerator shield is largely governed by the simple line-of-sight propagation of the cascade generating particles (> 150 MeV) produced at the target. These particles have an attenuation length that is independent of their energy.

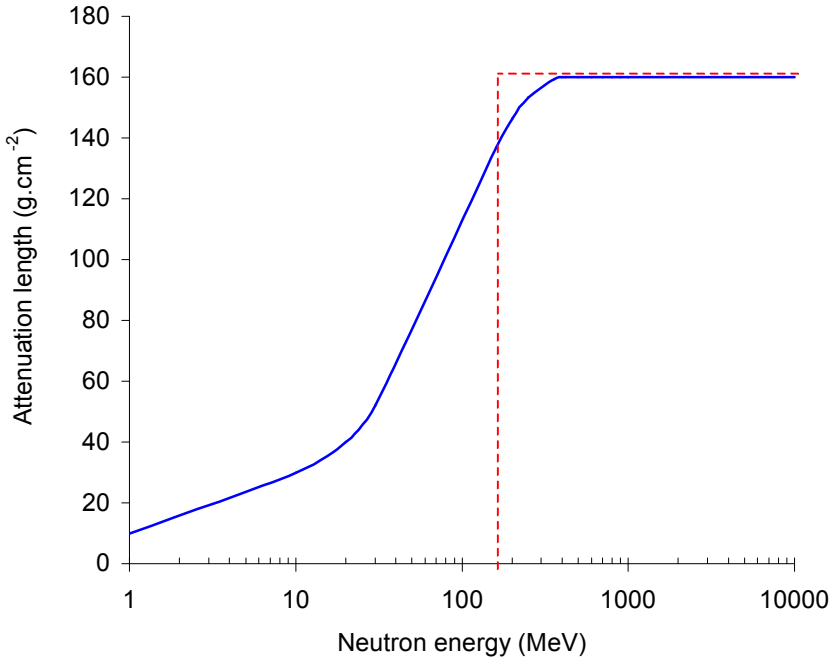

Figure 40 – Neutron attenuation length as a function of energy. The step-like function assumed in the Moyer model calculations is shown by the dashed line.

Using experimentally determined values for the source strength and for the angular distributions of the emitted hadrons, the following expression is obtained for the transverse shielding calculations for the typical accelerator geometry shown in Figure 41 [21]:

$$H = \frac{\Psi(E_p) N e^{-\beta\theta} e^{-\frac{D}{\sin\theta}}}{R^2 / \sin^2\theta}, \qquad (73)$$

where:

$\Psi(E_p) = 2.8 \times 10^{-13} E_p^{0.8}$ Sv.m^2,

$\beta = 2.3$ radians^{-1},

$D = \sum \frac{d_i}{\lambda_i}$,

N = number of protons interacting,

E_p is the proton energy in GeV.

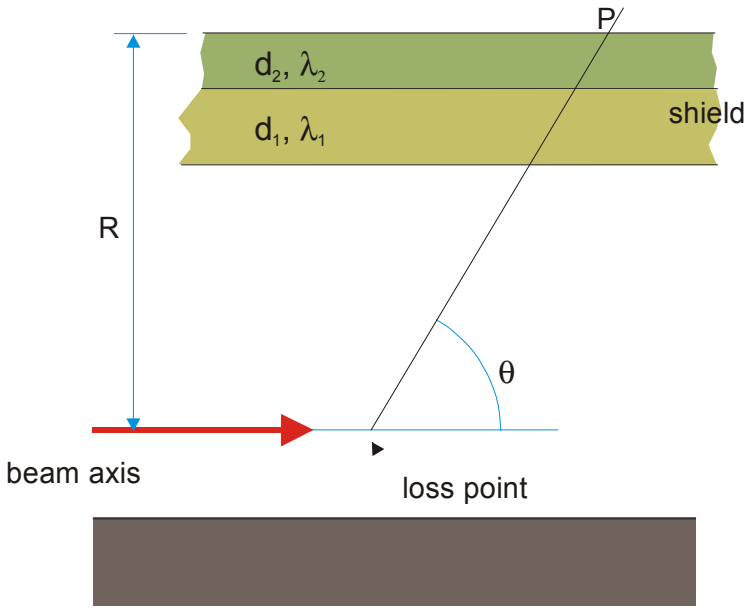

Figure 41 – Accelerator geometry used in the Moyer model calculations

For our calculations, the following attenuation length values were used [21]:

Concrete (2.35 g.cm^{-3}):	50 cm
Earth (1.8 g.cm^{-3}):	69 cm
Iron (7.4 g.cm^{-3}):	20.81 cm

6.3.2 Proton energies below 1 GeV

At energies below about 1 GeV protons lose a significant fraction of their energy by ionization before undergoing an inelastic reaction with a target nucleus. The secondary charged particles will most likely have lost all its energy by ionization before they can further cause spallation. Therefore the cascade neutrons produced by the incident protons will be the major component of the secondary radiation to be taken into account for shielding calculations.

As a consequence, for proton energies below 1 GeV the two basic assumptions for the high energy shielding model are no longer valid:

(1) The average neutron energy will be less than 150 MeV and consequently their attenuation mean free path in the shield will change with energy.

(2) The ionisation energy losses of both the primary protons and the secondary charged hadrons become important, inhibiting the full development of the hadronic cascade. As a consequence the approximate proportionality of the dose equivalent source term to the incident proton energy will no longer hold.

Analysis of experimental shielding data and results from Monte-Carlo calculations in this energy range show that it is still possible to use a simple analytical model of the form:

$$H = \frac{H_0 e^{-d/\lambda \sin\theta}}{R^2/\sin^2\theta}, \tag{74}$$

provided one uses the proton energy dependent values for the dose equivalent source term H_0 and for the neutron attenuation lengths λ [11,23].

In chapter 4 we have already derived the expressions (60) and (61) for the dose equivalent source term H_0.

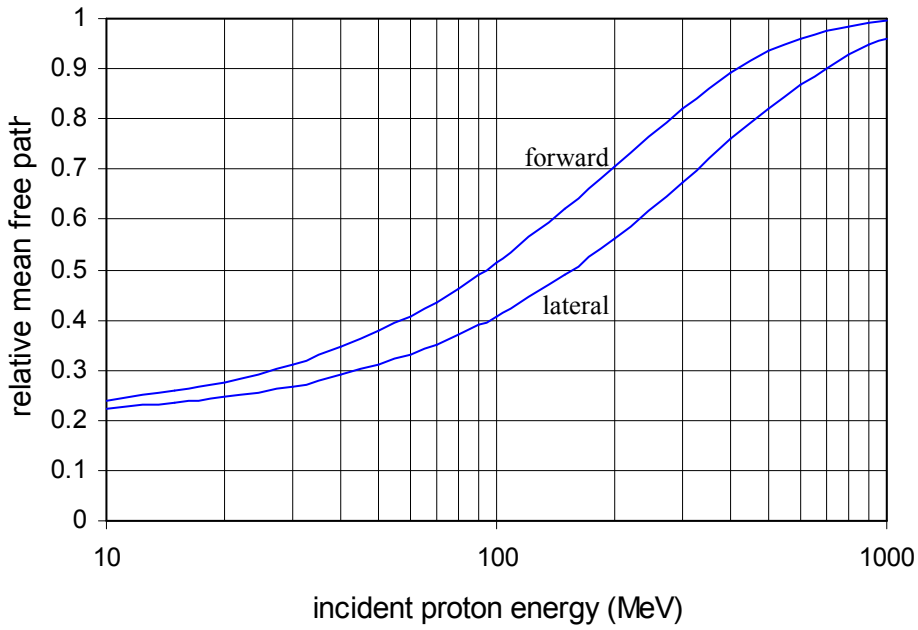

Figure 42 – Secondary particle attenuation mean free path in concrete, as a function of primary proton energy, relative to high energy mean free path.

The average secondary particle energy from interactions of protons below 1 GeV will be less than 150 MeV and their attenuation mean free path will therefore vary in the shield with energy. A review of experimentally determined radiation attenuation in concrete exposed laterally to secondary radiation from proton interactions of different energy showed that these mean free paths, expressed as a fraction of the limiting value at high energies λ_0 can be written as [11,23]

$$\lambda = \lambda_0 \left(1 - 0.8e^{-\alpha E}\right) \quad (75)$$

where α = 3 and E is the incident proton energy in GeV.

Computations of secondary radiation attenuation mean free paths show that the expression (75) can also be used in the forward direction, but with a value for α of 5.

Figure 42 shows these relative secondary particle attenuation mean free paths as a function of primary proton energy.

7. Radiation monitoring

7.1 Introduction

The main purpose of radiation protection measurements is to assess the actual and/or potential radiation exposure of people. Radiation measurements could also be used to obtain information about the energy distribution of leakage radiation, in order to determine the required shielding reinforcements. Permanent monitoring systems can be installed, providing interlocks to the accelerators.

Although one is interested in the dose in biological tissue, the measurement will of course be made via a probe of a different material. A given radiation monitor will use a specific effect (physical or chemical) that occurs in the interaction between radiation and matter, giving the monitor reading (e.g. electrical current). A radiation monitor will only be useful if there is a simple relationship, independent of the radiation energy over a sufficiently large energy range, between on the one hand the monitor reading and the absorbed dose in the probe medium, and on the other hand between the absorbed dose in the probe medium and the absorbed dose in biological tissue.

Radiation monitoring is a very specific topic. Accurate measurements are only possible if a full understanding of the secondary radiation fields exists, as well as a thorough knowledge of the instrument's characteristics and its limitations. A detailed discussion goes beyond the scope of this introductory course. We limit ourselves to a short description of the most commonly used instruments for photon and neutron measurements.

7.2 Charged particles detectors

7.2.1 Gas ionisation detectors

7.2.1.1 Principle of operation

Radiation passing through gases will lead to excitation or ionisation of the gas molecules, while electron-hole pairs will be created in semiconductors.

The mean energy w required to create an ion pair in a gas is more or less independent of the type and energy of the interacting particle, as well as of the nature of the gas, as illustrated in table 19.

	H_2	He	O_2	Ar	Air
electrons	36.3	41	31.0	26.4	34.0
alpha particles	36.5	44	32.4	26.4	35.3

Table 19 – Mean energy required to create an ion pair in different gases.

The number of ion pairs generated by a particle of energy E, which is completely absorbed in the gas, is given by

$$N_p = E/w \tag{76}$$

The dose rate dD/dt in the corresponding gas will be given by

$$\frac{dD}{dt} = \frac{w}{\rho_g V_g} \frac{dN_p}{dt} \tag{77}$$

where ρ_g and V_g stand for the density and volume of the gas. When the ions and electrons are separated via an electric field, the following relation exists between the ionisation current I and the dose rate (in case of charge collection without losses)

$$\frac{dD}{dt} = \frac{w}{e \rho_g V_g} I \tag{78}$$

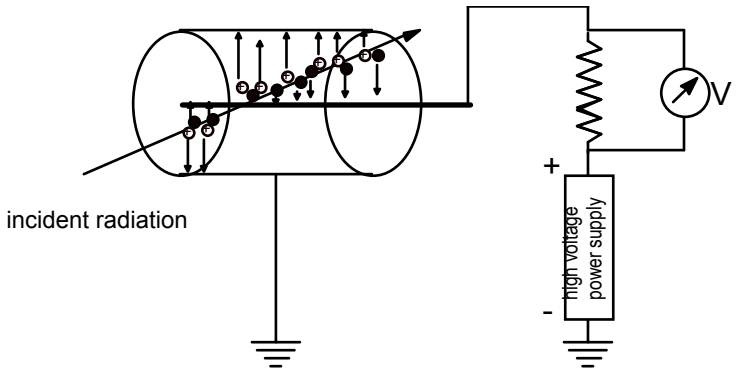

Figure 43 – Principle of a gas-filled ionisation monitor

The probe of a gas ionisation detector is a gas-filled volume, in which an electric field exists between two electrodes.

The collection of the charge carriers will depend on the applied voltage, the electrode configuration and the type of gas. The collected charge varies generally as a function of the applied voltage as shown in figure 44 (for cylindrical geometry). Five regions can be distinguished, as explained in table 20.

7.2.1.2 Ionisation chambers

Ionisation chambers are of great importance in radiation protection measurements. In the saturation range, the expression (78) is valid.

The portable ionisation chamber survey meter is certainly the reference instrument in the radiation survey around electron accelerators, where the bremsstrahlung radiation is the dominant secondary radiation.

In ionisation chambers there is always some loss in signal current, owing to recombination of the primary ions before they are collected at the electrodes, Especially when

used in pulsed radiation fields (linear accelerators, circular accelerators during injection, ..) significant signal losses could occur under certain extreme conditions.

Range	*Process*	*Radiation monitor*
I: recombination range	The generated charge carriers migrate to the corresponding electrodes, with recombination and diffusion losses.	
II: saturation range	Collection of charge carriers occurs with negligible loss due to recombination and diffusion. All primary generated charge carriers are collected.	Ionisation chamber
III: proportional range	The electrons are sufficiently accelerated to ionise the gas themselves. The collected charge is greater than the primarily generated charge.	Proportional counter
IV: restricted proportionality range	Space charge effects start to play a role, and recombination occurs.	
V: Geiger-Mûller range	The discharge covers the entire electrode configuration.	Geiger Müller counter
VI: continuous discharge range		

Table 20 – Different regions of operation of a gas-filled radiation monitor.

The collection efficiency f is the ratio of the number of ions collected to the number of ions formed by radiation in the gas. For steady radiation, detected by a parallel-plate chamber, f is given by [18]:

$$f = (1+x)^{-1} \approx 1 - x \tag{79}$$

where

$$x = \frac{1}{6}\frac{\alpha}{ek_1k_2}\left(\frac{qd^4}{V^2}\right) = \frac{1}{6}m^2\left(\frac{qd^4}{V^2}\right)$$

with:

α: recombination coefficient ($cm3 \cdot s^{-1}$),

k_1,k_2: mobilities of positive and negative ions respectively ($cm^3 \cdot s^{-1} \cdot V^{-1}$). The mobility is approximately inversely proportional to gas pressure. For air, at NTP, $k_1 \approx k_2 \approx 1.35\ cm^3 \cdot s^{-1} \cdot V^{-1}$,

q: ionisation rate ($C \cdot cm^{-3} \cdot s^{-1}$). It is equal to the saturation ionisation current (A) divided by the irradiated gas volume (cm^3),

e: electronic charge ($1.602\ 10^{-19}$ C),

d: the electrode spacing (cm),

V: the chamber bias voltage (V),

m^2: for air at NTP, $m^2 = 4.\ 10^{12}\ V^2 \cdot C^{-1} \cdot cm^{-1} \cdot s$.

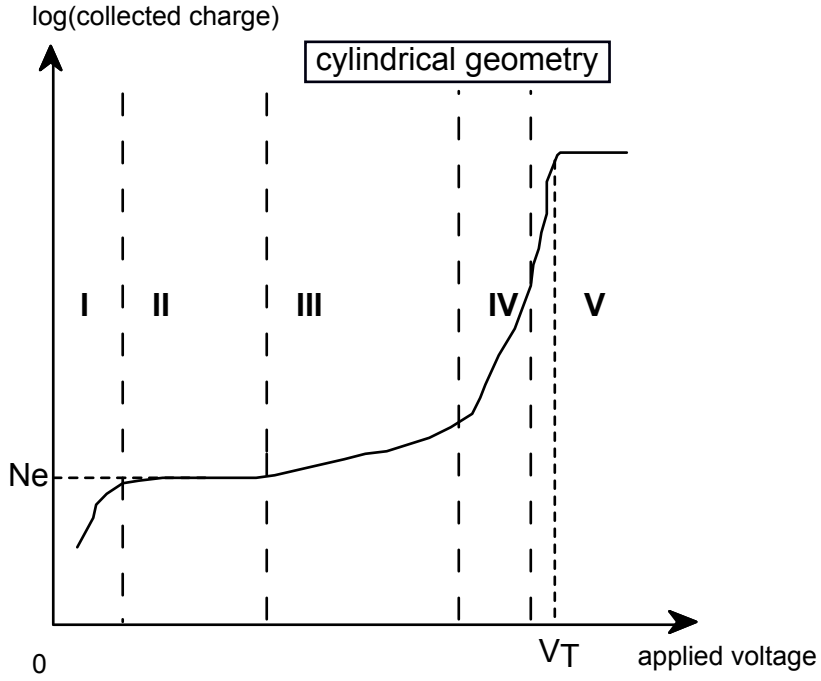

Figure 44 – different regions of operation of a gas-filled radiation monitor.

In the case of pulsed radiation, where the pulse length is much shorter than the ion collection time T_C, the collection efficiency is given by [18]:

$$f = u^{-1} \ln(1+u) \approx 1 - u/2 \tag{80}$$

where:

$$u = \frac{\alpha}{(k_1 + k_2)e}\left(\frac{\rho_0 d^2}{V}\right) = \mu\left(\frac{\rho_0 d^2}{V}\right)$$

with:

ρ_0: the initial density of positive or negative ionisation charge released by one radiation pulse ($C \cdot cm^{-3}$),

μ: for air at NTP, $\mu = 3.3\ 10^{12}\ V \cdot C^{-1} \cdot cm$.

The collection time T_C is given by

$$T_C = \frac{2d^2}{(k_1 + k_2)V}$$

For cylindrical or other chamber geometries closely related formulae apply.

In the case of electronegative gases (e.g. air, O_2, NH_3, NO, ...) the electrons attach themselves quickly to a molecule. Then k_2 is about equal to k_1 because the negative and positive charge carriers have the same mass and therefore diffuse at the same rate. In noble gases and some other gases (H_2, N_2, CO_2, BF_3, ...) the negative charge carriers are primarily free electrons with much greater mobility k_2. In these gases, k_2 is about two orders of magnitude larger, and recombination effects are correspondingly less severe.

7.2.1.3 Geiger-Müller counters

Geiger-Müller counters operate in the region V of figure 44. The output charge pulses from the detector are independent of the amount of ionisation produced by the incident particle. Their magnitude is constant, and depends only on the amount by which the applied voltage exceeds the threshold voltage V_T. The multiplication rate of the initial ionisation is very high (Townsend avalanche). A positive ion sheath is formed around the entire anode, and moves slowly to the cathode. The space charge produced by this positive ion sheath lowers the effective potential of the anode to such an extent that no further electron multiplication takes place and the discharge thus quenches. However, when the positive ions reach the cathode they may eject electrons which can reactivate the detector and produce new discharges. Several methods exist for suppressing these oscillatory discharges. In case of a noble gas filling, the most common quenching technique exists in adding a small quantity of a halogen gas, usually bromine, to the gas filling of the detector.

The Geiger-Müller counter is certainly the most handy survey monitor which is used to detect radiation. From the principle of its operation it indeed detects radiation, rather than measuring it. Its reading will therfore often be expressed in events per time (e.g. counts per minute). They come in very compact, light weight monitors. Their high sensitivity and fast response time make them indispensable for all sorts of radiation checks, especially when they are equipped with an audible alarm. Therefore, if some radiation is detected by a Geiger-Müller detector, accurate measurements should be made with an ionisation chamber.

Geiger-Müller counters have a relative long deadtime, because of the discharge process and the consequent slow collection of the positive charges. This dead time is typically of the order of 100 µs. Therefore G-M counter will largely underestimate dose rates in pulsed radiation. Indeed, in pulsed accelerators, the pulse length is most of the time << 100 µs, and because of its high dead time, the GM counter will not be able to detect more than one count per pulse!

7.2.2 Thermoluminescent dosimeters (TLDs)

Thermoluminescence is one of the possible processes that can occur in certain solids. Radiation can create a redistribution of the electrons in the different energy levels. One should assume that between the valence and the conduction band two types of centres exist: activators and traps respectively. Due to the effect of ionising radiation, electrons can be excited out of the valence band to the conduction band. A number of them will immediately recombine with the holes in the activator centres, emitting fluorescent radiation. The others will be captured by the traps. If the material is afterwards heated, these electrons will reach the conduction band again, and some of them will recombine with the activator holes, emitting thermoluminescent light. The principle of this is illustrated in figure 45.

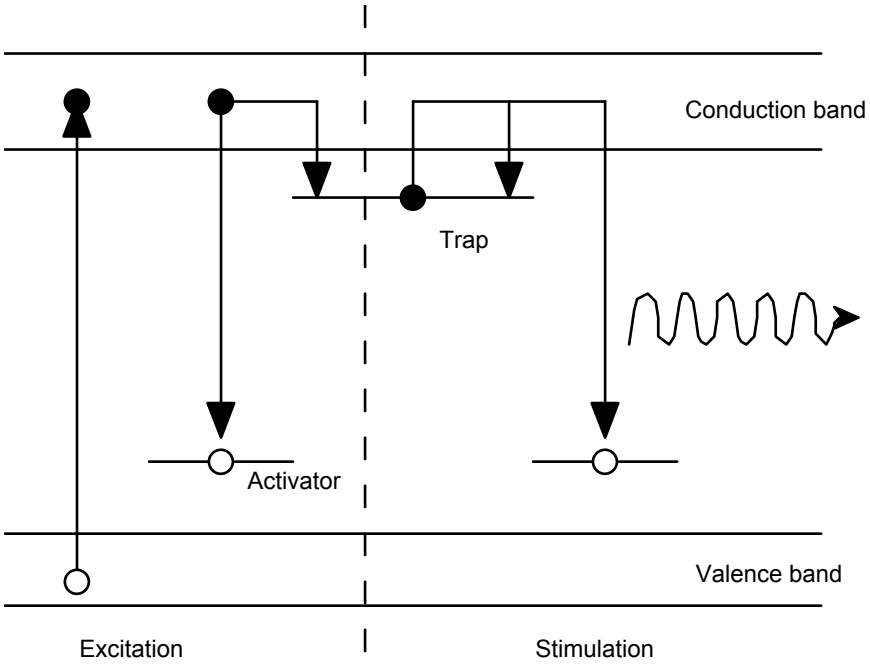

Figure 45 - Principle of thermoluminescent detectors

Reaction	Q value (MeV)
Elastic scattering ^{6}Li	-
Inelastic scattering ^{6}Li	-1.47128
^{6}Li(n,α)^{3}H	4.786
^{6}Li(n,p)^{6}He	-2.7336
Elastic scattering ^{7}Li	-
Inelastic scattering ^{7}Li	-0.477484
^{7}Li(n,d)^{6}He	-7.76382
Elastic scattering ^{19}F	-
Inelastic scattering ^{19}F	-0.11
^{19}F(n,p)^{19}O	-4.0363
^{19}F(n,d)^{18}O	-5.76892
^{19}F(n,t)^{17}O	-7.55613

Table 21 - Selected neutron interactions in LiF materials

The use of LiF thermoluminescent material for neutron detection uses the reactions listed in table 21.

The cross-sections for ^{6}Li and ^{7}Li behave in a similar way, except for the huge cross section for the reaction ^{6}Li(n,α)^{3}H (see figure 46). Combinations of ^{6}LiF and ^{7}LiF detectors therefore allow a rough separation of the thermal neutron contribution in mixed neutron-gamma fields.

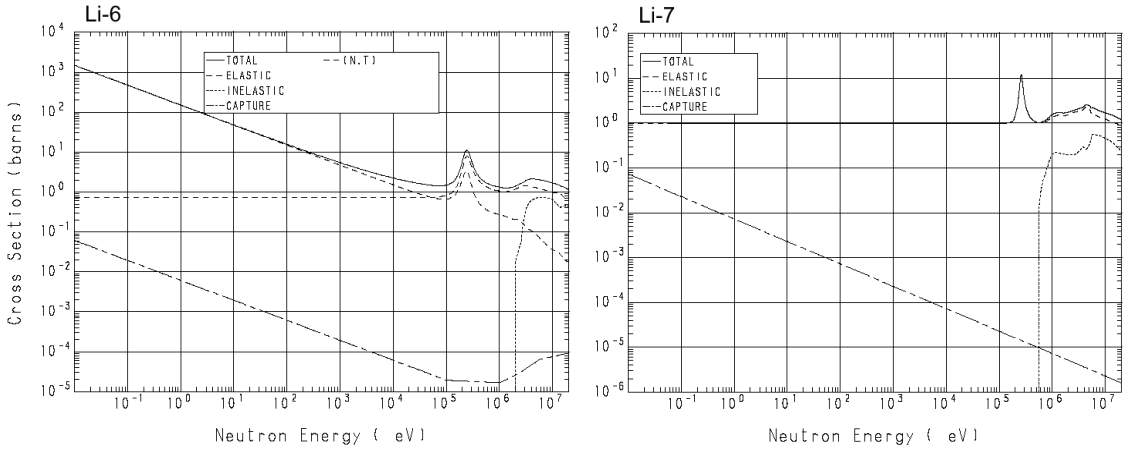

Figure 46 - Neutron cross-sections for ^{6}Li and ^{7}Li (copyright © 1997 JAERI [7]). The ^{6}Li(n,α)^{3}H cross section is indicated as (N,T) in the Li-6 graph.

7.2.3 Semiconductor detectors

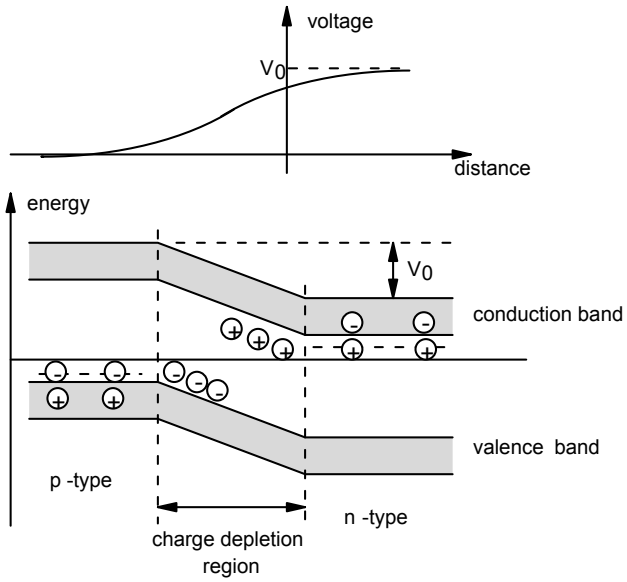

Figure 47 - Schematic representation of the electron band structure near a p-n junction

Figure 47 illustrates the principle of p-n junction detectors. In the junction region between a n-type and a p-type semiconductor, the donor levels in the n-type material are fully ionized and the excess electrons supplied by them to the conduction band diffuse across the junction to the

p-type side, where some may recombine with the holes. Similarly the acceptor levels nearest the junction are fully ionized and the excess holes created by them in the valence band also diffuse across the junction to the n-type side where again some may recombine with electrons. This results in a space charge due to the fixed fully ionized donors and acceptors which gives rise to a potential barrier V_0 and creates a region depleted of free carriers. The ionization produced by a charged particle passing through the charge depletion region can be readily detected. If an external reverse bias voltage V_B is applied to the junction such that the n-type part is made more positive with respect to the p-type part the depth of the charge-depleted region is increased. It is this increase in depth of the charge depletion region by the application of a reversed bias voltage which is the basic factor governing the properties of p-n junction detectors.

7.3 Neutron detectors

7.3.1 Moderated thermal neutron detectors

A moderated thermal neutron detector consist of a detector with a high efficiency to thermal neutron placed inside a moderator-attenuator whose structure is such that the response function of the instrument reproduces the conversion curve from neutron fluence to H*(10) ambient dose equivalent over a wide range of energies.

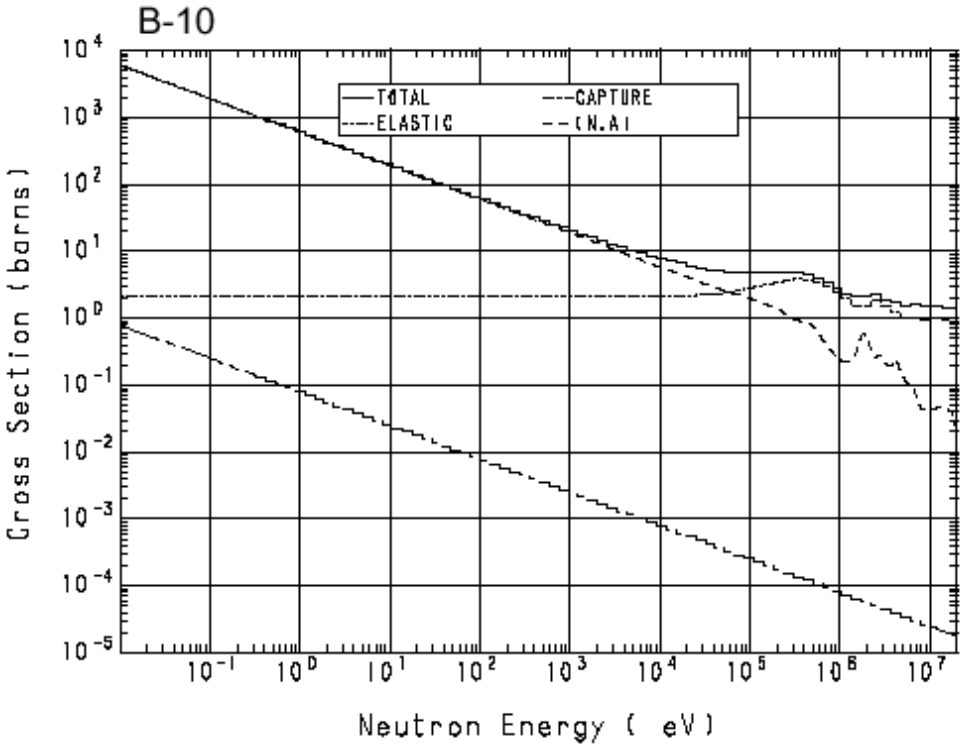

Figure 48 - Neutron cross-sections of ^{10}B, including the $^{10}B(n,a)^7Li$ cross section (reference [7])

BF_3 filled detectors use the reaction:

$$n + {}^{10}_{5}B \rightarrow \begin{cases} \alpha + {}^{7}_{3}Li + 2.310\,MeV\,(94\%) \\ \alpha + {}^{7}_{3}Li + 2.792\,MeV\,(6\%) \end{cases} \tag{81}$$

where the alpha particle that is produced is detected.

^{3}He filled proportional counters use the reaction:

$$n + {}^3He \rightarrow p + {}^3H + 765keV \tag{82}$$

where both the proton and the ^{3}H are detected.

These gas proportional detectors are efficient only for thermal (low energy) neutrons. This can be seen from figures 48 and 49, showing the relevant neutron cross-sections for both detectors. These figures are copyright (c) 1997 by the Japan Atomic Energy Research Institute (JAERI) and are copied with kind permission of JAERI [7].

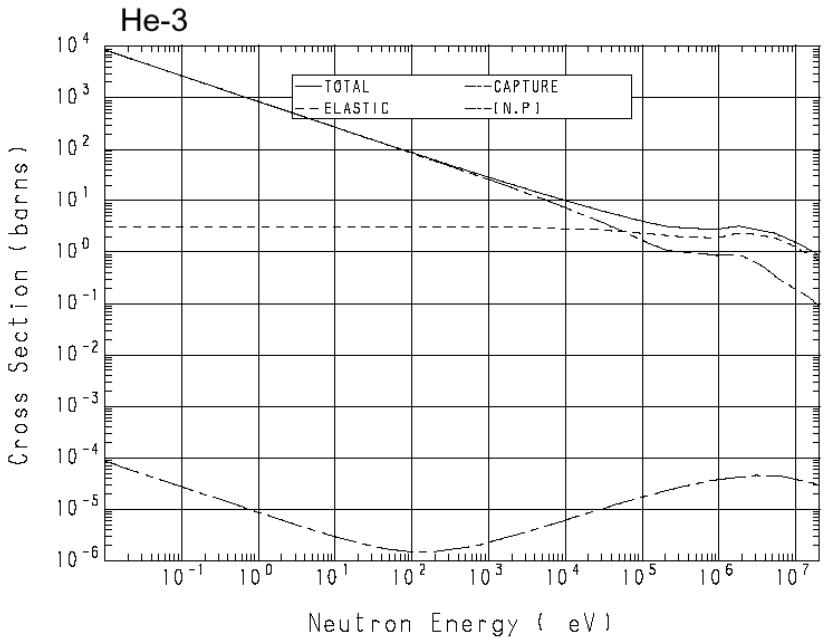

Figure 49 - Neutron cross-sections of ^{3}He, including the ^{3}He (n,p) ^{3}H cross section (reference [7])

It is therefore necessary to slow down the neutrons to a level where the probability of interaction is statistically significant. Many modern moderated neutron monitors are based on the original design from Andersson and Braun [26].

The original Andersson Braun neutron rem counter consists of a BF_3 proportional counter surrounded by a shield made of polyethylene and boron plastic that gives the appropriate amount of moderation and absorption to the impinging neutrons to obtain a response as a function of neutron energy in accordance with the rem.n^{-1}.cm^2 curve published in the US National Bureau of Standards Handbook 63 in 1957, known as the Radiation Protection Guide (RPG) for neutrons.

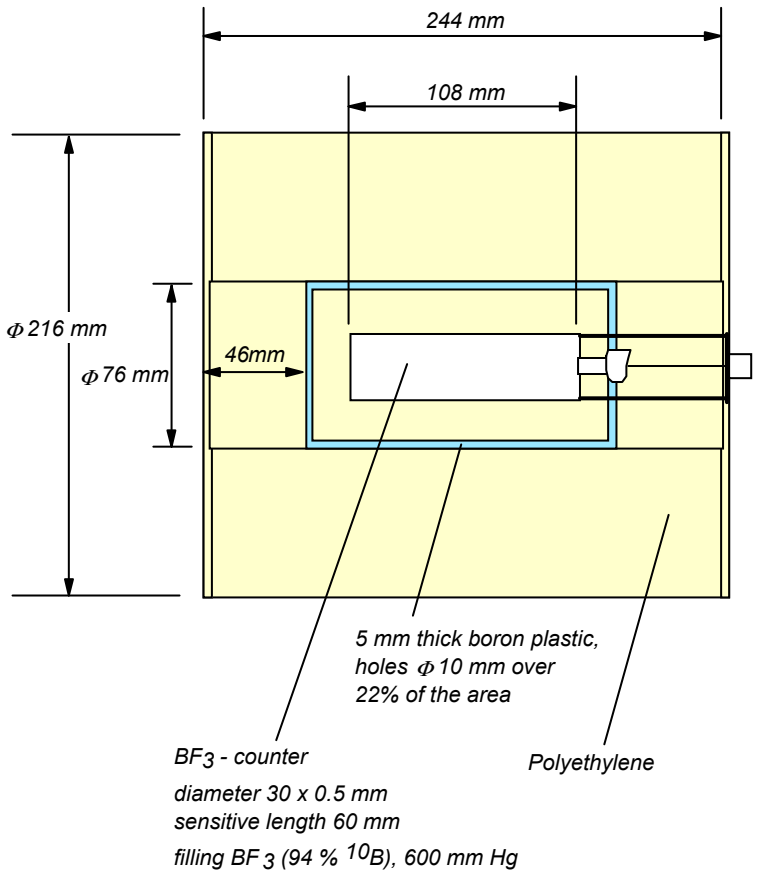

Figure 50 - Andersson - Braun neutron rem counter NRC III [26]

Figure 50 shows the design of their Neutron Rem Counter NRC III, designed as a portable monitor (total weight 8.5 kg).

Figure 51 shows the comparison between the measured response of the NRC III counter and the RPG from the US NBS Handbook 63, as a function of neutron energy, for radiation at right angles to the detector axis and for radiation parallel to the detector axis [26]. The counter has a useful energy range from thermal neutrons up to about 15 MeV.

Figures 52 and 53 show two examples of modern moderated neutron meters. The Studsvik neutron monitor 2222 uses a BF_3 counter with a polyethylene and boron plastic moderator. The LB 6411 rem counter from EG&G Berthold consists of a ^{3}He proportional counter inside a 25 cm polyethylene moderator sphere, including internal Cd absorbers and perforations.

The Radiation Protection Group of Milan of the INFN has developed a new Andersson-Braun type monitor. Based on a BF3 counter, the complex moderator/attenuator that includes polyethelene and boron doped synthetic rubber moderators with perforations, surrounded by a lead layer, has allowed to extend the monitor's useful energy range up to several 100 MeV [27, 28]

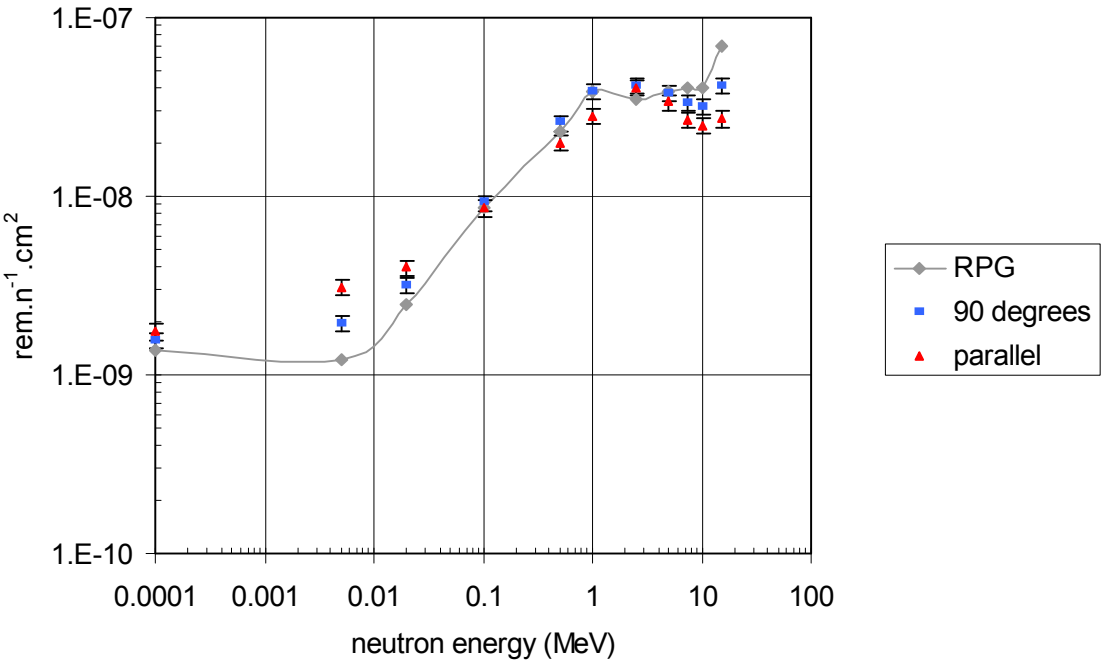

Figure 51 – Comparison between the response of the neutron rem counter NRC III and the RPG from the US NBS Handbook 63, as a function of neutron energy, for radiation at right angles to the detector axis and for radiation parallel to the detector axis [26].

Figure 52 – The Studsvik neutron monitor 2222

Figure 53 – The EG&G Berthold LB 6411 ambient dose equivalent rate meter

7.3.2 Superheated emulsions

Superheated emulsions consist of uniform dispersions of over-expanded halocarbon and/or hydrocarbon droplets suspended in a tissue equivalent polymeric or aqueous gel. The principle of these superheated emulsions is similar to the operation of bubble chambers, since long used in high-energy physics.

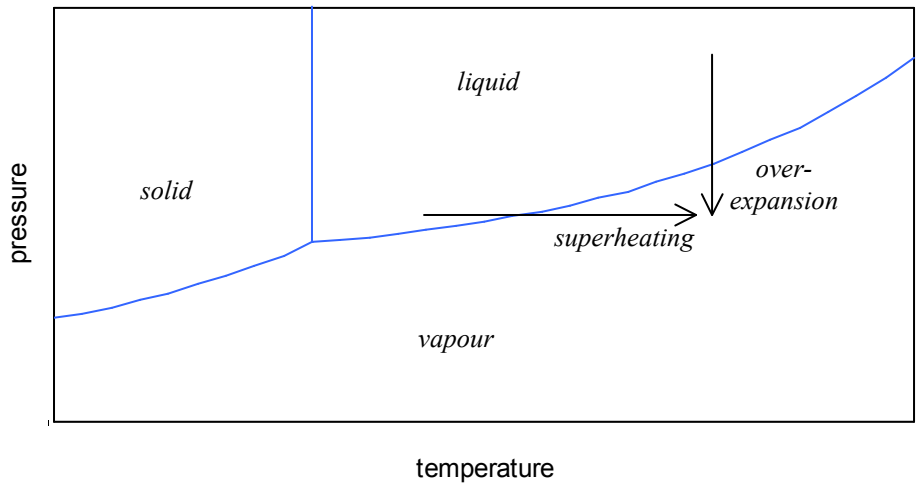

Figure 54 – Phase diagram of a material

A fluid is superheated (or over-expanded) when it is in liquid form at temperature and pressure values corresponding to the vapour region (see phase diagram in figure 54). This metastable state is normally fragile and short-lived due to heterogeneous nucleation starting from microscopic particles or gas pockets present at the interface surfaces. However, a superheated fluid can be kept stable by fractionating it into droplets, dispersed into an immiscible

and inert host fluid. This process called emulsification creates perfectly smooth spherical interfaces, free from nucleating impurities or irregularities. The droplets should be moderately superheated, i.e. their operating temperature should be close to the boiling point, and the emulsifier material must be clean and de-gassed to be free of heterogeneous nucleation sites.

The use of superheated emulsions as radiation detectors is based on the fact that charged particles generate trails of sub-microscopic vapour cavities inside the droplets. When these cavities exceed a critical size they keep growing until the whole droplet evaporates. Sub-critical cavities however collapse back to the liquid phase under the action of external pressure and surface tension. The energy and the critical size being necessary for bubble nucleation depend on the composition and the degree of superheat of the emulsion.

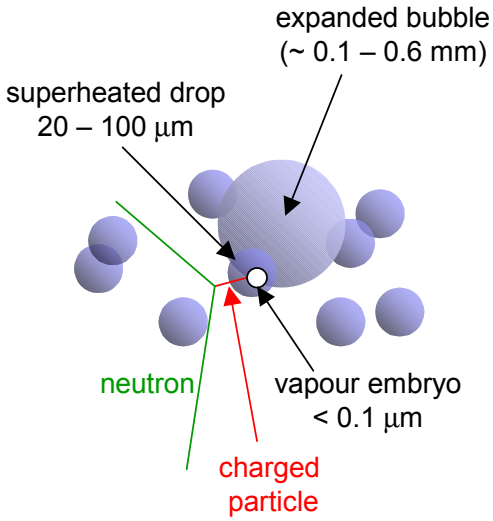

Figure 55 – Bubble formation steps in superheated emulsions (reference [28]).

Superheated emulsions are able to detect neutrons and discriminate low ionising radiations, such as photons and electrons. The bubble formation is induced by highly ionising charged particles generated through neutron interactions inside or next to the superheated droplets.

Various passive dosimeters based on superheated emulsions exist, meeting the current requirements on energy dependence of the response and on minimum detection threshold. These dosimeters rely on the optical counting of the bubbles, which remain trapped in the polymer gel after their formation. This counting can be done by eye or by means of automated camera systems.

Active devices are counting the bubble nucleation acoustically: the rapid bubble expansion associated with the boiling of superheated droplets is accompanied by oscillating pressure pulses with a duration of ~ 10 ms, which can be easily recorded using piezo-electric transducers.

Figure 56 shows the fluence energy response of the REMbrandt superheated drop detector versus the fluence to ambient dose equivalent conversion factor (ICRP-60) (taken from reference [30]).

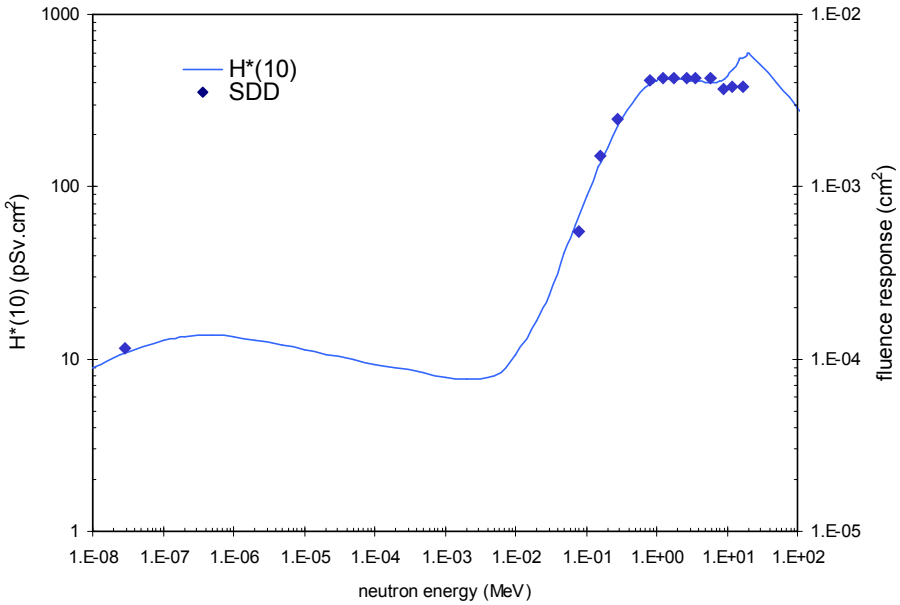

Figure 56 - Fluence energy response of the REMbrandt superheated drop detector versus fluence to ambient dose equivalent conversion factor (ICRP-60) (taken from reference [30]).

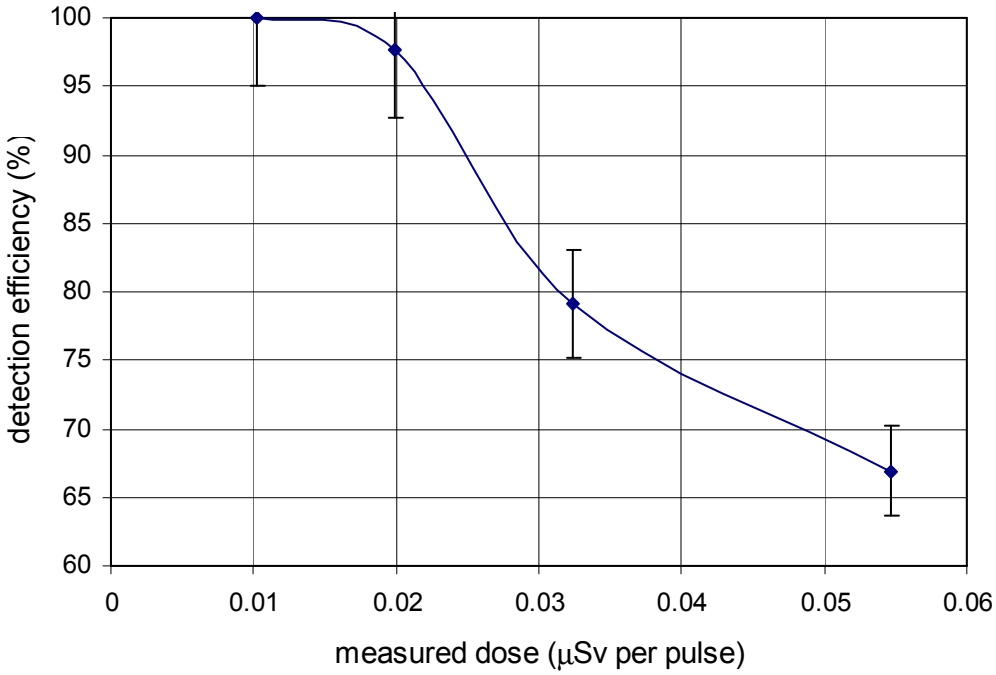

Figure 57 - Measured pulsed radiation efficiency of the Apfel REMBrandt monitor, giving the detection efficiency (%) as a function of the measured dose (μSv) per pulse, for a repetition frequency of 1 Hz.

An idea of the efficiency to detect pulsed radiation of the REMbrandt monitor is obtained from figure 57, showing the detection efficiency as a function of the measured dose per pulse. These data were obtained by the author at the ESRF using 1 μs long beam pulses with a repetition frequency of 1 Hz.

Finally, using different superheated liquids having different detection thresholds it is in principle possible to carry out neutron spectroscopy measurements.

7.3.3 Operational dosimetry

7.3.3.1 Diode-based electronic dosimeters

Combining semiconductor junction detectors with neutron sensitive converters, one can develop electronic dosimeters sensitive to neutrons. The difference in signal between a diode, covered with a ^{10}B implanted polyethylene converter and a diode without this converter provides a measurement for the neutron dose equivalent, as shown schematically in figure 58.

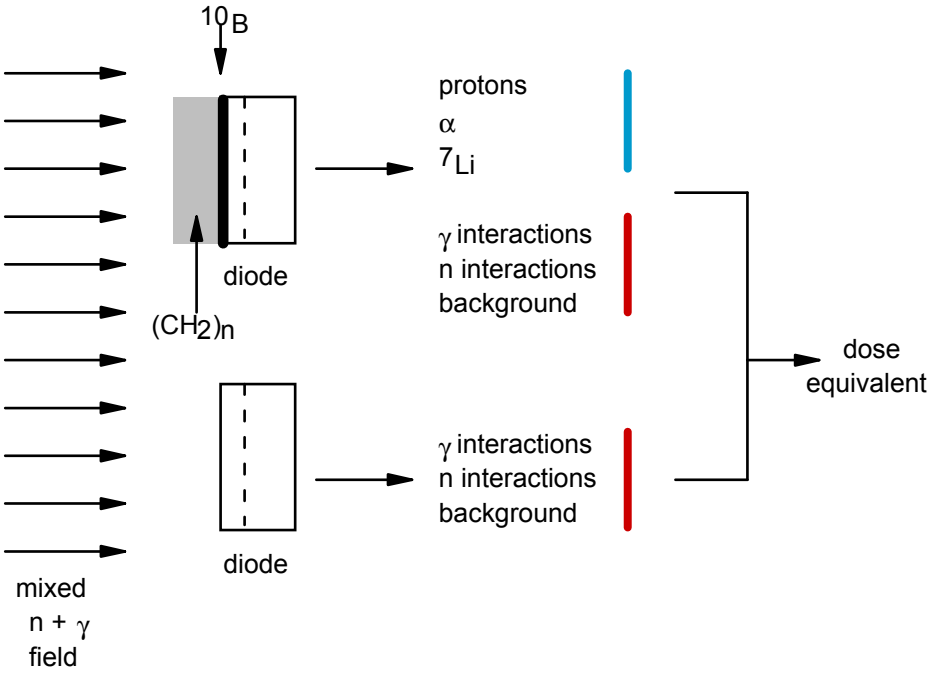

Figure 58 – Schematic diagram of electronic neutron dosemeter

Figure 59 shows the EPD-N electronic dosimeter from the company Siemens, giving dose equivalent readings for photons and neutrons. For neutrons it is supposed to give reliable results in the energy range from thermal energies to about 15 MeV [31].

7.3.3.2 Direct ion storage (DIS) dosimeters

A recent development in personal dosimetry is the Direct Ion Storage (DIS) technology. The DIS dosimeter combines the use of miniaturized ion chambers and MOSFET analog memory technology.

The operation principle of MOSFETs is well known: in the case of a p-substrate and n-type source and drain, thermal diffusion creates a positive charge on the metal strip between the

p-type silicon and the SiO_2 layer, creating an n-type inversion layer in the p-type substrate, near the metal boundary. By changing the bias voltage of the floating gate, the width of this inversion layer is modified. The resistance between source and drain can therefore be modified via the floating gate bias voltage.

Figure 59 – Picture of the EPD-N photon and neutron electronic dosimeter from the company Siemens [31].

When using MOSFETs as analog memory devices, a charge is put on the floating gate by putting a tunnelling current through the insulating oxide surrounding the floating gate; the oxide is a perfect insulator under typical low bias voltages but can indeed be made sufficiently conductive to charge (or discharge) the floating gate when applying a sufficiently high bias voltage.

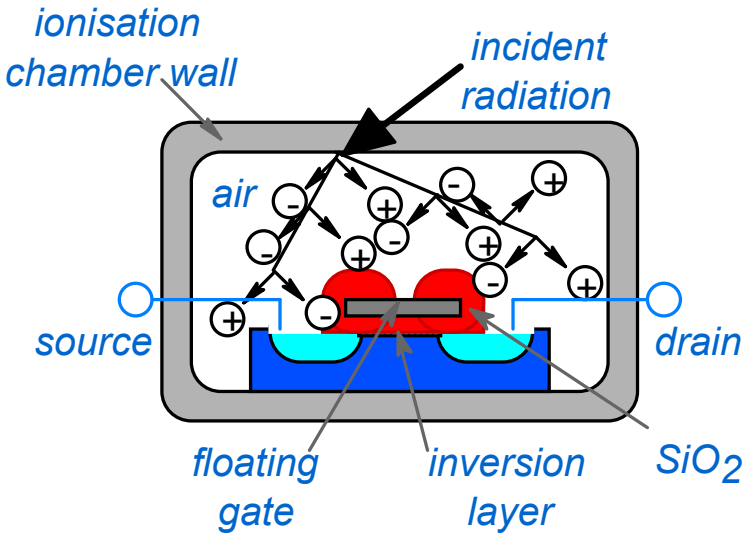

Figure 60 – Principle of a Direct Ion Storage dosimeter

The principle of the DIS dosimeter is directly based on this analog memory operation. Figure 60 shows the schematic layout of a DIS dosimeter. An opening in the oxide layer surrounding the floating gate is foreseen, such that the floating gate comes in direct contact with the air of the ionisation chamber into which the MOSFET is placed; the MOSFET's substrate being electrically connected to the ionisation chamber's conducting wal. The floating gate is initially put to a positive bias voltage (typically 30 V) and acts as the positive electrode of the ionisation chamber, attracting the electrons produced inside the air volume by the secondary radiation created in the chamber wall. The positive bias voltage of the floating gate thus linearly changes with the number of electrons collected (proportional to the integrated dose) and a resistive measurement between source and drain gives a direct indication of the dose.

Figure 61 shows a photograph of a photon-sensitive DIS badge (used for X-rays, γ and β radiation), developed by the company RADOS Technology [32]. The distance between the chamber wall and the floating gate is 2 mm, a 30 V bias therefore creates a field strength of 15 $kV.m^{-1}$, sufficient to measure dose rates up to 10 $Sv.h^{-1}$ without saturation (the bias voltage should not decrease below 10 $kV.m^{-1}$, defining the dose range of the device). A dose of 1 μSv typically decreases the floating gate bias with 2 mV. Inside one DIS badge 5 individual ionisation chambers are incorporated to obtain the required range from 1 mSv up to 40 Sv, and to measure both the deep and shallow ambient dose equivalents. The walls of the chambers are made of tissue equivalent A-150 plastic. The three ion chambers used to measure the deep dose equivalents have an input wall thickness of $1g.cm^{-2}$, whereas the two chambers used to measure the shallow dose equivalent have an input window of 7 $mg.cm^{-2}$.

Figure 61 – Photograph of the photon-sensitive DIS badge developed by the company RADOS Technology [32].

DIS neutron badges are also being developed by RADOS Technology for neutron dosimetry. Dosimeters with a big response to fast neutrons are built using wall material consisting of tissue equivalent A-150 plastic mixed with polyethylene. The recoil protons from the (n,p) reaction are detected. The detection of neutrons of lower energies, especially thermal neutrons, is enhanced by adding ^{10}B or ^{6}Li to the wall material under the form of BN or $LiNO_3$ [32]. Figure 63 shows the energy response of these neutron DIS dosimeters [33].

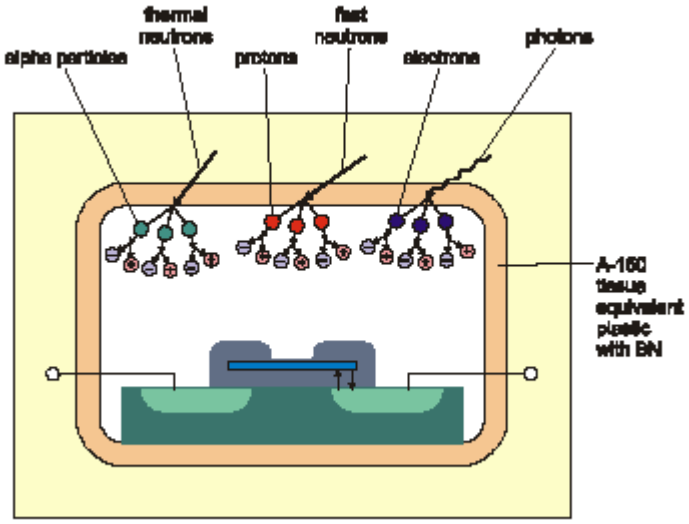

Figure 62 – Principle of neutron detection in DIS dosimeters (taken from reference [33].

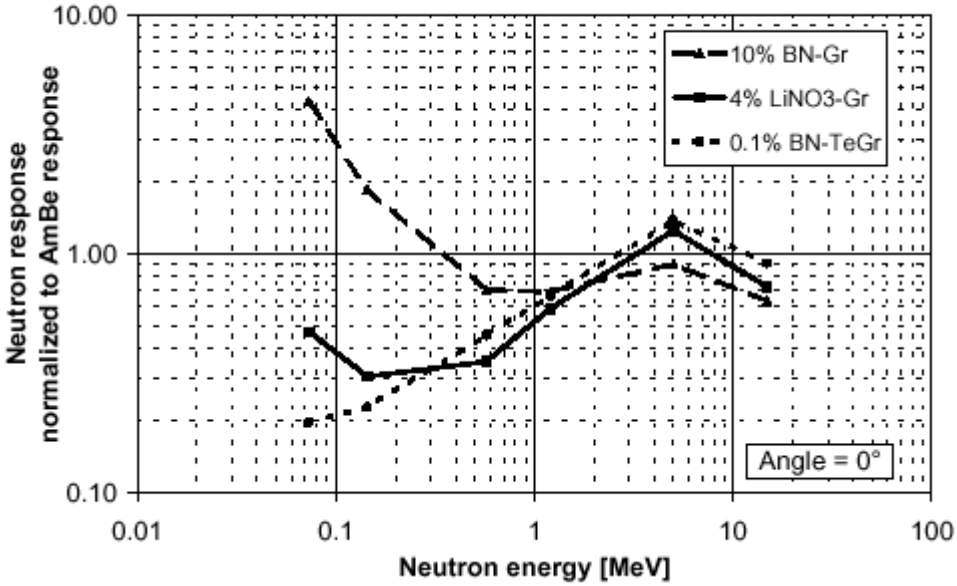

Figure 63 – Neutron response of DIS neutron dosimeter [33].

7.4 Area monitors

Area monitors could be foreseen in those (accessible) areas where the radiation fields are not constant, but depend largely on the operation parameters of the accelerator, and where certain modes of operation could lead to excessive dose rates. These instruments are essentially ionisation chamber monitors provided with local and/or remote readout and alarm displays. They can be actively interlocked to the accelerators to switch off the accelerator in case of an alarm

reading. If one relies effectively on these monitors, a self-checking provision is recommended via a small priming source, which has to produce a small ionisation current. Where neutrons may be produced it is good practice to install both a gamma and a neutron monitor.

In bigger installations, it may be very difficult to satisfactorily span the entire facility with area monitors, since very localized leaks may be overlooked. Therefore regular routine radiation checks with portable survey meters (ionisation chambers or Geiger-Müller counters) are always recommended.

8. Personnel Safety systems

8.1 Role of the personnel safety system

The shielding of the accelerator tunnels and experimental rooms guarantees that during the operation of the accelerator the effective dose levels are sufficiently low outside these areas. The role of the Personnel Safety System (PSS) is to guarantee that nobody can be present inside the accelerator tunnel and experimental areas while the accelerator is operational. In a more general way, the PSS must guarantee that:

- No prompt radiation source can be switched on in a room before one is certain that nobody is still present in this room;
- If the presence of a person is detected inside a room, all prompt radiation sources inside this room are immediately switched off.

Note that the protection against induced radioactivity is less straightforward and will rely on administrative measures.

8.2 Requirements

Independent of national and/or international legal requirements, any PSS must meet a number of general requirements.

The entire system must be redundant, in the sense that two independent safety systems exist, where each system fulfils its role as PSS described above. This redundancy must be maintained throughout the entire system. This means that any individual interlock has been doubled (e.g. two door-switches per door-wing, two contacts per emergency stop), one interlock cabled into the first logic diagram and the second interlock cabled into the second logic diagram. The requirement for redundancy also implies that at least two accelerator subsystems must be interlocked, where switching off each individual sub-system alone results in the immediate halt of the prompt radiation sources.

The PSS must be an active safety system: a PSS power failure must automatically put the installation in a safe situation, i.e. all prompt radiation sources switched off.

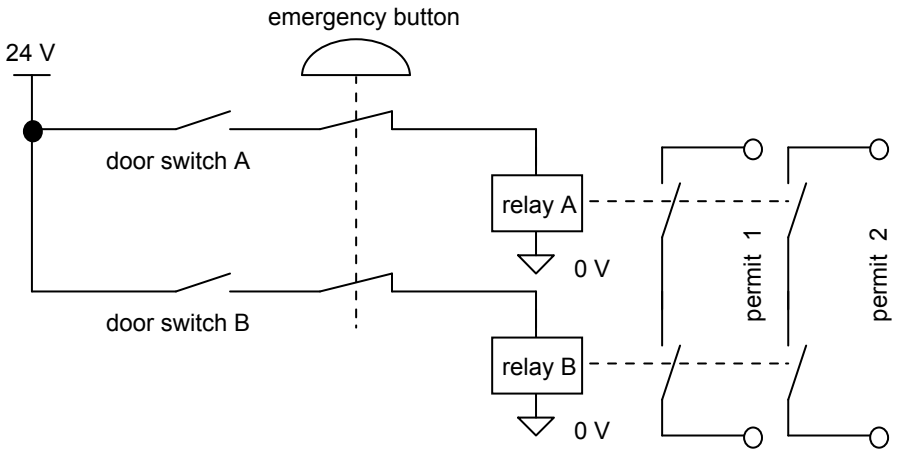

Figure 64 - Simple safety circuit illustrating the PSS requirements for redundancy

Figure 64 shows a simple PSS circuit for a simple active and redundant system where a permit to switch on an equipment would require that a door is closed and an emergency stop has not been pressed.

It is important that the PSS provides all the functionalities requested by the accelerator people, as long as the required modes of operation are not in contradiction with safety considerations.

From experience we know that the level of safety obtained with a properly designed PSS will be essentially determined by human factors. This aspect should therefore not be underestimated. Failures due to human errors can be avoided via:

- The design of the PSS should take the human factor into account: the search routes defined in the tunnels should automatically force people to span the entire area; if necessary wide-angle mirrors should be installed, at the end of a search warning sirens and beacons should be activated before any accelerator can be switched on, etc.
- All people working around the accelerators must be trained in all aspects of the PSS.

8.3 Technology

Both systems using hardwired relay logic or systems using Programmable Logical Controllers (PLCs) are reliable and failsafe and the final choice between these two technologies will be essentially based on legal requirements and/or philosophical considerations.

Independent of the technological choice the PSS should be clearly separated from the control system of the accelerator. Mixing the two systems would lead to unavoidable conflicts related to the maintenance of the system. Indeed a formal retesting of the PSS is required after any intervention on it. The number of people intervening on the PSS as well as the number of interventions should be limited to the strict minimum. Therefore the PSS should only raise accelerator permits and switch off accelerators in emergency cases, but the normal accelerator control (on/off) should be external to the PSS.

8.4 Layout of the PSS

We can distinguish different subsystems in the PSS. The area interlocks deal with securing the different accelerator rooms. This part includes the searches, the emergency stops as well as the door interlocks and danger signs. The accelerator interlocks deal with the permits of the interlocked accelerators. The interlocked radiation monitors will also be included in the PSS. These different subsystems are linked together via the logic circuitry, the central part of the PSS.

Before an accelerator can be switched on, one must guarantee that nobody is present inside any of the rooms where the switching on of the accelerator will create radiation hazards. This condition is met by the so-called search. The search is a visual inspection of the entire accelerator room. One (or more) person enters the tunnel and searches the entire room, making sure that any person still inside is leaving. The search is implemented in such a way that the entire area is effectively covered and that it is impossible for a person to re-enter the area behind the search-team. The first condition is met by locating search buttons in appropriate places, the second condition is met by interlocking all secondary doors at the start of the search and this may require the presence of at least two people in the search team.

Once a tunnel is searched the PSS must guarantee that nobody can enter before the search is tripped. This is done by interlocking all access doors. The ultimate safety here comes from the door switches: as soon as a door is opened the loss of the door switch contacts trips the search. However, extra safety barriers are provided by door-locks or by blocking the opening of motorized doors, as well as by illuminated “no access” signs indicating the status of the tunnel.

Inside all tunnels sirens and flashing beacons are switched on for a given period of time, before the accelerator permit will be raised. This can be combined with the diffusion of a message over the loudspeaker system. This must allow people who were left accidentally inside the tunnel after the completion of the search to react by pressing an emergency stop before the accelerator would be switched on (see hereafter).

Emergency stop buttons are installed inside the tunnels, in such a way that wherever a person is, at least one emergency stop can be easily reached within a short distance and without having to crawl under or over equipment. Pressing an emergency stop button trips the search and therefore immediately switches off all prompt radiation sources or prevents them from being switched on. It is good practice to use the same emergency stops for both the radiation safety (via PSS) and electrical safety: apart from tripping the search, pressing an emergency stop will switch off all electrical power inside the tunnel, except for the lighting.

References

1. M.J. Berger, S.M. Seltzer, “Stopping powers and ranges of electrons and positron”, National Bureau of Standards report NBSIR 82-2550, 1982
2. Shielding against high energy radiation, Landolt-Börnstein new series, volume I/11, Editor H. Schopper, Springer-Verlag, 1990
3. National Institute of Standards and Technology, Photon Cross Sections Database, http://physics.nist.gov/PhysRefData/Xcom/Text/XCOM.html
4. A.T. Nelms, “Graphs of the Compton energy-angle relationship and the Klein-Nishina formula from 10 keV to 500 MeV, National Bureau of Standards, Cir. 542, Washington DC, 1953
5. J.H. Hubbell, “Photon cross-sections, attenuation coefficients and energy absorption coefficients, National Bureau of Standards Report NSRDS-NBS 29, Washington DC, 1969
6. John R. Lamarsh, “Introduction to Nuclear Reactor Theory”, Addison-Wesley, 1972
7. JENDL-3.2: Nakagawa T., Shibata S., Chiba S., Fukahori T., Nakajima Y., Kikuchi Y., Kawano T., Kanda Y., Ohsawa T., Matsunobu H., Kawai M., Zukeran A., Watanabe T., Igarasi S., Kosako K. and Asami T.; J. Nucl. Sci. Technol., 32(12), 1259-1271 (1995).
8. M.F. Kaplan, Concrete radiation shielding, John Wiley & Sons, NY, 1989
9. J.F. Janni, *Calculations of energy loss, range and probability of inelastic nuclear collisions for 0.1 to 1000 MeV protons*, Atomic Data Nucl. Data Tab. **27**, 147 (1982)
10. *Nuclear data for neutron and proton radiotherapy and for radiation protection*, ICRU report 63, International Commission on Radiation Units and Measurements, Bethesda, Maryland, 2000
11. A.H. Sullivan, A guide to radiation and radioactivity levels near high energy particle accelerators, Nuclear Technology Publishing, 1992
12. *Review of Particle Properties*, Phys. Lett. B, **204**, 1 (1988)
13. D.M. Skyrme, The evaporation of neutrons from nuclei bombarded with high energy protons”, Nucl. Phys. **35**, 177 (1962)
14. ICRP, “Recommendations of the International Commission on Radiological Protection”, ICRP Publication 60. Annals of the ICRP 21(1-3) Pergamon Press, Oxford, 1991
15. ICRU, “Quantities and units in radiation protection dosimetry”, ICRU Report 51. International Commission on Radiation Units and Measurements, Bethesda, Maryland, 1993
16. ICRU, “Conversion coefficients for use in radiological protection against external radiation”, ICRU Report 57. International Commission on Radiation Units and Measurements, Bethesda, Maryland, 1998
17. B. Dörschel, V. Schuricht and J. Steuer, The Physics of Radiation Protection, Nuclear Technology Publishing, 1996
18. W.P. Swanson, Radiological Safety Aspects of the Operation of Electron Linear Accelerators, IAEA Technical Reports Series no. 188, Vienna, 1979
19. IAEA Photonuclear Data Library, http://www-nds.iaea.or.at/photonuclear/
20. Levinger, Modified Quasi-deuteron model, Physics letters 82B(1979)181

21. R. H. Thomas and G. R. Stevenson, *Radiological safety aspects of the operation of proton accelerators*, IAEA Technical Reports Series no. 283, Vienna (1988)

22. D. R. Perry, "Neutron dosimetry methods and experience on the 7-GeV proton synchrotron, Nimrod", Neutron Monitoring (Proc. Symp. Vienna, 1966), IAEA, Vienna (1967) 35

23. K. Tesh, "A simple estimation of the lateral shielding for proton accelerators in the energy range 50 to 1000 MeV", Radiat. Prot. Dosim. **11**(3), 165 (1985)

24. M. Barbier, Induced Radioactivity, North Holland Publishing Company, 1969

25. H.J. Moe, "Advanced Photon Source: Radiation Safety", DOE Safety Review, Argonne National Laboratory, Chicago, 1990

26. I. O. Andersson and J. Braun, "A neutron rem counter", Nucleonik 6(5), 237 (1964)

27. Birattari C., Esposito A., Ferrari A., Pelliccioni M. and Silari M, "*A Neutron Survey Meter with Sensitivity Extended up to 400 MeV",* Radiat. Prot. Dosim. **44**, 193-197 (1992).

28. Birattari C., E. Esposito A., Ferrari A., M., Pelliccioni M., Rancati T. and Silari M., "*The extended range neutron rem counter "LINUS": Overview and latest developments"*, Radiat. Prot. Dosim. **76**, No.3, 135-148 (1998).

29. F. d'Errico, Nucl. Instr. And Meth. In Phys. Res. B 184, pp. 229 – 254 (2001)

30. F. d'Errico et al., Radiat. Protrct. Dosim. 65 (1-4), pp. 397-400 (1996)

31. www.siemens.co.uk/env-sys/uk/electronic_dosimetry/ EPD-N.pdf

32. V.K. Mathur, "Ion Storage dosimetry", Nucl. Instrum. And Meth. In Phys. Res. B 184, pp. 190-206 (2001)

33. C. Wernli et al., "Neutron dosimetry with ion chamber-based DIS systems", IRPA-10, Hiroshima, Japan, May 2000